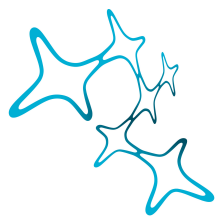


DEVELOPMENT AND PHYSIOLOGY OF SIGNAL INTEGRATION IN THE DNLL

Julian AMMER



Graduate School of
Systemic Neurosciences
LMU Munich

Munich, July 2013

Dissertation

DEVELOPMENT AND PHYSIOLOGY OF
SIGNAL INTEGRATION IN THE DNLL

Julian Ammer

Graduate School of Systemic Neurosciences
Ludwig-Maximilians Universität München

Submitted July 2013

First reviewer and supervisor: PD Dr Felix FELMY

Second reviewer: Prof Benedikt GROTHE

External reviewer: Prof Eckhard FRIAUF

Date of oral defense: 21.11.2013

Contents

Abstract	IV
1 Introduction	1
1.1 Sound localization	2
1.1.1 Interaural level differences	4
1.1.2 Interaural time differences	5
1.1.3 The precedence effect	8
1.1.4 Processing of binaural cues in the DNLL	9
1.1.5 Persistent inhibition alters processing in the inferior colliculus	12
1.2 Motivation	13
1.3 Developmental refinement of neuronal circuits	13
1.4 Integration of synaptic inhibition	16
2 Physiological development of DNLL neurons	20
3 Long lasting inhibition in the DNLL	36
4 Discussion	68
4.1 Implications of fast and precise signaling in the mature DNLL . . .	68
4.2 Synergistic actions as cellular mechanism of persistent inhibition . .	71
4.2.1 NMDA receptor dependent input amplification	72

4.2.2	Synaptic mechanisms	73
4.2.3	Postsynaptic integration	74
4.3	Persistent inhibition and the precedence effect	77
	References	82
	Nomenclature	96
	Appendix	97

Abstract

The auditory system uses interaural disparities to compute the location of sound sources. In natural auditory environments, sounds are reflected from a multitude of objects. The reflections can arrive at the listener's ear multiple times and from different angles in space. As a consequence these reflections cause binaural cues that carry distracting directional information and pose a challenge to the accurate localization of the primary sound source. The auditory system deals with this challenge by selectively suppressing the directional information of echoes, a process known as the precedence effect. An initial step in the physiological implementation of this process is thought to be mediated by the dorsal nucleus of the lateral lemniscus (DNLL). In response to a leading sound, the DNLL generates a GABAergic persistent inhibition in its contralateral counterpart that lasts long enough to suppress responses to trailing sounds for tens of milliseconds. At the same time DNLL neurons are able to respond very reliably and fast to binaural stimulation.

To get more insight into the biophysical specializations that enable the DNLL neurons to fulfill their physiological task, we first studied the physiological development of DNLL neurons. Building on the information of this first study, we investigated the cellular mechanisms that could underlie the generation of persistent inhibition.

As neurons are tuned to their specific function in the mature circuit during postnatal development, we assessed the relevant physiological parameters of DNLL neurons in acute brain slices of 9 - 26 day old Mongolian gerbils. The maturation of intrinsic and synaptic properties lead to an improvement of fast and precise signal integration in DNLL neurons. DNLL neurons turn into fast spiking neurons with fast membrane time constants and brief action potentials. In accordance, synaptic glutamatergic and GABAergic current kinetics accelerate with age. Together, these changes reduce the latency and jitter of action potential responses to incoming sig-

nals. Furthermore, although NMDA receptor mediated current is downregulated and its kinetics accelerate with age, it still contributes to action potential generation in mature animals. Taken together, DNLL neurons are developmentally tuned to respond with temporally precise action potentials and high firing rates.

Importantly, this fast processing does not contradict the creation of persistent inhibition. Rather, the high firing rates that mature DNLL neurons can sustain form the basis of a series of interacting cellular mechanisms that control the duration of inhibition in the DNLL of mature Mongolian gerbils depending on presynaptic activity. Activity-dependent GABA spillover and asynchronous release translate high presynaptic firing rates into a prolongation of GABAergic IPSCs. Passive integration of hyperpolarizing inhibition additionally prolongs IPSPs depending on the conductance amplitude, due to the non-linear membrane relaxation between GABA-reversal and resting potential. The resulting IPSP efficiently suppresses action potential generation for a duration matching *in vivo* findings. Thus, these cellular mechanisms work in synergy to achieve an activity-dependent control of inhibition that gates information during the categorization of echoes.

Taken together, the cellular properties described here enable DNLL neurons to take part in signal processing on very different time scales. On the one hand, they are able to transmit information fast and reliably. On the other hand, they display a slow filter property that adds context to the processing of binaural cues.

1 Introduction

Our perception of the auditory environment is not an accurate representation of the physical acoustic scene, but a processed and filtered interpretation. The auditory system extracts the auditory information that is relevant to us and allows us to orient in the auditory environment. At the same time, other distracting information is suppressed. An example of this selective filtering of auditory information is the suppression of directional information of reverberations during sound localization (reviews e.g.: Blauert, 1997; Litovsky et al., 1999; Blauert and Braasch, 2005; Litovsky and McAlpine, 2010). In a surrounding with sound reflecting objects, a sound emitted from a single sound source arrives at our ears multiple times: First through a direct path and then through longer reflected pathways. The binaural auditory cues caused by the first wavefront carry the relevant information to localize the sound source correctly. The reflections arrive with a delay and from different angles in space compared to the direct sound, causing binaural cues that carry distracting directional information. The initial sound localization structures in the auditory brainstem compute the location of every incoming reflection. Only at a later processing stage is the distracting information identified and tagged to enable a facultative suppression (Pecka et al., 2007). How this context-dependent filtering may be implemented on a cellular basis in Mongolian gerbils is the main focus of this work. In the following, I will first briefly outline the initial stages of binaural processing involved in sound localization and then describe the circuit thought to

underlie the identification of echoes in more detail.

1.1 Sound localization

Sound is a pressure wave. When it hits the ear, it travels through the auditory canal and causes vibrations of the tympanic membrane. The tympanic membrane transmits its vibrations to the three inner ear ossicles which serve to conduct the signal to evoke a travelling wave in the fluid filled cochlea. The sensory epithelium of the cochlea is the Organ of Corti, located on the basilar membrane. The elasticity of the basilar membrane decreases from basal to apical end and displays resonance to vibrations at different frequencies along this axis (von Békésy, 1970). Thus, sounds of different frequencies cause vibrations at different positions along the cochlea. This place code of frequency is called "tonotopy" and is preserved at many levels along the auditory pathway. Inner hair cells in the Organ of Corti transform the mechanical signal in the cochlea into an electrical signal. These highly specialized receptor cells excite the ganglion neurons which form the auditory nerve that projects to the cochlear nucleus (CN).

At the level of the auditory nerve, the incoming sound signal has been decomposed into different frequency channels. In these frequency channels intensity and temporal information of the sound is encoded in the rate and timing of action potentials (APs). For low frequencies, auditory nerve fibers carry specific timing information as they are able to phase lock their APs to a specific phase in a cycle of a pure tone (Rose et al., 1967).

In contrast to other sensory systems such as the somatosensory or visual system, information regarding the location of objects is not available at the level of the sensory receptors. Instead, the auditory system uses spectral cues and interaural disparities to compute the location of a sound source (Grothe et al., 2010).

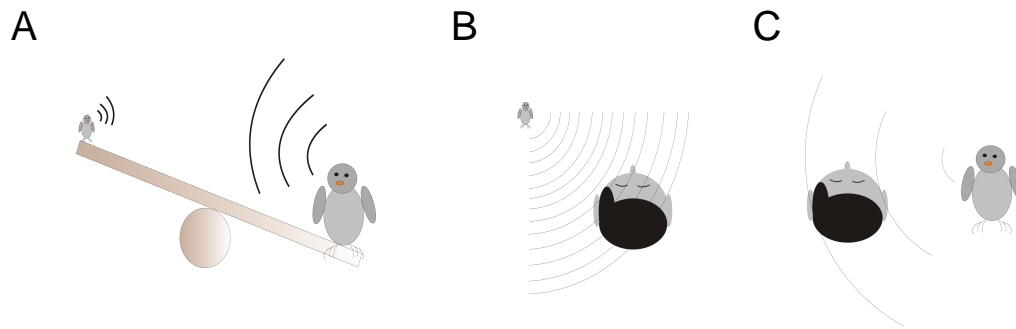


Figure 1.1: **A** Two birds singing. The small bird emits high frequency sounds. The big heavy bird emits low frequency sounds. **B** When high frequency sounds hit the head of the listener, the sound intensity is attenuated by the head. **C** For low frequencies, sounds are not attenuated, but timing differences can be computed when the wavelength is longer than the head width. Modified from Grothe et al. (2010); Porres (2012).

Spectral cues are used for localization in the vertical plane. Depending on the elevation of a sound source, notches in the frequency spectrum which are largely caused by the pinna lead to characteristic signals that code for elevation (Grothe et al., 2010). Interaural disparities are used for sound localization in the horizontal plane. Different neural mechanisms serve to localize high and low frequency sounds. For high frequency sounds, sound intensity is attenuated by the head and pinnae leading to differences in sound intensity level at the two ears (interaural level differences, ILDs) which can be used to estimate the azimuthal sound location (Figure 1.1).

Low frequency sounds are hardly attenuated by the head. In this case, microsecond differences in the arrival time between both ears (interaural time differences, ITDs) are used to determine sound location. This strategy can be used only for frequencies for which the wavelength of the tone is longer than the head width. Otherwise the computation of phase differences during ongoing tones becomes ambiguous. The usage of these two strategies in different frequency regions is called the duplex theory of sound localization (Rayleigh, 1907). Simplified, the structures

in the auditory brainstem that compute ILDs and ITDs are the lateral and medial superior olive (LSO and MSO).

1.1.1 Interaural level differences

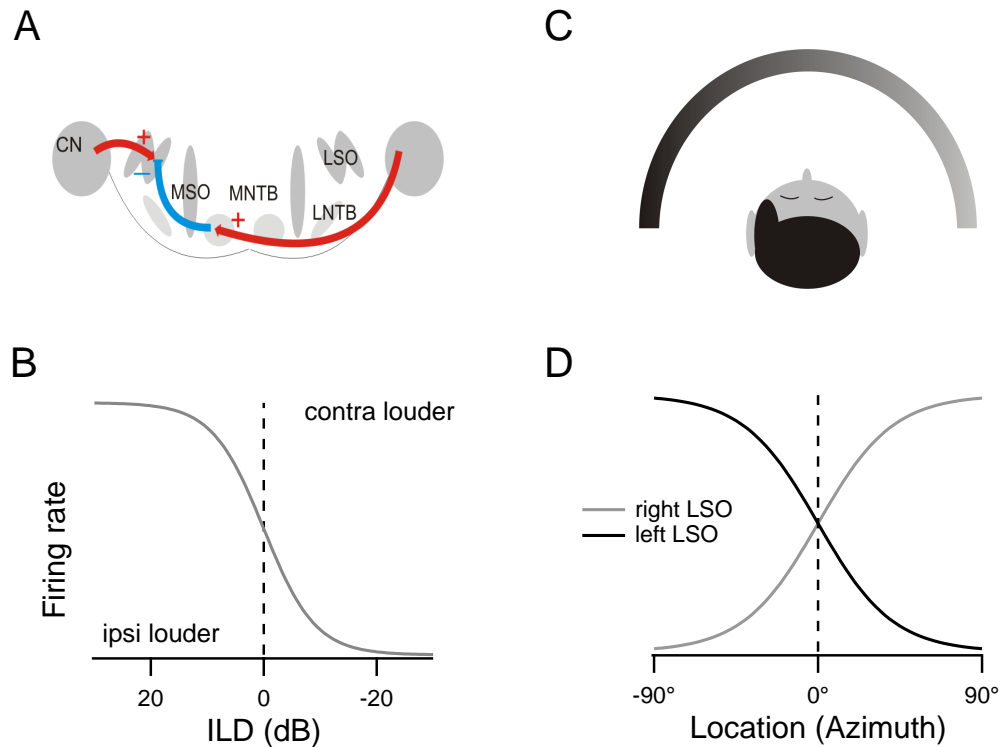


Figure 1.2: ILD processing in the LSO. **A** Circuit diagram with excitatory projections in red and inhibitory projections in blue. CN cochlear nucleus, MSO medial superior olive, LSO lateral superior olive, MNTB medial nucleus of the trapezoid body, LNTB lateral nucleus of the trapezoid body. **B** Schematic response curve of a LSO neuron. Response rate is maximal for ILDs favouring the ipsilateral ear and decreases for ILDs favouring the contralateral ear. **C, D** Representation of azimuthal sound source location through the population codes of the LSOs in both hemispheres. The population response of each LSO is maximal for sounds on the ipsilateral side. The population responses of the two LSOs intersect at 0 ILD which corresponds to sound from the front. Modified from Grothe et al. (2010); Porres (2012).

The computation of ILDs in the LSO can be thought of as a subtraction mechanism (Moore and Caspary, 1983; Sanes, 1990; Grothe et al., 2010). Ipsilateral sound intensity is represented in the excitatory input from the spherical bushy cells

in the anterior ventral cochlear nucleus (AVCN)(Cant and Casseday, 1986). Contralateral sound intensity is encoded in the inhibitory input from the medial nucleus of the trapezoid body (MNTB)(Spangler et al., 1985; Sanes, 1990). The glycinergic cells of the MNTB relay the information they receive from the globular bushy cells of the contralateral AVCN through the Calyx of Held. Strikingly, the faithful transmission at this large synapse as well as the thicker axons compensate for the longer distance and enable inhibition to play a role even at the onset of a sound stimulus (Grothe et al., 2010). The integration of the two opposing inputs in the LSO leads to characteristic ILD functions (Figure 1.2). If the sound on the ipsilateral side is louder, excitation in the LSO dominates and the neuron responds with a high firing rate. If the sound intensity at the contralateral ear is increased, stronger inhibition via the MNTB is recruited that finally suppresses firing in the LSO neuron (Boudreau and Tsuchitani, 1968). Thus, neurons in the right LSO are primarily excited by sounds in the right hemifield while neurons in the left LSO are excited by sounds in the left hemifield. If the population codes of the two LSOs are considered together (Figure 1.2D), a two channel code that unambiguously codes for horizontal location in space results (Park et al., 2004; Grothe et al., 2010).

1.1.2 Interaural time differences

Equivalent to the coding of ILDs, a two channel code of ITDs is probably used in mammals for sound localization at low frequencies (McAlpine et al., 2001; Brand et al., 2002; Grothe, 2003; McAlpine and Grothe, 2003; Grothe et al., 2010; Lesica et al., 2010). The original theoretical suggestion of the Jeffress model (Jeffress, 1948) only seems to hold true for birds (Grothe et al., 2010; Lesica et al., 2010; Ashida and Carr, 2011). In the Jeffress model, sound location is mapped at the single neuron level. The creation of such a map requires coincidence detection of two

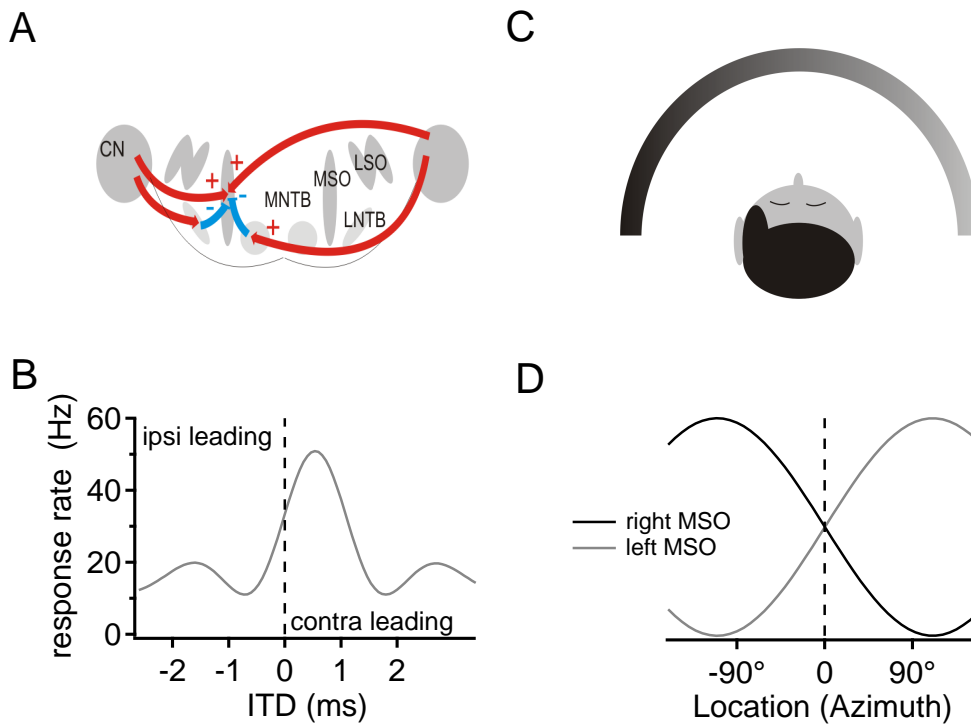


Figure 1.3: ITD processing in the MSO. **A** Circuit diagram with excitatory projections in red and inhibitory projections in blue. CN cochlear nucleus, MSO medial superior olive, LSO lateral superior olive, MNTB medial nucleus of the trapezoid body, LNTB lateral nucleus of the trapezoid body. **B** Schematic response curve of one MSO neuron. The peak of the response curve is shifted to ITD values favouring the contralateral ear. The slope of the response function lies in the physiologically relevant range. **C, D** Representation of azimuthal sound source location through the population codes of the MSOs in both hemispheres. The population responses of the two MSOs intersect at 0 ITD which corresponds to a sound directly from the front. Modified from Grothe et al. (2010); Porres (2012).

excitatory inputs in neurons arranged systematically along a delay line axis. Along this delay line axis, ITDs are compensated by different axonal conduction times of the two inputs (Jeffress, 1948). If the two excitatory inputs arrive simultaneously, the firing rate in the coincidence detectors becomes maximal (Grothe et al., 2010; Ashida and Carr, 2011).

The situation is different in mammals. Although the MSO receives two excitatory inputs and the temporal code is transformed into a rate code through a very precise

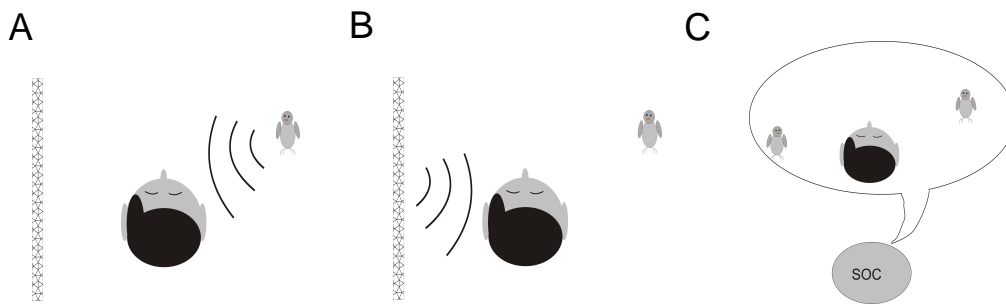


Figure 1.4: Sound source representation in the superior olivary complex (SOC). A bird emits a sound that hits the listener in a reverberant environment through **A** a direct path and **B** a reflected pathway. **C** The SOC does not differentiate between direct and indirect sounds but responds to every incoming sound wave. Thus, at this stage of binaural processing the bird call is represented as if coming from multiple locations.

coincidence detection mechanism, the peaks of the rate response curves are shifted outside of the range of naturally occurring ITDs (Figure 1.3). Thus, the maximal firing rates in MSO neurons do not code for sound location (McAlpine et al., 2001; Brand et al., 2002). The shift in the peak of the response curves is probably largely caused by the inhibitory inputs from the MNTB and the lateral nucleus of the trapezoid body (LNTB) (Brand et al., 2002; Pecka et al., 2008 but see Roberts et al., 2013; van der Heijden et al., 2013). This shift causes the steepest slope of the ITD response function to fall within the physiologically relevant range (McAlpine et al., 2001; Brand et al., 2002; Grothe et al., 2010). In this way, ITDs can be ideally distinguished on the basis of the response rate. Analogous to the two channels coding for ILDs, the population tuning curves from both hemispheres are combined to unambiguously code for a specific location in space (Figure 1.3).

Taken together, the exquisitely precise temporal information that is conveyed by the inputs to the MSO neurons is converted into a rate code by the very precise integration of MSO neurons.

The computation of ITDs and ILDs requires numerous cellular specializations from the receptor cells to the first stages of binaural convergence in the MSO and

LSO. These specializations enable signal processing on very fast time scales. However, this considerable speed makes it difficult for these nuclei to process signal variations on slower time scales (Figure 1.4). To achieve a meaningful percept of auditory space the information present at the superior olivary complex (SOC) has to be further processed and filtered in a context-dependent manner.

1.1.3 The precedence effect

Fluctuations of binaural cues on fast time scales can carry misleading information, caused by reflections or interference of multiple sound sources (Meffin and Grothe, 2009). Thus, additional processing of information on a slower time scale is necessary to enable a meaningful interpretation of the auditory environment. In a real acoustic environment, sounds are reflected from a multitude of reflecting surfaces such as walls or trees. The reflections are attenuated yet spectrally similar copies of the original sound and can arrive at the listener's ear multiple times and from different angles in space (Litovsky et al., 1999).

Psychophysically and physiologically, the processing of reflections is mostly studied with a very simplified two tone paradigm. A leading sound representing the primary sound source and a lagging sound representing a single reflection are presented at variable time delays (reviewed in Blauert, 1997; Litovsky et al., 1999). Depending on the delay, the perception of the two sounds changes. At very short delays (<1ms) a summation of the two sound locations occurs, an effect known as summing localization. For longer delays the leading sound dominates the perception of sound location, while the lagging sound is perceived as a reverberation but is not localized. This phase is called localization dominance and lasts until the echo threshold is reached. When the echo threshold is crossed for even longer delays, two separate sound sources are perceived and localized. The time to echo threshold varies from 5 to tens of milliseconds depending on the stimulus and experimental

conditions (Litovsky et al., 1999). This sequence of behavioral effects is summarized as the precedence effect (Wallach et al., 1949; Blauert, 1997; Litovsky et al., 1999). Apart from mammals (for Mongolian gerbils: Wolf et al., 2010), precedence has been described in birds, insects and amphibians (Spitzer et al., 2003; Lee et al., 2009; Marshall and Gerhardt, 2010). This widespread occurrence shows the general importance of the precedence effect in auditory perception. In mammals, putative physiological correlates of precedence have been described at various levels of the auditory system, from the auditory nerve to the auditory cortex (Litovsky et al., 1999; Litovsky and McAlpine, 2010). The most common described neuronal correlate is a suppression of the neural response to a sound by a preceding tone. The duration of suppression increases gradually along the auditory pathway (Litovsky et al., 1999). The first stage in the binaural pathway, in which a substantial suppression of a neural response to a lagging sound appears, is the dorsal nucleus of the lateral lemniscus (DNLL). Importantly, the information from the lagging sound is not lost during this suppression, but instead the sound is identified as an echo (Pecka et al., 2007). This identification leads to a facultative suppression of the directional information of the echo. Under some behavioral conditions, however, the directional information can be retrieved and echo suppression breaks down (Clifton, 1987). How this echo identification process is thought to be implemented on a neuronal level will be described in the following after a brief introduction to the neural circuitry and processing of the DNLL (section 1.1.4.1).

1.1.4 Processing of binaural cues in the DNLL

The rate coded information from the initial sound localization stages in the SOC is transmitted to the DNLL via direct excitatory synapses. The DNLL receives excitation from the contralateral LSO and ipsilateral MSO (Glendenning et al., 1981; Shneiderman et al., 1988; Siveke et al., 2006; Kelly et al., 2009). The LSO also

provides glycinergic inhibition to the ipsilateral DNLL (Glendenning et al., 1981; Glendenning et al., 1992; Oliver, 2000). In addition, the DNLL receives excitatory inputs from the contralateral CN (Kelly et al., 2009).

In line with its inputs, the DNLL contains neurons that are sensitive to both ILDs and ITDs (Aitkin et al., 1970; Brugge et al., 1970; Li and Kelly, 1992; Kelly et al., 1998; Seidl and Grothe, 2005) and is primarily excited by sounds from the contralateral side (Glendenning et al., 1992; Markovitz and Pollak, 1993; Oliver, 2000; Siveke et al., 2006). Interestingly, the representation of ITDs is enhanced in the DNLL compared to the MSO (Kuwada et al., 2006; Pecka et al., 2010). For neurons with low preferred frequencies this effect is achieved by a reduction in inter-trial response variability (Pecka et al., 2010). For neurons with higher preferred frequencies the representation is enhanced through an increase in dynamic range. The increased dynamic range is achieved by keeping the peak response rates in the DNLL as high as in the SOC, but reducing the trough rates of the response curve (Pecka et al., 2010). Generally, DNLL neurons can respond with high sustained rates to binaural stimulation (Markovitz and Pollak, 1994; Seidl and Grothe, 2005; Siveke et al., 2006; Pecka et al., 2010). Only a minority of cells respond exclusively at the sound onset (Siveke et al., 2006).

The DNLL itself is a mainly GABAergic nucleus (Saint Marie et al., 1989) that sends strong projections via the commissure of Probst to the contralateral DNLL and to both ipsi- and contralateral inferior colliculi (IC) (Adams and Mugnaini, 1984; Chen et al., 1999; Kelly et al., 2009). The inhibitory commissural projections seem to target mainly the soma of DNLL neurons (Iwahori, 1986; Oliver and Shneiderman, 1989), that seem to constitute a heterogeneous population of cells ranging from bipolar to multipolar morphology (Kane and Barone, 1980; Bajo et al., 1993; Wu and Kelly, 1995b; Campos et al., 2001). It is this commissural connection, that reciprocally inhibits the two DNLLs, that is key to the filtering of the directional

information of lagging sounds.

1.1.4.1 Persistent inhibition

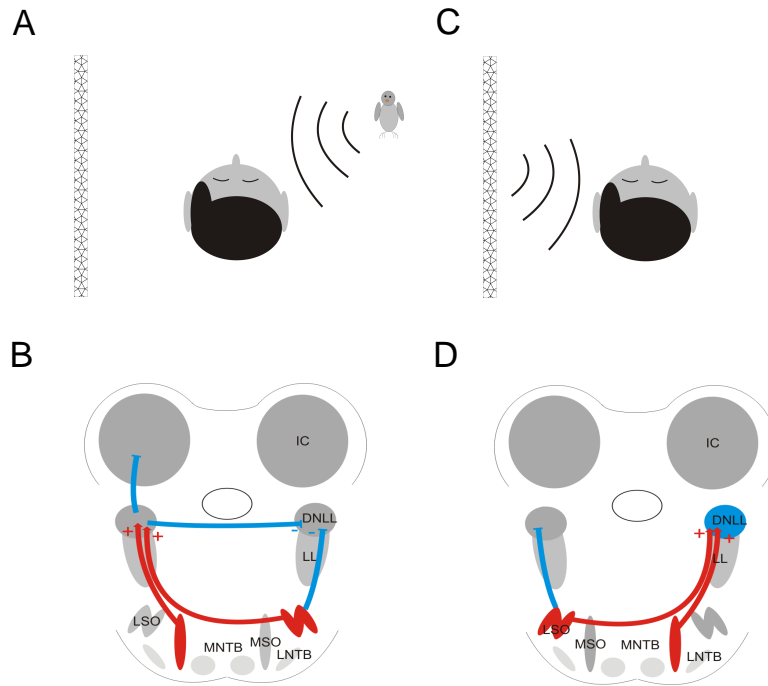


Figure 1.5: Persistent inhibition in the DNLL. **A** Sound arrives at the right ear through the direct pathway **B** The right LSO and/or left MSO are activated and excite the left DNLL. The DNLL itself inhibits neurons in both ICs and the right DNLL. **C** When the reflected sound arrives at the left ear, **D** the other LSO/MSO pair becomes active but fails to excite the DNLL as the inhibition by the first soundwave still persists. Modified from (Pecka et al., 2007; Porres, 2012).

In addition to the properties that the DNLL inherits from the SOC, it adds a different computational quality to binaural processing by introducing a context-dependent filter property that is necessary to identify distracting localization cues. The DNLL generates a $GABA_A$ receptor mediated persistent inhibition (PI, Figure 1.5) long enough to inhibit responses to lagging sounds for tens of milliseconds in the contralateral DNLL even after cessation of presynaptic activity (Yang and Pollak, 1994; Burger and Pollak, 2001; Pecka et al., 2007). The duration of the PI has been pro-

posed to match the echo threshold during behavioral performance (Pecka et al., 2007).

Three different cellular mechanisms could potentially underlie the PI (see also Porres et al., 2011; Porres, 2012):

First, persistent activity in the presynaptic inhibitory neuron could continuously supply inhibitory input. This hypothesis is supported from data in rats (Wu and Kelly, 1995b; Kelly and Kidd, 2000). However, no prolonged spiking has been found in gerbils (Siveke et al., 2006; Pecka et al., 2007).

Second, single trailing spikes from many presynaptic neurons could arrive with some temporal jitter and thereby suppress activity over an extended period. This possibility, however, would also require delayed presynaptic activity to some extent. In addition, the jittered arrival of inhibitory input seems too unreliable a mechanism to produce PI repeatedly and reliably on a single trial level.

Third, the properties of the GABA_A receptor mediated inhibition or the integration properties of DNLL neurons could be such that APs are suppressed for a long time after the last presynaptic AP. The basis of this last hypothesis can be ideally studied in *in vitro* slice preparations. Previously, the slow IPSC kinetics in juvenile gerbils *in vitro* have been proposed to underlie the PI (Pecka et al., 2007; Saunier-Rebori, 2008). Yet, whether this holds true for GABAergic kinetics in adult animals is not known and constituted the motivation for the first, developmental study of this thesis (section 2).

1.1.5 Persistent inhibition alters processing in the inferior colliculus

The PI in the DNLL has immediate consequences on signal processing in IC. During the PI, a population of neurons in the IC is relieved from inhibition by the DNLL and responds to lagging sounds from directions to which they were previously unre-

sponsive (Burger and Pollak, 2001; Pecka et al., 2007). There are different possible interpretations of this additional activity in the IC. The disinhibition could corrupt the population code in the IC and thus lead to an ambiguous representation of sound source location for lagging sounds (Burger and Pollak, 2001). In this scenario, the PI would lead to a loss of directional information. Yet, as localization information can be retrieved under some behavioral conditions (Clifton, 1987), the additional activity in the IC could also be used as a tag that identifies the sound as an echo for a later facultative suppression of echoes in higher centers (Pecka et al., 2007).

1.2 Motivation

Taken together, the DNLL is an important source of inhibition in the auditory brainstem. The reciprocal connection between the two DNLLs constitutes an ideal circuit motif for the flexible categorization of sounds during echo suppression (Mysore and Knudsen, 2012). To gain more insight into the biophysical specializations that enable DNLL neurons to fulfill their physiological task, we first studied the physiological development of DNLL neurons (section 2). Building on the information of this first study, we investigated the cellular mechanisms that could underlie the generation of PI (section 3). As both studies are presented in the form of a manuscript, each of them already contains a specific introduction. Thus, the following paragraphs will rather provide a more general view on the topics of developmental refinement and the role of inhibition in neuronal circuits.

1.3 Developmental refinement of neuronal circuits

In the first study, we describe the postnatal development of the intrinsic membrane properties of DNLL neurons and the maturation of the main synaptic inputs to the

DNLL.

During postnatal development neurons are tuned towards their specific function in the mature circuit. This tuning involves morphological and electrophysiological changes at the cellular and synaptic level. Plasticity on the level of synapses often entails pruning and reorganization of synapses. Prominent examples of these plastic changes are found in the sound localization circuits of the SOC. In the LSO, elimination of glycinergic synapses from the MNTB sharpens the tonotopic distribution of MNTB-LSO connections after hearing onset (Kim and Kandler, 2003). In the MSO, a relocation of inputs takes place at a single cell level. Normal early acoustic experience causes a relocation of glycinergic synapses to the soma from a previously homogenous distribution along the whole cell surface (Kapfer et al., 2002; Werthat et al., 2008). The concentration of inhibitory synapses at the soma potentially reduces temporal filtering along the dendrites and enhances the temporal accuracy of inhibitory inputs, an important feature for coincidence detection. Rearing gerbils in omnidirectional noise inhibits the proper pruning of the synapses (Kapfer et al., 2002; Werthat et al., 2008) and disrupts the normal development of ITD tuning curves (Seidl and Grothe, 2005). Together with the pruning of synapses, the dendritic tree of neurons is refined (Rietzel and Friauf, 1998; Rautenberg et al., 2009).

In addition to these coarse changes in synaptic location, the fine structure of synapse morphology can be altered (Ford et al., 2009) to allow faster clearance of transmitter from the synaptic cleft (Cathala et al., 2005). This fast clearance can lead to a faster decay of synaptic currents, which is a common effect observed during maturation. Besides structural changes, the acceleration in synaptic kinetics can also be caused by changes in receptor subunit composition (e.g. for NMDA: Cathala et al., 2000; Lopez de Armentia and Sah, 2003, AMPA: Joshi et al., 2004, GABA: Peden et al., 2008, Glycine: Singer et al., 1998). Often observed is a down-

regulation of NMDA receptors which, in some circuits, might only be important for the plastic changes during development, but which are not useful when fast signals are processed (Futai et al., 2001; Franks and Isaacson, 2005). In the MNTB, NMDA receptor mediated current accelerates but is maintained during development (Steinert et al., 2010). However, the contribution of the NMDA component to electrical signaling seems small. Instead, calcium influx through NMDA receptors has been suggested to play a role in nitric oxide signaling (Steinert et al., 2010).

Important for the functioning of inhibitory circuits is the change in chloride reversal potential that occurs in many brain regions during postnatal development (reviews: Ben-Ari, 2002; Blaesse et al., 2009; Friauf et al., 2011). In the first days after birth, the chloride reversal potential is usually positive, leading to depolarizing synaptic events upon release of inhibitory transmitter that can even trigger APs, for example in the LSO (Kullmann and Kandler, 2001). In the LSO, the depolarization was suggested to be important to activate Cav1.3 channels that are crucial for the proper development of the nucleus, synaptic pruning and the hyperpolarizing shift in the chloride reversal potential (Kandler et al., 2009; Hirtz et al., 2011; Hirtz et al., 2012). The mechanism underlying the hyperpolarizing developmental shift is the increased expression and/or localization of the K-Cl transporter KCC2 to the membrane (Balakrishnan et al., 2003). In the adult mammalian auditory system inhibition is hyperpolarizing in all nuclei studied so far (Friauf et al., 2011).

Together with the maturation of synapses, intrinsic membrane properties develop, usually leading to faster membrane time constants and lower input resistance (Kandler and Friauf, 1995; Magnusson et al., 2005; Scott et al., 2005). The AP properties change and often lead to faster spiking neurons during development (Taschenberger and von Gersdorff, 2000; Cathala et al., 2003; Magnusson et al., 2005; Scott et al., 2005; Etherington and Williams, 2011). These changes have partly been described in the rat DNLL, where the membrane time constants of DNLL neurons

accelerate until P18 and neurons are able to follow higher rates (Ahuja and Wu, 2000). Yet, there appear to be some species-specific differences as even juvenile neurons possess very fast time constants compared to gerbils (Ahuja and Wu, 2000; Porres et al., 2011).

In vivo, DNLL neurons of juvenile gerbils at P14 are hardly tuned to ITDs at all and at P15 the response rates are still much lower than in the adult (Seidl and Grothe, 2005). At P31 the mature *in vivo* ITD tuning curves can be observed (Seidl and Grothe, 2005). Yet, little is known about the development of cellular properties of DNLL neurons in gerbils during this period. Moreover, at the start of this thesis no *in vitro* recordings in mature gerbils had been published.

The goal of the first study in this thesis was thus twofold. First, we aimed to describe the physiological development of DNLL neurons to see which cellular parameters are tuned during late postnatal development and are thus important for its physiological function in the mature circuit. This question may be of general interest from a biophysical point of view as DNLL neurons *in vivo* exhibit very fast firing and sustain peak firing rates as high as in the SOC (Pecka et al., 2010) while displaying this very long lasting inhibition (Pecka et al., 2007). What cellular specializations a neuron needs to fulfill these tasks is unclear. Second, our goal was to define a stage at which DNLL neurons are mature to study the cellular mechanisms that underlie PI in the mature animal.

1.4 Integration of synaptic inhibition

In the second study we aimed to understand the role of GABA_A receptor mediated inhibition in the mature DNLL that produces PI.

Inhibition in neuronal circuits fulfills various different functions. It can alter coding properties of neurons by modulating the rate or timing of the spiking output

(Pouille and Scanziani, 2001; Brand et al., 2002; Chance et al., 2002; Mitchell and Silver, 2003; Wehr and Zador, 2003; Vida et al., 2006; Silver, 2010). It can also act as a gate by fully suppressing the propagation of activity (Tsuchitani and Boudreau, 1967; Sanes, 1990; Wehr and Zador, 2005; Kremkow et al., 2010).

In the auditory system inhibition is involved in shaping the response properties at many processing stages (Pollak et al., 2002; Grothe, 2003; Pollak et al., 2003; Trussell, 2012). One special feature of the auditory brainstem which makes it an ideal model system to study inhibition is the organization of its different nuclei. This organization leads to assemblies of inhibitory projection neurons like the DNLL which can be studied more easily than, for instance, interneurons in the cortex that are part of an intricate network.

The inhibition in the DNLL is inhibition in the classical sense: the suppression of action potentials for a certain time upon release of inhibitory transmitter. The question is, what cellular mechanisms cause such a strong and long lasting inhibition, which is at the same time variable in duration depending on sound pressure level.

Generally, effectiveness and duration of inhibition depend on the location of synapses as well as on synaptic and intrinsic properties of the neuron. Inhibition targeting the soma or proximal dendrites is often used towards efficient suppression of the spiking output, whereas dendritic inhibition performs more subtle computations (Miles et al., 1996; Liu, 2004; Wilson, 2007; Lovett-Barron et al., 2012; Chiu et al., 2013).

For the open duration of an inhibitory receptor channel, inhibition exerts a shunting influence on incoming excitation by increasing the conductance of the cell membrane (Fatt and Katz, 1953; Coombs et al., 1955). Apart from inherent receptor properties, activity-dependent processes such as spillover of transmitter (Alger and Nicoll, 1982; Overstreet and Westbrook, 2003; Farrant and Nusser, 2005; Balakrishnan et al., 2009; Tang and Lu, 2012) and asynchronous release (Lu and

Trussell, 2000; Hefft and Jonas, 2005; Best and Regehr, 2009; Tang and Lu, 2012) can slow down the conductance decay at inhibitory synapses. These mechanisms have been proposed to play a role in the prolongation of GABAergic inhibitory postsynaptic currents (IPSCs) in the juvenile gerbil (Saunier-Rebori, 2008; Porres et al., 2011). Spillover describes the process during which transmitter diffuses out of the synaptic cleft and acts on extra-synaptic receptors or even neighboring synapses (Huang, 1998). Late binding of these transmitters then prolongs the decay of synaptic currents. A high concentration in the synaptic cleft can on its own already lead to a delayed clearance and prolonged synaptic decay without spillover (Balakrishnan et al., 2009; Barberis et al., 2011). Asynchronous or delayed release is caused by build-up of calcium during periods of high activity in the presynaptic terminal (Ravin et al., 1997; Zucker, 1999). The increased intracellular calcium decouples the release from single APs so that vesicles may fuse long after the last AP, thereby leading to asynchronous release that can continue for hundreds of milliseconds after an action potential train (Goda and Stevens, 1994; Atluri and Regehr, 1998; Lu and Trussell, 2000; Hefft and Jonas, 2005).

Besides these synaptic mechanisms, filtering through the membrane of the postsynaptic neuron can additionally prolong the inhibitory effect beyond the duration of receptor opening for hyperpolarizing inhibition (Coombs et al., 1955; Eccles, 1961). Active intrinsic conductances can further shape the inhibitory postsynaptic potential (IPSP) and either prolong or curtail the inhibitory effect (Stuart, 1999; Williams and Stuart, 2003; Wilson, 2005; Hardie and Pearce, 2006; Kopp-Scheinflug et al., 2011). Whether the integration of inhibition in the DNLL contributes to the long duration of PI *in vivo* is unknown. Reports about the expression of hyperpolarization-activated nonspecific cationic current (I_h) in the DNLL (Fu et al., 1997; Koch et al., 2004) indicate that IPSPs may rather be shortened by a fast return to rest as seen in other auditory nuclei (Bal and Oertel, 2000;

Koch and Grothe, 2003; Leao et al., 2006; Felix et al., 2011; Kopp-Scheinflug et al., 2011).

In summary, many factors that potentially control the duration of inhibition in the DNLL are unknown. In the second study (section 3) we thus aimed to describe the GABAergic kinetics and test for activity-dependence of the IPSC decay at a developmental stage where *in vivo* activity is fully developed. In addition, we investigated the contribution of postsynaptic integration to PI in DNLL neurons as well as the mechanisms that shape the resulting IPSPs. Finally, we investigated how the IPSPs interact with incoming excitation and which parameters are essential to effectively suppress APs for a duration matching PI *in vivo*.

2 Physiological development of DNLL neurons

Contributions

Julian Ammer (J.J.A.), Benedikt Grothe (B.G.), and Felix Felmy (F.F.) conception and design of research; J.J.A. and F.F. performed experiments; J.J.A. and F.F. analyzed data; J.J.A., B.G., and F.F. interpreted results of experiments; J.J.A. and F.F. prepared figures; J.J.A. and F.F. drafted manuscript; J.J.A., B.G., and F.F. edited and revised manuscript; J.J.A., B.G., and F.F. approved final version of manuscript.

The manuscript was published in the *Journal of Neurophysiology* (Ammer et al., 2012). The American Physiological Society permits whole published articles to be reproduced without charge in dissertations and posted to thesis repositories. Full citation is required.

Late postnatal development of intrinsic and synaptic properties promotes fast and precise signaling in the dorsal nucleus of the lateral lemniscus

J. J. Ammer, B. Grothe, and F. Felmy

Division of Neurobiology, Department of Biology II, Ludwig-Maximilians University Munich, Martinsried, Germany

Submitted 23 June 2011; accepted in final form 24 November 2011

Ammer JJ, Grothe B, Felmy F. Late postnatal development of intrinsic and synaptic properties promotes fast and precise signaling in the dorsal nucleus of the lateral lemniscus. *J Neurophysiol* 107: 1172–1185, 2012. First published November 30, 2011; doi:10.1152/jn.00585.2011.—The dorsal nucleus of the lateral lemniscus (DNLL) is an auditory brain stem structure that generates a long-lasting GABAergic output, which is important for binaural processing. Despite its importance in binaural processing, little is known about the cellular physiology and the synaptic input kinetics of DNLL neurons. To assess the relevant physiological parameters of DNLL neurons, their late postnatal developmental profile was analyzed in acute brain slices of 9- to 26-day-old Mongolian gerbils. The observed developmental changes in passive membrane and action potential (AP) properties all point toward an improvement of fast and precise signal integration in these neurons. Accordingly, synaptic glutamatergic and GABAergic current kinetics accelerate with age. The changes in intrinsic and synaptic properties contribute nearly equally to reduce the latency and jitter in AP generation and thus enhance the temporal precision of DNLL neurons. Furthermore, the size of the synaptic NMDA current is developmentally downregulated. Despite this developmental reduction, DNLL neurons display an NMDA-dependent postsynaptic amplification of AP generation, known to support high firing rates, throughout this developmental period. Taken together, our findings indicate that during late postnatal development DNLL neurons are optimized for high firing rates with high temporal precision.

binaural processing; passive membrane properties; action potential properties; input-output function; synaptic inputs

THE DORSAL NUCLEUS of the lateral lemniscus (DNLL) lies within the fibers of the lateral lemniscus (LL) ventral to the inferior colliculus (IC; Fig. 1A). The DNLL contains mainly GABAergic neurons (Adams and Mugnaini 1984; Roberts and Ribak 1987; Saint Marie et al. 1997; Vater et al. 1997; Winer et al. 1995) of heterogeneous morphology (Bajo et al. 1993; Iwahori 1986; Kane and Barone 1980; Wu and Kelly 1995). Despite this heterogeneity, these neurons stain almost homogeneously for parvalbumin (PV) in guinea pig (Caicedo et al. 1996), rabbit (Kuwada et al. 2006), rat (Lohmann and Friauf 1996), and bat (Vater and Braun 1994). DNLL neurons receive ascending excitatory inputs from neurons of the ipsilateral medial superior olive (MSO) (Glendenning et al. 1981; Kelly et al. 2009; Oliver 2000; Shneiderman et al. 1988; Siveke et al. 2006) and from the contralateral lateral superior olive (LSO) (Oliver 2000). A strong reciprocal connection between the bilateral DNLL nuclei exists through the commissure of Probst (Glendenning et al. 1981; Kelly et al. 2009; Oliver and Shneiderman

1989; Shneiderman et al. 1988). Thus the GABAergic output that DNLL neurons generate is at the same time equivalent to one of their major inputs. Besides this reciprocal GABAergic connection, the DNLL projects bilaterally to the IC (Adams 1979; Bajo et al. 1993; Gonzalez-Hernandez et al. 1996; Shneiderman et al. 1988).

In accordance with the circuit's anatomy, DNLL neurons process binaural sound information (Brugge et al. 1970; Burger and Pollak 2001; Kelly et al. 1998; Kuwada et al. 2006; Markovitz and Pollak 1994; Meffin and Grothe 2009; Pecka et al. 2007, 2010; Seidl and Grothe 2005; Siveke et al. 2006; Yang and Pollak 1994). At the level of the DNLL the binaural information has become more robust compared with the MSO (Pecka et al. 2010). The temporal precision in response to sound stimulation, judged by the vector strength, is high in DNLL neurons (Seidl and Grothe 2005; Siveke et al. 2006) and apparently maintained compared with superior olivary complex (SOC) neurons (Brand et al. 2002; Pecka et al. 2008; Smith et al. 1998; Tollin and Yin 2005; Yin and Chan 1990). The physiology of the DNLL is suited to suppress the information of bilateral spurious cues (Meffin and Grothe 2009) and is thought to account for the suppression of sound information during reverberations (Burger and Pollak 2001; Pecka et al. 2007). These features are related to the physiological hallmark of the DNLL, the long-lasting persistent inhibition provided to the contralateral counterpart and the IC (Burger and Pollak 2001; Faingold et al. 1993; Pecka et al. 2007; Yang and Pollak 1994). On the behavioral level, this GABAergic inhibition might underlie the precedence effect. This perceptual phenomenon (Blauert 1997; Litovsky et al. 1999; Zurek 1987) describes the suppression of the ability to localize echoes.

Besides the importance of the GABAergic inputs, the properties of the excitatory inputs are crucial for defining the DNLL's output signal. In these neurons postsynaptic integration of excitatory inputs leads to faithful high-frequency firing, sometimes with a small number of additional action potentials (APs) trailing the stimulation (Porres et al. 2011). The fidelity of generating APs at high rates depends also on the synaptic NMDA component. In turn, the duration of the GABAergic output signal correlates with both the number and the rate of generated APs (Porres et al. 2011). This correlation suggests that in DNLL neurons a synergy between the excitatory integration and the GABAergic release exists, which adjusts the time course of the GABAergic output signal to the physiologically required duration.

Other cellular parameters that define the physiological properties of DNLL neurons have been partially described in juvenile gerbils (Porres et al. 2011) and in more mature rats (Ahuja and Wu 2000; Wu and Kelly 1995). There exist

Address for reprint requests and other correspondence: F. Felmy, Div. of Neurobiology, Dept. of Biology II, Ludwig-Maximilians Univ. Munich, Großhadernerstr. 2, D-82152 Martinsried, Germany (e-mail: felmy@zi.biologie.uni-muenchen.de).

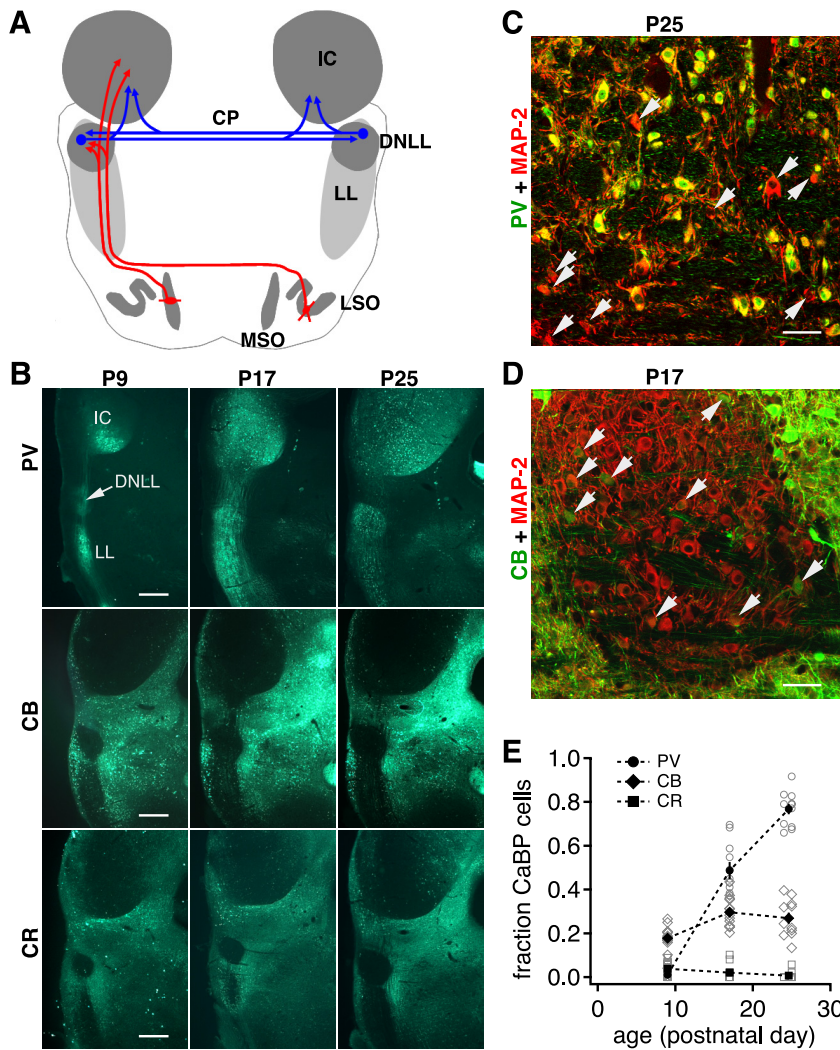


Fig. 1. Developmental profile of the expression of calcium binding proteins (CaBPs). *A*: schematic drawing of the neuronal circuit of the dorsal nucleus of the lateral lemniscus (DNLL). IC, inferior colliculus; MSO, medial superior olive; LSO, lateral superior olive; LL, lateral lemniscus; CP, commissure of Probst. GABAergic connections in blue, glutamatergic projections in red. *B*: overview of the developmental changes of CaBP expression in the DNLL. CR, calretinin; CB, calbindin; PV, parvalbumin; P, postnatal day. Scale bar, 500 μm . *C*: overlaid image of confocal scans of a P25 slice stained for PV and microtubule-associated protein (MAP)-2. Arrows indicate cells that were regarded as PV negative. Colors as indicated; scale bar, 50 μm . *D*: same as *C* but for a P17 slice stained for CB and MAP-2. Arrows indicate cells that were judged as CB positive. *E*: the fraction of cells that express specific CaBPs changed during late postnatal development. Open symbols correspond to a single quantified DNLL section ($n = 11\text{--}15$ sections from 3 or 4 animals; squares, CR; diamonds, CB; circles, PV); filled symbols represent average values.

substantial species-specific differences in some passive membrane properties. In rats the membrane time constant (τ_m) is approximately fourfold and the input resistance (R_{in}) approximately twofold smaller compared with gerbils. Despite these differences, the resting potential and the firing behavior of DNLL neurons are similar (Ahuja and Wu 2000; Porres et al. 2011; Wu and Kelly 1995). In general, the APs are brief as in other auditory brain stem areas, and almost all cells respond with sustained firing during long-lasting current injections.

During development the progressive change of a given cellular parameter carves out its most important features. Thus investigating the late postnatal development of intrinsic and synaptic properties reveals the functionally most relevant parameters of the neurons studied. For DNLL neurons the most important cellular parameters are those that define the firing precision and integration properties, especially as these neurons fire with high temporal fidelity at high rates (Brugge et al. 1970; Kuwada et al. 2006; Pecka et al. 2010; Seidl and Grothe 2005; Siveke et al. 2006) and, at the same time, integrate inhibition over several milliseconds (Burger and Pollak 2001; Pecka et al. 2007; Yang and Pollak 1994).

MATERIALS AND METHODS

Slice preparation. All experiments complied with institutional guidelines and national and regional laws. Animal protocols were reviewed and approved by the Regierung of Oberbayern according to the Deutsches Tierschutzgesetz for the AZ 55.2-1-54.2531.8-211-10. Slices were prepared from Mongolian gerbils (*Meriones unguiculatus*) at postnatal days (P) 9–26. Animals were decapitated, brains were removed in dissection solution containing (in mM) 50 sucrose, 25 NaCl, 25 NaHCO_3 , 2.5 KCl, 1.25 NaH_2PO_4 , 3 MgCl_2 , 0.1 CaCl_2 , 25 glucose, 0.4 ascorbic acid, 3 *myo*-inositol, and 2 Na-pyruvate (pH 7.4 when bubbled with 95% O_2 and 5% CO_2), and 200- μm -thick transverse slices containing the DNLL were taken with a VT1200S vibratome (Leica, Wetzlar, Germany). Slices were incubated in extracellular recording solution (same as dissection solution but with 125 mM NaCl, no sucrose, 2 mM CaCl_2 , and 1 mM MgCl_2) at 36°C for 45 min, bubbled with 5% CO_2 and 95% O_2 .

Electrophysiology. After incubation slices were transferred to a recording chamber attached to a microscope (BX50WI, Olympus, Hamburg, Germany) equipped with gradient contrast illumination (Luigs and Neumann, Ratingen, Germany) and continuously perfused with extracellular solution. All recordings were carried out at near-physiological temperature (34–36°C). Cells were visualized and imaged with a TILL Photonics system (Gräfelfing, Germany) composed of an Imago CCD camera, a Poly-IV monochromator, and its control unit. Voltage- and current-clamp recordings were performed with an EPC10/2 amplifier (HEKA Elektronik, Lambrecht, Germany). For

voltage-clamp recordings access resistance was compensated to a residual of 3 M Ω of its initial value; data were acquired at 20–40 kHz and filtered at 3 kHz. In current-clamp mode the bridge balance was set to 100% after estimation of the access resistance. For whole cell voltage-clamp recordings an internal solution consisting of (in mM) 105 Cs-gluconate, 26.7 CsCl, 10 HEPES, 20 TEA-Cl, 5 Cs-EGTA, 3.3 MgCl₂, 2 Na₂-ATP, 0.3 Na₂-GTP, 3 Na₂-phosphocreatine, and 5 QX-314 (pH 7.2) was used. For whole cell current-clamp recordings the internal recording solution consisted of (in mM) 145 K-gluconate, 5 KCl, 15 HEPES, 2 Mg-ATP, 2 K-ATP, 0.3 Na₂-GTP, 7.5 Na₂-phosphocreatine, and 5 K-EGTA (pH 7.2).

Synaptic inputs were stimulated with a concentric bipolar electrode (MCE-100X, Scientific Products) that was placed in the fiber tracts of the LL or the commissure of Probst (Fig. 1A). The stimulation was triggered by the EPC10/2 and conveyed with a stimulator unit (model 2100, A-M Systems, Scientific Products) that allowed manual adjustment of the stimulation strength. Stimulations were applied as a biphasic voltage deflection of 200- μ s total duration. Synaptic currents were pharmacologically isolated. GABAergic inputs were isolated with 0.5 μ M strychnine, 20 μ M DNQX, and either 50 μ M D-AP5 or 10 μ M R-CPP. Excitatory inputs were isolated in the presence of 0.5 μ M strychnine and 10 μ M SR95531, and in some cases to isolate the AMPA receptor-mediated component either 50 μ M D-AP5 or 10 μ M R-CPP was added additionally.

Immunohistochemistry and confocal microscopy. Immunohistochemistry was carried out in tissue from animals between P10 and P25. The animals were anesthetized (0.5% chloral hydrate, 0.2 ml/10 g body wt) and perfused with phosphate-buffered saline (PBS) containing 0.1% heparin and 155 mM NaCl for ~5 min before the perfusion was switched to 4% paraformaldehyde. After 20-min perfusion the brains were removed and postfixed overnight. Brains were washed twice in PBS, and brain slices of 40- to 60- μ m thickness were taken with a VT1000S vibratome (Leica). Standard immunohistochemistry procedures were carried out to stain free-floating slices with primary antibodies (Abs) for calretinin (CR; monoclonal anti-mouse Ab, clone 6B3 or polyclonal anti-rabbit Ab, catalog no. 7699/3H, Swant, Bellinzona, Switzerland), calbindin (CB; polyclonal anti-rabbit Ab, catalog no. CB38a, Swant), PV (polyclonal anti-rabbit Ab, catalog no. PV 28, Swant), and microtubule-associated protein 2 (MAP-2; polyclonal anti-chicken Ab, catalog no. CH22103, Neuromics, Acris Antibodies, Hildesheim, Germany). Secondary Abs were applied the following day for 2 h at room temperature. These were conjugated with Alexa 488 (Molecular Probes, Invitrogen, Karlsruhe, Germany), or Cy3 (Dianova, Hamburg, Germany). Slices were mounted in Vectashield medium (H-100, Vector Laboratories, AXXORA, Lörach, Germany), and confocal scans were taken with a Leica SP System. Images were acquired with a \times 25 objective (0.75 NA), leading to a pixel size of 0.781 nm².

Data and statistical analysis. Electrophysiological data were analyzed with IGOR Pro (WaveMetrics, Lake Oswego, OR) and Microsoft Excel. Spontaneous postsynaptic currents were extracted by a custom-written template matching routine (Couchman et al. 2010). The weighted decay time constant was derived from a biexponential function fit to the data and calculated according to $\tau_w = \tau_1 \cdot \text{amplitude}(\tau_1) / \text{amplitude}(\tau_1) + \tau_2 \cdot \text{amplitude}(\tau_2) / \text{amplitude}(\tau_2)$. Immunocytochemistry was quantified as described previously (Felmy and Schlegelburger 2004). In brief, each positively stained cell in each fluorescence channel was marked in Adobe Photoshop and counted. Results are presented as means \pm SE. Significance was determined with either paired or unpaired Student's *t*-test in Excel or, for more than two groups of samples, with a one-way ANOVA test followed by a multiple-comparison Tukey-Kramer test in IGOR Pro. Linear regression analysis was performed with a Tukey-type test on multiple regressions in IGOR Pro. The significance level was set to $P < 0.05$ for all cases.

RESULTS

The goal of this study was to comprehensively describe the functional late postnatal development of DNLL neurons. During the developmental period from P9 to P26 gerbils transform from nonhearing to nearly mature hearing animals, with hearing onset around P12 (Finck et al. 1972; Ryan et al. 1982a; Smith and Kraus 1987). We investigated the expression of calcium binding proteins (CaBPs) during maturation to evaluate the neuronal heterogeneity and then characterized the development of the intrinsic properties and the synaptic inputs of DNLL neurons. This investigation was complemented by estimating the impact of the observed developmental changes in intrinsic and synaptic properties on the precision of AP generation and the translation of excitatory synaptic charge into APs in DNLL neurons at different developmental stages.

Development of calcium binding proteins. The profile of CaBP expression changes during late postnatal development in many mammalian auditory brain stem nuclei (Felmy and Schlegelburger 2004; Lohmann and Friauf 1996). To describe the developmental expression profile of CaBPs in the DNLL, overview images (Fig. 1B) were complemented by analyzing confocal images of the center of this nucleus. Single confocal sections were used to count the MAP-2-positive cells as reference and the number of cells coexpressing a specific CaBP (Fig. 1, C–E). PV expression was developmentally regulated and was found in the neuropil and the cellular structures of the DNLL (Fig. 1B). PV staining of cells of different shape colocalized with MAP-2 expression (Fig. 1C). The fraction of PV-expressing cells increased from near absence in P9 to 0.76 ± 0.02 in P25 animals (Fig. 1E). CB expression appeared nearly absent in overview images (Fig. 1B). However, several cells of different shapes marked positive for CB in all sections (Fig. 1D). The percentage of cells expressing CB was ~25% and showed only a modest change during late postnatal development (0.17 ± 0.01 in P9 to 0.26 ± 0.02 in P25). CR expression was largely absent at all ages tested (Fig. 1B), with a negligible fraction of positively stained neurons (Fig. 1E). Thus, similar to rats (Lohmann and Friauf 1996), the DNLL of gerbils shows a mixed PV and CB expression pattern throughout late postnatal development. It might therefore be expected to encounter two distinct cellular behaviors in DNLL neurons segregated according to the relative CaBP expression pattern.

Development of passive membrane properties. The passive membrane properties of neurons such as resting membrane potential (E_{rest}), τ_m , R_{in} , and cell capacitance (C_m) influence the integration of synaptic inputs and hence adjust the neuronal input-output function.

To describe the development of these parameters in DNLL neurons of gerbils, four age groups were investigated (P9/10, P13, P17, and P23–26). Experimentally, these parameters can be estimated from a small voltage deflection close to the resting potential imposed by small hyperpolarizing current injections (5–10 pA, 500 ms, at least 50 repetitions per cell; Fig. 2A). E_{rest} did not change significantly during the developmental period investigated (Fig. 2B; P9/10: -58.7 ± 1.2 mV; P13: -59.5 ± 1.4 mV; P17: -60.8 ± 1.7 mV; P23–26: -59.8 ± 0.9 mV; ANOVA, $P > 0.05$). Exponential functions were fitted to the onset and offset of the voltage response, and for each cell an average value of τ_m was calculated. The population average of τ_m became significantly shorter during late postnatal develop-

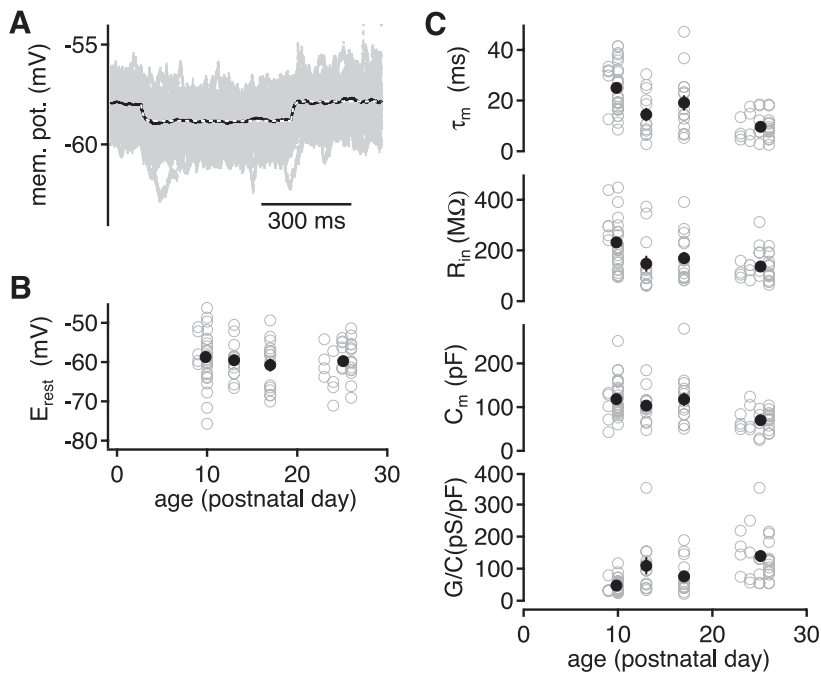


Fig. 2. Passive membrane properties indicate a developmental decrease in the integration time window. *A*: voltage response of a P24 DNLL neuron to a -5 pA current step of 500 ms. The 50 single-trial voltage responses are shown in gray and the average in black. A single-exponential function was fitted to the onset and offset of the average voltage response (white dashed lines). *B*: resting potential (E_{rest}) of the DNLL neurons as a function of age. E_{rest} was measured as the average membrane potential before the onset of the hyperpolarizing current injection, as shown in *A*. Open symbols represent single cells (P9/10: $n = 31$, P13: $n = 12$, P17: $n = 15$, P23–26: $n = 29$); filled symbols represent the averages of the 4 age groups. *C*: passive membrane properties given as a function of age. *Top*: membrane time constant (τ_m) taken from the exponential fits shown in *A*. *Upper middle*: input resistance (R_{in}) calculated from the steady-state voltage deflection in *A* and the applied current amplitude. *Lower middle*: membrane capacitance (C_m) calculated from τ_m and R_{in} . *Bottom*: calculated leak conductances of each neuron ($G = 1/R_{in}$) normalized with the corresponding C_m . Symbols as in *B*.

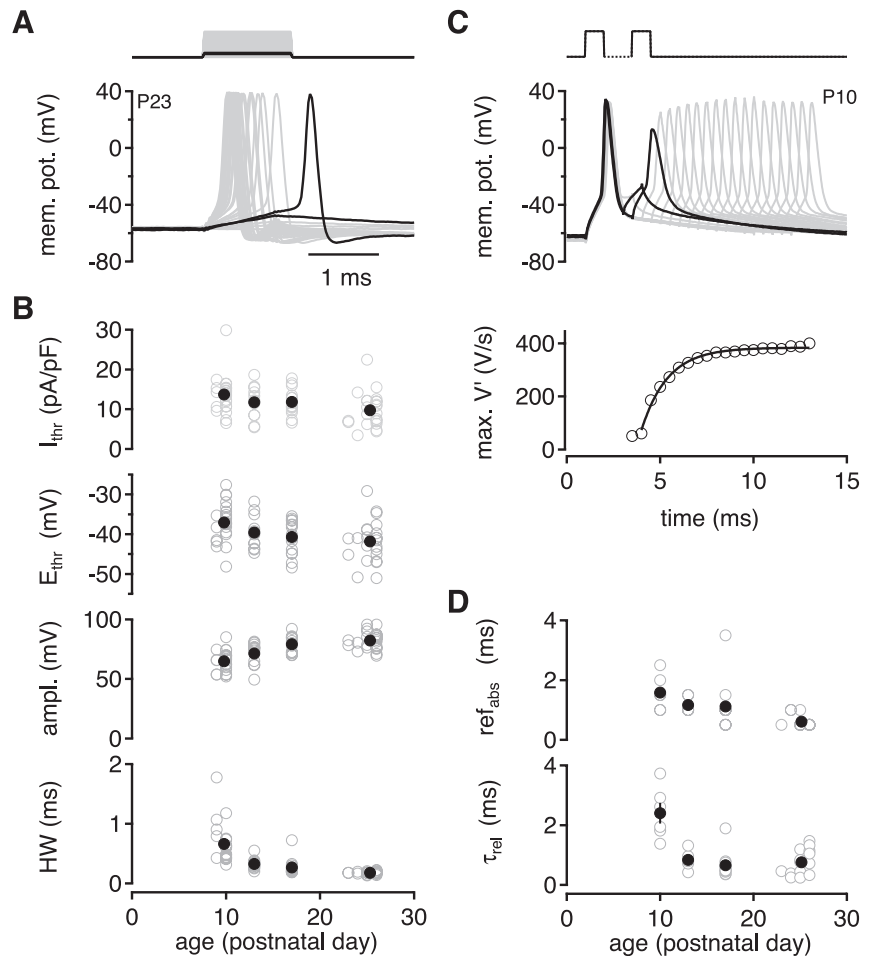
ment (Fig. 2C; P9/10: 25.0 ± 1.7 ms; P13: 14.5 ± 2.6 ms; P17: 19.1 ± 3.0 ms; P23–26: 9.6 ± 0.9 ms; Tukey-Kramer P9/10 vs. P23–26: $P < 0.05$). During the same developmental period R_{in} decreased 1.7-fold (P9/10: 231 ± 20 M Ω ; P13: 148 ± 31 M Ω ; P17: 170 ± 24 M Ω ; P23–26: 137 ± 10 M Ω ; Tukey-Kramer P9/10 vs. P23–26: $P < 0.05$). The effective cell size, C_m , is proportional to τ_m/R_{in} and decreased significantly during development (Fig. 2C; P9/10: 118 ± 8 pF; P13: 104 ± 11 pF; P17: 118 ± 15 pF; P23–26: 70 ± 4 pF; Tukey-Kramer P9/10 vs. P23–26: $P < 0.05$). This reduction in apparent cell size led to further analysis of the specific leak conductance (the inverse of R_{in} , normalized with C_m). The specific leak conductance showed that the membrane of DNLL neurons became significantly leakier during this developmental period (Fig. 2C; P9/10: 47 ± 4 pS/pF; P13: 108 ± 26 pS/pF; P17: 76 ± 15 pS/pF; P23–26: 140 ± 16 pS/pF; Tukey-Kramer P9/10 vs. P23–26: $P < 0.05$). Therefore, the changes in estimated cell size and specific leak conductance lead to smaller membrane time constants, allowing for a temporally more precise synaptic integration. Note that, consistent with earlier reports (Porres et al. 2011), the variability between cells even in a single age group was substantial. However, for no age group was a segregation of the data into two distinct subclasses, as might be expected from the relative CaBP expression patterns, observed.

Development of action potential and firing properties. Besides the basic membrane properties that influence the integration time course, the properties of AP generation and firing behavior are important determinants describing the excitability and the output pattern of a neuron. APs were elicited with a 1-ms current injection ranging from 0 to 2.5 nA incremented in 100-pA steps (Fig. 3A). From the first suprathreshold trial the values of the current and voltage threshold and the AP amplitude and half-width were extracted (Fig. 3B). During the late postnatal development the current threshold (I_{thr}) of the AP normalized to cell size decreased significantly (Tukey-Kramer P23–26 vs. P9/10, P13, P17: $P < 0.05$) from 13.7 ± 1 pA/pF in P9/10 animals to 9.7 ± 0.9 pA/pF in P23–26 animals. The

voltage threshold (E_{thr}) of AP generation between P9/10 and P23–26 decreased significantly from -37.0 ± 1.0 mV at P9/10 to -41.8 ± 1.0 mV at P23–26 (Tukey-Kramer P9/10 vs. P23–26: $P < 0.05$). The AP height was defined as the voltage difference from E_{thr} to the peak of the AP and increased significantly with age (Tukey-Kramer P23–26 vs. P9/10, P13: $P < 0.05$), reaching a deflection of 82.2 ± 1.5 mV in the most mature animals. The same significant change was observed when AP height was determined from rest and is opposite to findings in the MSO, where somatic AP height decreases during development (Scott et al. 2005). A major developmental alteration occurred in the AP duration measured as AP half-width. The AP half-width decreased almost fourfold from 663 ± 67 μ s in P9/10 to 177 ± 5 μ s in P23–26 (Tukey-Kramer P23–26 vs. P9/10, P13: $P < 0.05$). It should be noted that, apart from the AP half-width in mature animals, all parameters related to AP generation showed a large cell-to-cell variability even within a single age group, without segregating into two distinct subclasses.

An important property of cells in the auditory brain stem pathways is how rapidly two APs can be generated in succession, or how long the refractory period after a single AP lasts. To estimate the refractory period, two current injections of 1 ms were delivered with interstimulus intervals ranging from 0.5 to 10 ms and incremented in 0.5-ms steps (Fig. 3C). The amplitude of the current injection was set to 300 pA above I_{thr} to ensure reliable generation of an AP with the control current injection. The absolute refractory period (ref_{abs}) was defined as the time window when no AP was generated upon the second current injection. The relative refractory period (τ_{rel}) was defined as the time constant of the recovery of the maximal AP velocity ($max V'$). To quantify τ_{rel} , a single-exponential function was fitted to the average of the $max V'$ values of each cell (Fig. 3C). During late postnatal development the ref_{abs} decreased significantly from 1.58 ± 0.24 ms in P9/10 animals (Tukey-Kramer P23–26 vs. P9/10: $P < 0.05$) to 0.61 ± 0.05 ms in P23–26 animals (Fig. 3D). An equally significant reduc-

Fig. 3. Neuronal excitability increases during late postnatal development. **A:** sub- and suprathreshold voltage responses were evoked by a short current pulse (1 ms, between 0 and 2.5 nA in 100-pA increments). The example shows recordings of a P23 neuron. The last subthreshold trial and the first suprathreshold trial are shown in black. The first action potential (AP) evoked with the lowest current injection was used for further analysis shown in **B**. **B:** development profile of AP thresholds and waveform. Open circles are single cells (P9/10: $n = 25$, P13: $n = 12$, P17: $n = 15$, P23–26: $n = 25$); filled circles are averages of the 4 age groups. Current threshold (I_{thr} , normalized to membrane capacitance; *top*) and voltage threshold (E_{thr} ; *upper middle*) were extracted from trials of the first suprathreshold response. AP amplitude (*lower middle*) reflects voltage difference from E_{thr} to AP peak. AP half-width (HW; *bottom*) was measured at half the AP amplitude from AP threshold. **C:** refractory period of AP generation was probed with a paired-pulse paradigm of 1-ms current injections adjusted to 300 pA above I_{thr} and the interspike interval incremented with 0.5 ms between 0.5-ms and 10-ms interspike intervals (ISIs; *top*). The last trial that evoked no second AP and the first that triggered an AP with both pulses are shown in black. AP refractory period was analyzed from the peak of the first derivative of the voltage responses shown in **A** ($\max V'$; *bottom*). The interspike interval of the first dual AP response was taken as the absolute refractory period (see **D**). The relative refractory period was determined by fitting a single-exponential function to $\max V'$ values starting from the last pulse that evoked no AP. **D:** AP refractory properties during the late postnatal development. *Top:* absolute refractory period (ref_{abs}). *Bottom:* relative refractory period (τ_{rel}) as a function of postnatal day. Open circles represent single cells (P9/10: $n = 6$, P13: $n = 6$, P17: $n = 13$, P23–26: $n = 14$); filled circles are averages of the 4 age groups.



tion (Tukey-Kramer P23–26 vs. P9/10: $P < 0.05$) was observed for τ_{rel} (Fig. 3D). The shorter refractory periods indicate that mature DNLL neurons are capable of firing higher rates of APs compared with immature neurons.

To investigate whether mature DNLL neurons sustain higher firing rates for prolonged periods, firing properties were investigated by analyzing the firing frequency and adaptation to a 500-ms step current injection with increasing intensity (–50 to 800 pA, 50-pA increments; Fig. 4A). Irrespective of age, all neurons showed sustained AP firing. However, the AP frequency increased about threefold from P9/10 to P23–26 at an injected current of 600 pA (Fig. 4B). In addition, the maximal firing frequency was computed for each neuron from the response to the 500-ms current injection that yielded the highest AP count. In accordance with the developmental decrease of the refractory period, this maximal firing rate increased about fourfold from P9/10 (78 ± 5 Hz) to P23–26 (212 ± 15 ; Tukey-Kramer P23–26 vs. P9/10, P13, P17: $P < 0.05$; Fig. 4C). As in the MSO (Scott et al. 2005) and the nucleus laminaris (Gao and Lu 2008), the current threshold to long steps normalized to the cell's size increased significantly during late postnatal development (Fig. 4C; P9/10: 1.2 ± 0.1 pA/pF; P23–26: 2.5 ± 0.3 pA/pF; Tukey-Kramer P23–26 vs. P9/10: $P < 0.05$). This apparent discrepancy to short current injections (Fig. 3B) can be explained by the interplay between the different pulse lengths and the developmental alterations in the membrane time constant (Fig. 2C). Short current pulses are

not sufficiently long to charge the membrane to equilibrium (Couchman et al. 2010). Compared with DNLL neurons in younger animals, P23–26 DNLL neurons with smaller τ_m will charge faster and get closer to the equilibrium of the membrane potential during a 1-ms current injection. Therefore, to depolarize the membrane potential to E_{thr} more current is needed in DNLL neurons of younger gerbils during short current injections compared with P23–26 neurons. The situation is different when longer pulses have enough time to charge the membrane potential to the equilibrium level (Fig. 4C). In this case the R_{in} determines the degree of depolarization. In accordance with the decreased R_{in} in P23–26 animals, these neurons display the highest current threshold for long pulses compared with other age groups.

Next, the AP frequency adaptation was analyzed for all cells by extracting the interspike intervals (ISIs) at each neuron's individual half-maximal frequency. Plotting these ISIs against their corresponding number (Fig. 4D) revealed that—in contrast to neurons from young animals—nearly no AP frequency adaptation existed at mature stages. Averaging the different age groups over the first 15 ISIs showed a clear developmental reduction in adaptation indicated by shallower slopes in Fig. 4D, *inset*. Furthermore, an increase in the number of neurons with a “pauser” firing behavior was found from P17 on. This increase was evident as a prolonged initial ISI in P17 but was mainly found in P23–26 data (Fig. 4D, *inset*). This prolonged initial ISI in older animals indicates the increased expression of

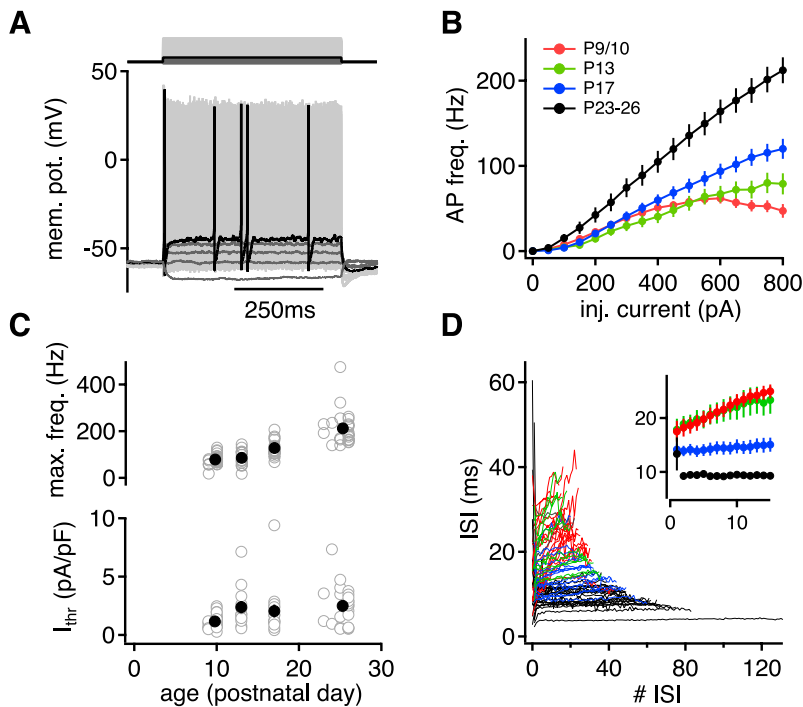


Fig. 4. AP frequency increases during late postnatal development. *A*: input-output functions were generated by current injections of 500-ms step ranging from -50 to 800 pA in 50 -pA increments. Example traces of a P24 neuron show subthreshold responses in dark gray and the first suprathreshold response in black. *B*: average input-output function for all 4 age groups (P9/10: $n = 24$, P13: $n = 12$, P17: $n = 15$; P23–26: $n = 23$). *C*: maximal firing frequency (*top*) for all individual neurons (open) and averages for each age group (filled). The input-output function (*B*) and the maximal frequency (*C*) were computed from the spike count over the whole 500-ms duration of the current injection. I_{thr} (*bottom*) represents the average current amplitude needed to evoke an AP with the protocol described in *A* normalized to the individual cell's membrane capacitance. *D*: duration of the ISI in milliseconds vs. number of the respective ISI for all cells at their individual half-maximal firing frequencies. *Inset*: pooled data for each age group for the first 15 ISIs. The different slopes indicate stronger adaptation in younger animals. Red, P9/10; green, P13; blue, P17; black, P23–26.

a fast transient potassium current during development. Taken together, our recordings suggest that developmental alterations in membrane properties and channel expressions produce DNLL neurons that are capable of precise AP firing at high rates.

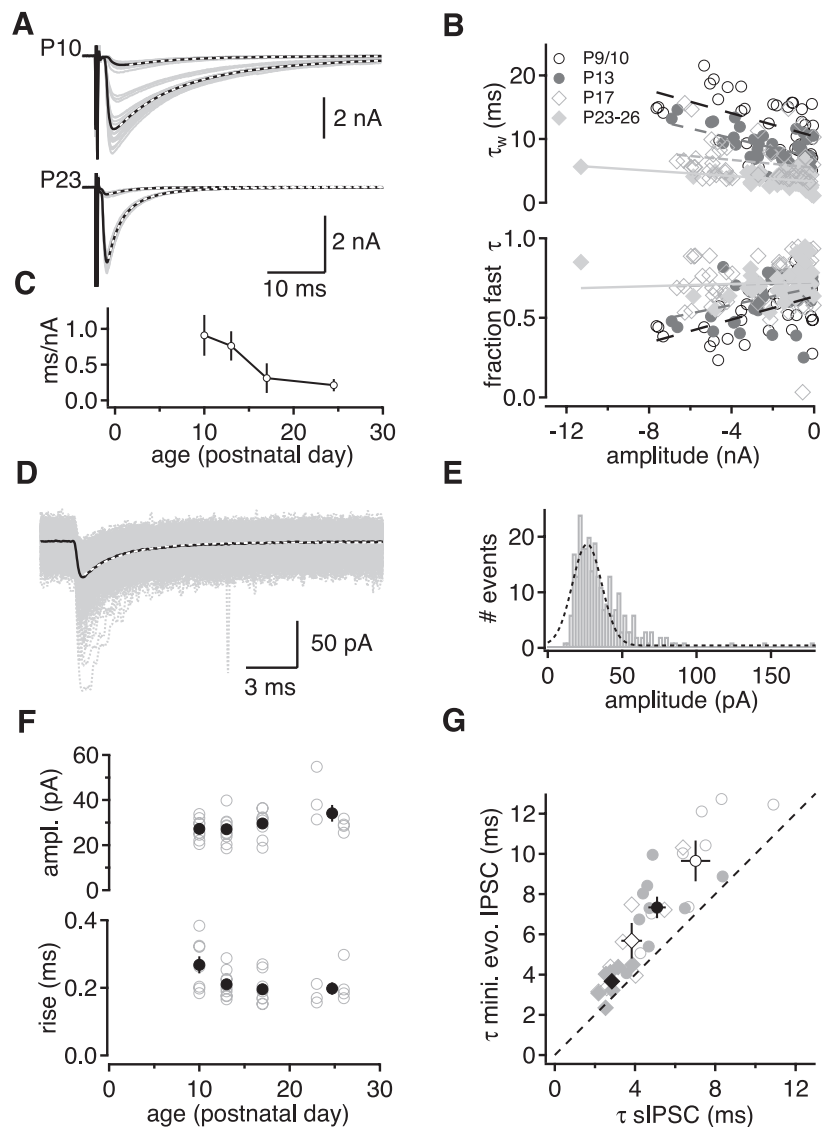
Development of GABAergic inputs to DNLL neurons. To analyze the properties of the GABAergic input, pharmacologically isolated GABAergic inhibitory postsynaptic currents (IPSCs) were evoked via the commissure of Probst with a single fiber shock at different intensities (Fig. 5*A*). For each stimulation intensity 10 trials were recorded to generate an average IPSC (Fig. 5*A*). From these average IPSCs the peak current and the decay time constant were determined. As the decay of these IPSCs was best fitted with a biexponential function, a weighted decay time constant was calculated. The initial observation was that during development the decay of the GABAergic IPSCs became significantly faster (Tukey-type test for elevations P23–26 vs. P9/10, P13, P17: $P < 0.05$; Fig. 5*B*). The developmental reduction of the decay time constant was partially dependent on an increase of the fast fraction of the decay time constant (Fig. 5*B*). A second important finding was that the decay time constants depended on the peak amplitude of the respective IPSCs (Fig. 5*B*). Large IPSCs tended to have a smaller fraction of the fast decay time constant and hence were more dominated by the slow decay kinetics of the GABAergic current. The dependence between the time course of the IPSC and its amplitude suggests a postsynaptic interaction of liberated neurotransmitter such as transmitter pooling or spillover (Balakrishnan et al. 2009; Farrant and Nusser 2005). Furthermore, the relationship between the weighted decay time constant and the IPSC amplitude appeared developmentally regulated (Fig. 5*B*). The slopes of these linear regressions decreased during development (Fig. 5*C*). Thus the time course of the IPSC shows less amplitude dependence in older animals compared with young animals,

indicative of a reduction of a possible postsynaptic contribution to the IPSC time course.

To estimate the minimal kinetics of the GABAergic inputs, spontaneous IPSCs (sIPSCs) were recorded in the same cells as the evoked IPSC. An average sIPSC was generated from all extracted sIPSCs of a given cell and fitted with a single-exponential function for later analysis (Fig. 5*D*). For all detected sIPSC events of a given cell a frequency histogram of the peak sIPSC amplitudes was generated and fitted with a Gaussian function to determine the mean of the sampled sIPSCs (Fig. 5*E*). The extracted sIPSC amplitude is considered to correspond closely to the quantal size of these inputs. During development the mean peak amplitude of the GABAergic sIPSCs became slightly larger, from 27.2 ± 1.7 pA in P9/10 animals to 34.1 ± 3.7 pA in P23–26 animals (Fig. 5*F*). The 20–80% rise time of the average GABAergic sIPSC indicated a slight reduction from P9/10 (0.27 ± 0.03 ms) to P23–26 (0.20 ± 0.02 ms) that, however, remained insignificant (Fig. 5*F*). In contrast, the decay time constants of the averaged GABAergic sIPSCs were reduced significantly during the late postnatal development (Fig. 5*G*). Thus the kinetics of both the evoked IPSCs and the sIPSCs become faster during development.

Next, we asked whether the developmental refinement of the time course of the evoked release can be explained by the developmental changes in sIPSC kinetics. Therefore, the time constants derived from the smallest evoked IPSCs were plotted as a function of the cell's sIPSC decay time constants (Fig. 5*G*). The size of the smallest evoked responses was not significantly different for the tested age groups (-527 ± 260 pA for P9/10 and -301 ± 81 pA for P23–26 animals). The decays of the evoked events were slower than those of the spontaneous events for all age groups (paired t -test $P < 0.05$), yet their relative difference remained constant for each age group during development and the variance of the rise time of

Fig. 5. GABAergic inputs to DNLL neurons accelerate during development. *A*: GABAergic inhibitory postsynaptic currents (IPSCs) evoked with different stimulation intensities for a P10 (*top*) and a P23 (*bottom*) neuron. Averages of 10 traces at a given stimulation intensity are shown in black and single trials in gray. The decay of the IPSCs was fitted with a biexponential function (white dotted line). *B*: the relation between decay time course and amplitude of GABAergic currents changed during development. *Top*: weighted decay time constants (τ_w) as a function of IPSC amplitude. *Bottom*: effect of IPSC amplitude on the fraction of the fast decay time constant for all different age groups. Lines represent linear regressions (P9/10: 36 IPSCs from 9 cells; P13: 40 IPSCs from 10 cells; P17: 48 IPSCs from 10 cells; P23–26: 40 IPSCs from 10 cells). *C*: averages of the slopes of linear regressions in *B* are plotted as a function of age. *D*: spontaneous IPSCs (sIPSCs) recorded in a neuron from a P26 animal. The average sIPSC (black trace) was used to calculate the 20–80% rise time (*F*) and to determine the decay time constant from a fit of an exponential function (white dotted line) (*G*). *E*: the histogram of sIPSC amplitudes from the same neuron as in *D* was fitted with a Gaussian, and the peak of this function was used to compare sIPSC amplitudes (*G*). *F*: sIPSC amplitudes (*top*) and rise times (*bottom*) as a function of age. Open symbols represent single cell values; filled symbols represent averages from a given age group. *G*: for all neurons in which both evoked and sIPSCs were recorded (P9/10: $n = 8$, P13: $n = 10$, P17: $n = 8$, P23–26: $n = 7$), the time constants of the sIPSCs are plotted vs. time constants of the smallest evoked IPSC. Throughout figure: open circles, P9/10; filled circles, P13; open diamonds, P17; filled diamonds, P23–26.



the evoked IPSCs remained unchanged. Together these findings indicate a developmentally unchanged precision of the release mechanism. These findings show that the developmental reduction of the decay time constants of the sIPSC can largely explain the acceleration of the evoked responses. Thus in mature animals GABAergic IPSCs follow a faster time course than previously suggested (Pecka et al. 2007).

Development of glutamatergic inputs to DNLL neurons. To investigate the development of glutamatergic inputs to DNLL neurons, the stimulation electrode was placed in the LL ventral to the DNLL. For a comparison between age groups the stimulation intensity was set to 20% above threshold of the minimally evoked excitatory postsynaptic current (EPSC). Glutamatergic inputs were segregated into synaptic AMPA and NMDA currents by recording at holding potentials of -70 and $+50$ mV, respectively. From 10–15 trials average evoked EPSCs were generated and fitted with an exponential function to quantify the amplitude and the decay time constant (Fig. 6A). The amplitude of the AMPA current was taken from the peak of the evoked current. To correct for developmental changes in the decay time constant of the NMDA component, the ampli-

tude value of the synaptic NMDA current was measured at the time indicated by its decay time constant (Fig. 6A). Under these conditions the peak amplitude of the synaptic AMPA currents did not change during late postnatal development (Fig. 6B, *top*). In contrast, the NMDA-to-AMPA ratio decreased significantly (Tukey-Kramer P23–26 vs. P9/10: $P < 0.05$) from 0.67 ± 0.10 at P9/10 to 0.27 ± 0.10 at P23–26, indicating a downregulation of the synaptic NMDA current (Fig. 6B, *bottom*). Furthermore, a developmental speeding of the AMPA- and NMDA-mediated components was observed. The decay time constant of the synaptic AMPA currents nearly halved from 4.04 ± 0.92 ms at P9/10 to 2.28 ± 0.45 ms at P23–26 (Fig. 6C), and the NMDA current became threefold faster, with decay time constants decreasing from 26.03 ± 1.3 ms at P9/10 to 8.10 ± 1.96 ms at P23–26 (Fig. 6C).

To estimate the minimal kinetics of the excitatory inputs to DNLL neurons, AMPA-mediated spontaneous EPSCs (sEPSCs) were recorded in the same cells. An average sEPSC was produced from all isolated sEPSCs of a given cell to determine the kinetics (Fig. 6D). The frequency histogram of all extracted peak sEPSC amplitudes of each cell was fitted with a Gaussian

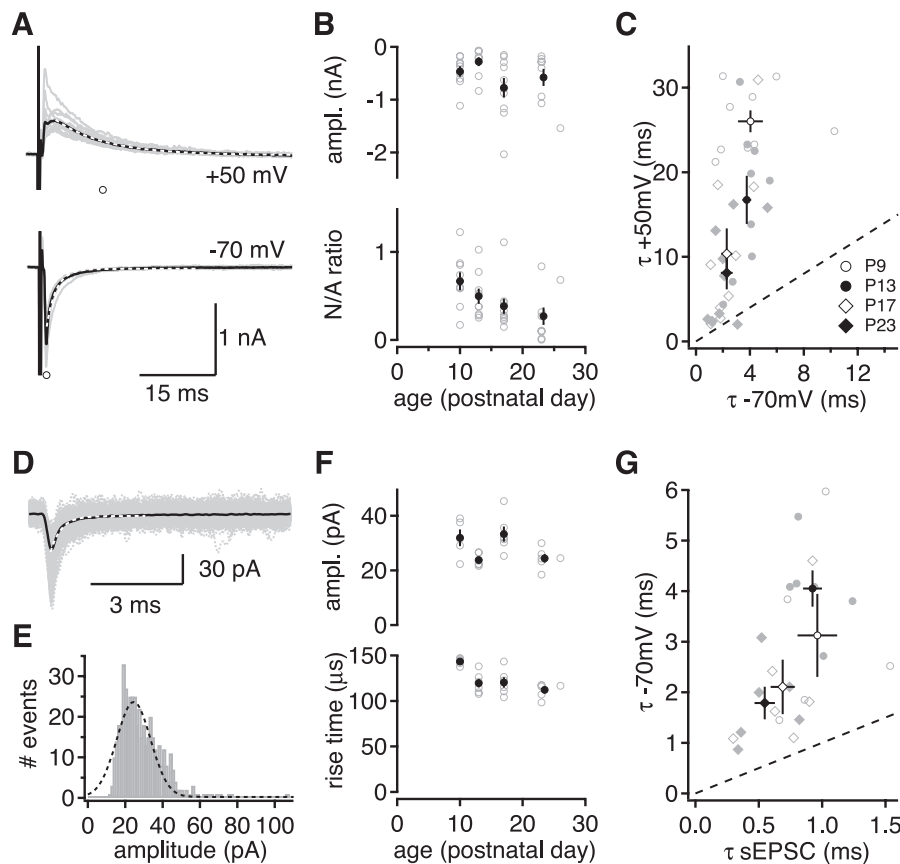


Fig. 6. Glutamatergic inputs to DNLL neurons accelerate during development. *A*: excitatory postsynaptic currents (EPSCs) evoked via the lateral lemniscus with stimulus intensity 20% above threshold. Traces of a P23 neuron exemplify the different decay time courses of EPSCs recorded at -70 and $+50$ mV. The decay time constants were extracted from a fit of an exponential function (white dotted line) to the average of 10–15 stimulation repetitions (black line; gray represents single trials). Values of EPSC amplitudes for recordings at $+50$ and -70 mV were taken at the location indicated by the open circles. For responses recorded at -70 mV the minimal value after the stimulation artifact was extracted. For responses recorded at $+50$ mV the value at the decay time constant was used. *B*: EPSC amplitudes recorded at -70 mV and evoked with 20% suprathreshold stimulation intensity as a function of age (top). Bottom: NMDA-to-AMPA (N/A) ratio derived from the amplitude measurements as a function of age (P9/10: $n = 10$, P13: $n = 9$, P17: $n = 10$, P23–26: $n = 9$). *C*: for all individual neurons, the decay time constants recorded at $+50$ mV are plotted vs. the decay time constants recorded at -70 mV. The dashed line indicates unity. *D*: spontaneous EPSCs (sEPSCs) recorded in a neuron of a P26 animal. The average sEPSC (black trace) was used to calculate the 20–80% rise time (*F*) and fitted with an exponential function (white dotted line) to determine the decay time constant (*G*). *E*: the histogram of sEPSC amplitudes was fitted with a Gaussian, and the peak of this fit was used to compare sEPSC amplitudes between neurons (*F*). *F*: sEPSC amplitude and rise time of the average sEPSC as a function of age. Open symbols represent single cell values; filled symbols represent average data of the specific age group. *G*: decay time constants of sEPSCs plotted vs. decay time constants of the smallest evoked EPSC for each cell. Gray symbols represent single cell values, black symbols represent average values of the specific age group (P9/10: $n = 5$, P13: $n = 6$, P17: $n = 6$, P23–26: $n = 6$), and dotted line indicates unity. Throughout figure: open circles, P9/10; filled circles, P13; open diamonds, P17; filled diamonds, P23–26.

function (Fig. 6*E*). The population average of the mean sEPSC amplitudes derived from the peaks of the Gaussian fits did not significantly change during development (Fig. 6*F*). In contrast, the rise time of the average sEPSCs accelerated significantly (Tukey-Kramer: P23–26 vs. P9/10: $P < 0.05$) during development (Fig. 6*F*).

To illustrate the developmental change of the decay kinetics of the EPSCs and the synchrony of release, the decay time constants of the sEPSC and the evoked EPSC were plotted against each other (Fig. 6*G*). Both the evoked EPSC and sEPSC decay time constants accelerated significantly during development (Tukey-Kramer: P23–26 vs. P9/10: $P < 0.05$). The average sEPSC decayed with a time constant of 0.92 ± 0.16 ms at P9/10 and with 0.55 ± 0.08 ms at P23–26, whereas the average evoked response decayed with a time constant of 4.05 ± 0.82 ms at P9/10 and with 1.79 ± 0.32 ms at P23–26. Similar to the GABAergic inputs, the difference between evoked EPSCs and sEPSCs was significant (paired t -test, $P <$

0.05 for P13, P17, P23–26), remaining three- to fourfold throughout development. Thus the reduction of the decay time constants of the sEPSC largely explains the acceleration of the evoked responses. Furthermore, our data show that during development the excitatory inputs to DNLL neurons became faster. The reduction in NMDA current might imply that the synaptic plasticity of DNLL neurons declines and that the NMDA-dependent amplification (Porres et al. 2011) becomes reduced.

Synaptic and intrinsic alterations contribute to the developmentally improved precision of AP generation. The ability to code signals fast and precisely is essential for neurons involved in binaural auditory processing. Developmental changes in intrinsic and synaptic properties have been shown to improve the precision of excitatory postsynaptic potential (EPSP)-AP coupling (Cathala et al. 2003), thus increasing response precision to incoming inputs. To dissect the influence of synaptic and intrinsic changes on the precision of AP generation in the

DNLL, we injected current waveforms simulating the EPSC kinetics of P9/10 (young) or P24–26 (mature) AMPA currents into neurons of P9/10 and P24–26 (Fig. 7A). The current amplitudes were scaled to evoke an AP in about half of the

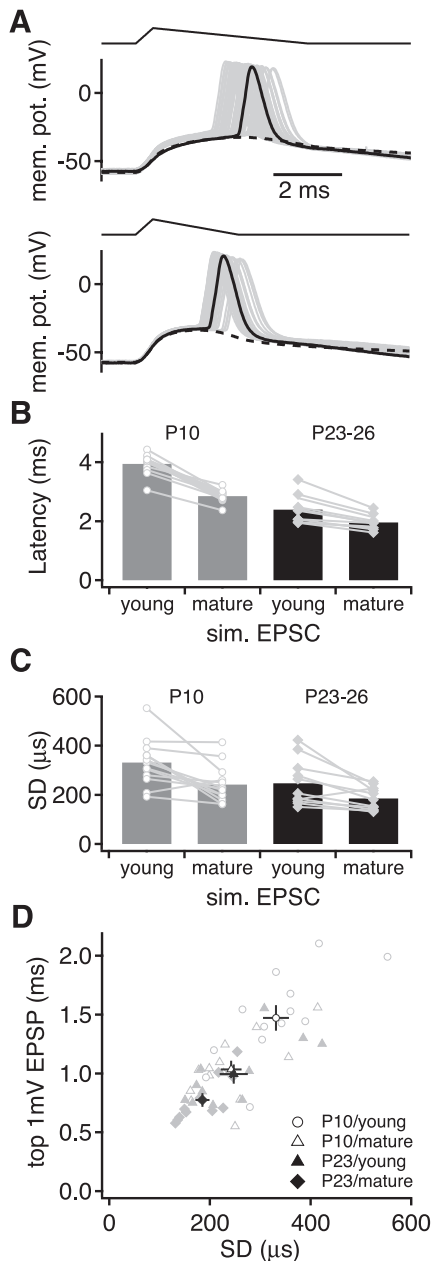


Fig. 7. Development of synaptic and intrinsic properties enhances precision of AP generation. *A*: current injections simulating the EPSC kinetics of P9/10 (*top*; young sim. EPSC, $\tau_{\text{decay}} = 4$ ms) or P23 (*bottom*; mature sim. EPSC, $\tau_{\text{decay}} = 2$ ms) AMPA currents scaled to evoke an AP in $\sim 50\%$ of trials. Example traces of a P9/10 neuron show AP responses in black or dark gray and average subthreshold response as black dotted line (52 APs at 56% success rate, *top*; 53 APs at 58% success rate, *bottom*). *B*: latency of AP response measured from the onset of the injected simulated EPSC for neurons of age P9/10 ($n = 13$) and P23–26 ($n = 11$). *C*: jitter of AP generation measured as standard deviation (SD) of AP response latency. *D*: time near AP threshold as a function of AP precision: time that the membrane potential remains within 1 mV of the maximum of the average subthreshold response (top 1 mV EPSP) plotted vs. the SD of the AP response latency for all cells and conditions. Gray symbols represent single neurons and black symbols average values.

trials (18–59%) to investigate AP precision directly at threshold and ensure comparability of data among cells.

The mean latency and the jitter of AP generation are classically used as measures for AP precision. During late postnatal development, the mean latency decreased from 3.9 ± 0.1 ms for the young EPSC and 2.9 ± 0.06 ms for the mature EPSC in P9/10 neurons to 2.4 ± 0.14 ms and 2.0 ± 0.08 ms in the P24–26 neurons, respectively (Fig. 7B; *t*-test: P9/10 young vs. P24–26 young $P < 0.05$; *t*-test: P9/10 mature vs. P24–26 mature $P < 0.05$). The jitter was reduced from $331 \pm 26 \mu\text{s}$ for the young EPSC and $242 \pm 21 \mu\text{s}$ for the mature EPSC in P9/10 neurons to $247 \pm 28 \mu\text{s}$ and $185 \pm 14 \mu\text{s}$ in the P24–26 neurons (Fig. 7C; *t*-test: P9/10 young vs. P24–26 young $P < 0.05$; *t*-test: P9/10 mature vs. P24–26 mature $P < 0.05$). Hence, the temporal precision of AP generation increases about twofold during postnatal development.

The contribution of the changes in the synaptic and intrinsic properties to AP precision can be estimated by comparing the responses to the two different simulated EPSCs within and between the two age groups. The mature EPSC waveform led in both P9/10 and P24–26 to significantly reduced latency and jitter (Fig. 7, *B* and *C*; all paired *t*-tests $P < 0.05$). The relative change for the mean latency and the jitter in response to young and mature injected current waveforms between P9/10 and P24–26 indicates the contribution of the intrinsic developmental alterations to the AP generation. An increase in temporal precision between 36% (mean latency) and 25% (jitter) is due to a change in the intrinsic properties. The synaptic contribution to the increase in temporal precision is accordingly estimated by calculating the relative change between young and mature current injections for both age groups. This revealed that between 21% (mean latency) and 26% (jitter) increase in temporal precision is due to the decrease in the synaptic decay time constant. Thus intrinsic and synaptic changes contribute nearly equally to the developmentally increased precision in AP generation.

Furthermore, it has been shown that the precision of AP generation depends on the time the membrane potential spends close to threshold (Rodríguez-Molina et al. 2007). Along this line both, the developmental stage and the choice of injected simulated EPSC influenced the time that the membrane potential remains within 1 mV of the maximum of the average subthreshold response (top 1 mV EPSP: P9/10 young 1.5 ± 0.1 ms; P9/10 mature 1.0 ± 0.1 ms; P24–26 young 1.0 ± 0.1 ms; P24–26 mature 0.8 ± 0.1 ms; besides P9/10 mature vs. P24–26 young all pairings are significantly different, *t*-test, $P < 0.05$). The time window that the membrane potential spends within 1 mV of AP threshold corresponded well to the observed jitter (Fig. 7D), again indicating that developmental changes in both intrinsic and synaptic properties lead to faster membrane potential dynamics near threshold and more precise AP generation.

NMDA current supports AP generation throughout development. Recently it was shown that the postsynaptic response of DNLL neurons is amplified in an NMDA-dependent manner (Porres et al. 2011), yet what the direct relation is between the NMDA current and the postsynaptic amplification was not explored. Here, we find that the synaptic NMDA component is developmentally reduced, which poses the question of whether the input amplification can be maintained during development and how the different synaptic charge is integrated at different

stages of development. In addition, the membrane potential influences the AP generation in DNLL neurons (Porres et al. 2011), and therefore perturbations of the cell by whole cell recordings might alter postsynaptic integration. During on-cell recordings the membrane potential is less affected by washout effects, but APs can still be reliably detected. Thus on-cell recordings are ideally suited to test whether NMDA currents are indeed capable of amplifying AP generation in DNLL neurons of different developmental stages.

First, to test the assumption that the current deflections recorded in on-cell mode represent APs, responses to different fiber stimulation intensities were recorded in on-cell mode and subsequently after break-in in the current-clamp whole cell configuration. The same stimulation intensities were repeated

10 times, and the responses were averaged for on-cell and current-clamp whole cell recordings (Fig. 8A). In general, the number of current deflections recorded in on-cell mode corresponded with the number of APs recorded in the whole cell configuration for both P23–26 ($n = 2$) and P14–15 ($n = 7$) (Fig. 8B). Thus the current deflections recorded in on-cell mode represent APs.

To directly test the involvement of NMDA currents in the generation of multiple APs upon a single stimulation event, synaptic NMDA currents were blocked by the specific antagonist *R*-CPP. For these experiments the stimulation strength was adjusted so that multiple APs were evoked initially (Fig. 8C). After bath application of *R*-CPP the number of APs recorded in on-cell mode was reduced to one (Fig. 8C). This

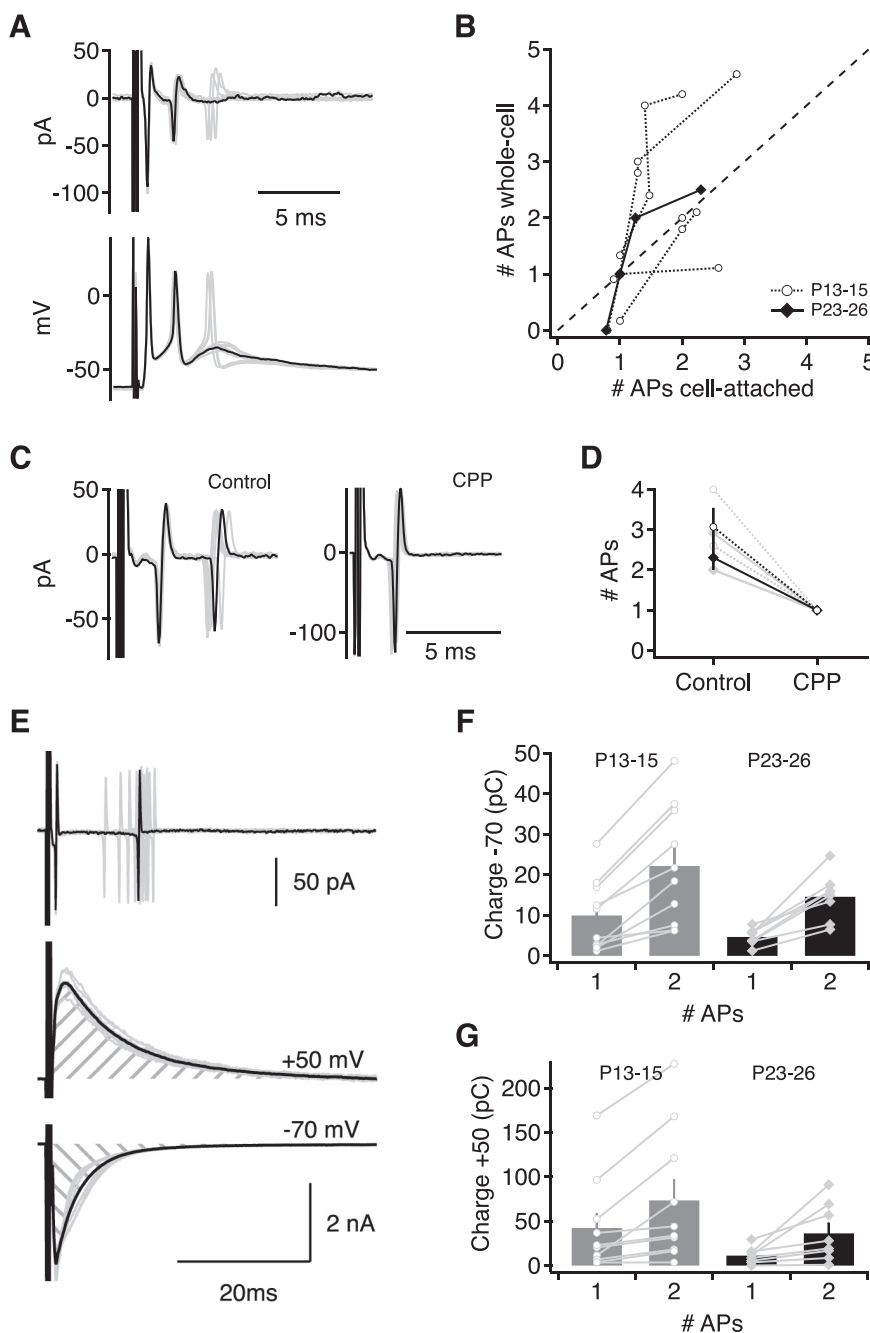


Fig. 8. NMDA currents enhance AP generation in DNLL neurons throughout late postnatal development. *A*: postsynaptic response of a P23 neuron to single stimulation events in on-cell voltage-clamp (*top*) and whole cell current-clamp (*bottom*) mode. Stimulation strength was the same before and after break-in to the cell. Ten repetitions are shown in gray, with single example traces highlighted in black. *B*: number of APs recorded in on-cell mode as a function of number of APs recorded in whole cell mode. Different stimulation intensities were applied for each cell. Stimulation intensities were adjusted to the same levels during on-cell and whole cell modes. P23 ($n = 2$) and P14–15 ($n = 7$) represent averages of number of APs from 10 trials. Dashed line indicates unity. *C*: on-cell recordings of evoked APs in a P23 neuron with the same stimulation strength before (Control; *left*) and after (*right*) *R*-CPP application. *D*: number of APs before and after the application of *R*-CPP recorded on-cell for 2 age groups: P14–15 (circles; $n = 3$) and P23–26 (diamonds; $n = 3$) neurons. Gray symbols represent single cells and black symbols average value. *E*: stimulation intensity was adjusted to produce either 1 (not shown) or 2 (*top*) APs during on-cell recordings. A single example of 10 repetitions is highlighted in black. After break-in, the glutamatergic inputs were recorded at +50 mV and –70 mV for the same stimulation intensities that corresponded to 1 (not shown) or 2 (*middle* and *bottom*) APs. Black trace represents average EPSC of 10 repetitions shown in gray. The synaptic charge was calculated from the average EPSC as indicated by the striped area. *F*: synaptic charge of EPSCs recorded at –70 mV evoked by stimulation intensities that elicited 1 or 2 APs: P13–15 neurons ($n = 10$) in gray, P23–26 ($n = 8$) in black. *G*: same as *F*, but for the EPSC charges recorded at +50 mV. Throughout figure: open circles, P13–15; filled diamonds, P23–26.

NMDA-dependent reduction in AP number was observed in all cells tested irrespective of age ($n = 3$ for P14/15 and $n = 3$ for P23–26; Fig. 8D). Thus the NMDA-dependent amplification is present throughout the late postnatal development, albeit the developmental reduction of the synaptic NMDA current shown above.

We next quantified the amount of the synaptic NMDA current involved in amplifying the postsynaptic response at different developmental stages (P13–14 and P23–26). Therefore, on-cell recordings of APs were followed after the break-in by voltage-clamp recordings at -70 and $+50$ mV (Fig. 8E). The stimulation strength was adjusted to two different intensities to evoke either one or two APs. From 10–15 synaptic stimulations an average EPSC was derived, and its charge was extracted and compared with the number of evoked APs (Fig. 8E). In mature animals the extracted EPSC charge correlating with two APs was about threefold larger compared with one AP at holding potentials of -70 and $+50$ mV (Fig. 8, F and G; $P < 0.05$). Similarly, for immature animals, a two- to threefold larger charge was correlated with two synaptically evoked APs compared with one (Fig. 8, F and G; $P < 0.05$). However, the absolute values for the EPSC charge indicated a developmental trend. The synaptic charge extracted at -70 mV was 4.7 ± 0.7 pC for one AP and 14.6 ± 2.0 pC for reliably triggering two APs in P23–26 animals (Fig. 8F). For immature animals (P13–15) 10.0 ± 2.8 pC and 22.2 ± 4.7 pC corresponded to one and two evoked APs, respectively (Fig. 8F). The charge transferred at $+50$ mV appeared smaller in mature compared with young animals. In P23–26 animals 11.2 ± 3.3 pC was associated with one AP and 36.3 ± 11.4 pC with two APs, whereas in P13–15 animals 42.3 ± 16.7 pC was extracted for one AP and 73.5 ± 23.6 pC for two APs (Fig. 8G). Therefore, a clear trend to smaller charges underlying the generation of one or two APs occurs during development (Fig. 8, F and G).

DISCUSSION

Here we report alterations of physiologically relevant parameters such as passive membrane properties, AP properties, size and kinetics of synaptic inputs, precision of EPSP-AP coupling, and the role of NMDA receptors in synaptically evoked AP generation during late postnatal development in DNLL neurons of Mongolian gerbils. This is complemented by quantifying the heterogeneity of the developmentally regulated CaBP expression pattern in the DNLL. Taken together, our findings show that DNLL neurons improve fast and precise signal integration during late postnatal development, a prerequisite to sustaining high firing rates with high temporal precision. The temporal precision of DNLL neurons fits to the high precision of lower stages of binaural processing and does not conflict with the DNLL's long-lasting GABAergic action found in *in vivo* recordings.

Expression of calcium binding proteins indicates two subpopulations of DNLL neurons. As described for other mammals (Caicedo et al. 1996; Kuwada et al. 2006; Lohmann and Friauf 1996; Vater and Braun 1994) DNLL neurons are predominantly parvalbuminergic in mature gerbils. The developmental increase in PV expression appears to correlate with the increased ability to hear (Finck et al. 1972; Ryan et al. 1982a; Smith and Kraus 1987) and use sound information in a relevant

manner (Kelly and Potash 1986). The increase of endogenous calcium buffers might be required to quench the possibly enhanced Ca^{2+} influx due to the increase in physiological firing frequencies at later developmental stages (Seidl and Grothe 2005). Similar to rats (Lohmann and Friauf 1996), a fraction of $\sim 25\%$ of DNLL neurons are calbindinergic throughout late postnatal development. These CB-positive cells appear morphologically indistinguishable from PV-positive cells. Furthermore, different CaBP expression appears not to be indicative of different intrinsic or synaptic properties of DNLL neurons. That the two CaBP subpopulations represent low- versus high-frequency tuning of DNLL neurons of gerbils is unlikely, as they are not clustered in a specific area related to the known tonotopy of this nucleus (Ryan et al. 1982b). It remains unclear whether the CB-positive fraction of DNLL neurons marks hypothesized subpopulations with specific functions (Meffin and Grothe 2009; Shneiderman et al. 1999) or an excitatory subpopulation, as it has been estimated that $\sim 15\%$ of DNLL neurons are noninhibitory (Saint Marie et al. 1997).

Development of cellular properties tunes DNLL neurons for fast and precise signal integration. A second anatomical alteration during late postnatal development is the reduction of the effective cell surface, as determined from the estimated cell capacitance. A developmental decrease in cell surface is common among neurons in the auditory brain stem (Chirila et al. 2007; Rautenberg et al. 2009; Rietzel and Friauf 1998; Rogowski and Feng 1981; Sanes et al. 1992). Such a decrease is of functional importance, as it allows faster charging of the membrane and therefore generates a shorter integration time window. A shortening of the integration time window is further promoted by the decrease in the specific input resistance of these neurons. Thus, similar to rats (Ahuja and Wu 2000), the developmental regulations of the passive membrane parameters lead to a speeding of cellular voltage responses. This acceleration suggests an improvement of the temporal precision in the information transfer from the SOC via the DNLL to the IC during late postnatal development. This improvement might underlie the capability of these neurons to respond with high temporal fidelity at high rates to sound stimulations (Brugge et al. 1970; Kuwada et al. 2006; Pecka et al. 2010; Seidl and Grothe 2005; Siveke et al. 2006).

During the late postnatal development the AP half-width decreases threefold. Such a reduction is common in the auditory brain stem and is observed in the MSO (Scott et al. 2005), the medial nucleus of the trapezoid body (Taschenberger and von Gersdorff 2000), and the avian nucleus laminaris (Gao and Lu 2008). In addition to the voltage threshold, the current threshold to short stimuli, which are more similar to the EPSC time course compared with long current injections, decreases in this developmental period. Together, these changes generate neurons that are more excitable and temporally more precise. This implication is illustrated by a decrease in the refractory period, an increase in AP firing frequency, and reduced AP firing adaptation. We suggest that an increase in sodium and potassium channel density together with a decrease in cell surface underlies the developmental increase in excitability. An increase in sodium channel density agrees with the reduction of E_{thr} during late postnatal development. An increase in potassium channel density is consistent with a reduction of R_{in} and the increased number of "pauser" neurons. Physiologically, this enhanced excitability might partially explain the

developmental increase of spike rates found in *in vivo* recordings (Seidl and Grothe 2005).

Besides the AP half-width, all physiological parameters show a large cell-to-cell variability in the DNLL. The source and the function of this variability remain unclear, as these parameters do not cluster in distinct populations, which would be expected for specific subcircuits. It is tempting to speculate that the cell-to-cell variability of the physiological parameters might match the different frequency contours in the gerbil DNLL (Ryan et al. 1982b). However, the best frequency of a neuron recorded in our slice preparation remains elusive, and it is unlikely that the variability matches a ventro-dorsal gradient. An alternative explanation for this cell-to-cell variability is that each cell makes use of the same subset of cell parameters with different weights to finally establish its physiologically required input-output function.

Implications of the developmental acceleration of GABAergic inputs to DNLL neurons. Synaptic stimulation showed that the kinetics of the GABAergic inputs to DNLL neurons accelerate 2.5-fold between P9/10 and P23–26. The decay time constants of GABAergic currents reported here differ notably from earlier reports (Pecka et al. 2007). The major difference between the recordings in these reports is the concentration of intracellular chloride. The level of intracellular chloride was recently shown to strongly affect the kinetics, especially the decay time course, of GABAergic currents (Houston et al. 2009). Compared with the earlier work (Pecka et al. 2007), this study employed lower intracellular chloride concentrations closer to normal physiological values. Therefore, we suggest that the GABAergic currents reported in the earlier work were approximately twofold too slow.

The action of the GABAergic inhibition is thought to be the cellular correlate for the persistent inhibition demonstrated in *in vivo* recordings (Burger and Pollak 2001; Pecka et al. 2007; Yang and Pollak 1994) that might underlie behavioral phenomena such as the precedence effect (Blauert 1997; Litovsky et al. 1999; Zurek 1987). It had been speculated that the time course of this GABAergic inhibition is mediated by a slow synaptic current (Pecka et al. 2007). Here, however, the time course of the fastest GABAergic currents measured does not directly match the predictions of the inhibitory time course from *in vivo* recordings (Burger and Pollak 2001; Pecka et al. 2007; Yang and Pollak 1994). This discrepancy can partially be explained by the membrane time constant that prolongs the inhibitory postsynaptic potential (IPSP) in respect to the IPSC drive. Two additional mechanisms might further help to explain the long-lasting GABAergic time course found *in vivo*. On the network level, the integration of many inputs with different latencies could generate a long-lasting inhibition in the target cells in the DNLL and IC. Second, synaptic mechanisms could prolong the GABAergic time course during ongoing activity. This idea is based on findings that show an increased IPSP decay time as a function of stimulation pulse number (Porres et al. 2011). Evidence that the time course of synaptic transmission might depend on the level of release is given here, as larger GABAergic currents decay slower than small currents. The underlying synaptic mechanism that prolongs the GABAergic IPSPs might be transmitter pooling (Balakrishnan et al. 2009), spillover (Farrant and Nusser 2005), a transition between phasic and asynchronous release (Lu and Trussell 2000), or changes in GABA receptor desensitization (Jones and Westbrook 1995). Thus the

fast-decaying single IPSC in mature animals can turn into a long-lasting inhibitory action by multiple mechanisms. Therefore, the developmental acceleration of both the synaptic and intrinsic parameters does not contradict the known long-lasting inhibition in the DNLL or IC. In contrast, it might increase the systems dynamic range, allowing for relatively short as well as long-lasting inhibition.

Development of excitatory inputs supports reliable signal transfer at high rates. Similar to nuclei in the SOC (Joshi and Wang 2002; Kandler and Friauf 1995; Koike-Tani et al. 2005; Magnusson et al. 2005; Taschenberger and von Gersdorff 2000), the size and kinetics of excitatory inputs to DNLL neurons are subject to developmental changes. The size of the NMDA current is developmentally downregulated. This decrease is inferred from the reduced NMDA-to-AMPA ratio together with the developmental invariance of the size of AMPA currents. Both the evoked NMDA and AMPA currents become faster in decay during late postnatal development. The kinetics of the excitatory inputs appear to be species specific, as the decay time constants obtained from rats (Fu et al. 1997) are about fourfold slower compared with those from gerbils.

From the developmental alterations of the synaptic AMPA and NMDA currents it is expected that APs are triggered less efficiently by excitatory synaptic inputs. The NMDA-dependent postsynaptic amplification (Porres et al. 2011) is therefore expected to be developmentally regulated. However, the developmentally increased excitability appears to counterbalance this expectation. This interpretation is consistent with the finding that less synaptic excitatory charge is required to generate APs in the postsynaptic DNLL neurons of mature gerbils.

Even at the oldest age tested, the decay time course of evoked AMPA currents is still about threefold slower than that of spontaneous events. The discrepancy between the AMPA decay time courses of evoked and spontaneous events can be interpreted as largely unsynchronized release. Interestingly, a rather sluggish excitatory transmission might be useful for DNLL neurons. Temporally extended excitatory inputs might allow DNLL neurons to faithfully follow the high firing rates of their presynaptic SOC neurons and produce failure-reduced synaptic information transfer (Brugge et al. 1970; Kuwada et al. 2006; Pecka et al. 2010; Siveke et al. 2006). We propose that the developmental acceleration of EPSC decays and their remaining unsynchronized release are balanced to allow DNLL neurons to optimize the trade-off between high AP precision and the sustaining of high firing rates. Such a mechanism could be important to keep up the AP firing rates in DNLL neurons and thereby induce a prolongation of the important GABAergic output signal in adult animals (Porres et al. 2011).

This study also allows for a comparison of the developmental changes of inhibitory and excitatory inputs to DNLL neurons. The refinement of synaptic GABA, AMPA, and NMDA currents occurs at similar developmental stages in DNLL neurons. Both inhibitory and excitatory inputs appear to mature until P23–26, with the largest change in size, kinetics, or both between P10 and P17. The similar developmental time course of the different synaptic inputs indicates that keeping the balance between excitation and inhibition is crucial throughout late postnatal development and during maturity.

Maturation of cellular properties enhances precision in EPSC/EPSP-AP coupling. The interaction between synaptic kinetics and intrinsic properties was analyzed in respect to their influence on AP precision. The acceleration of both the synaptic decay kinetics and τ_m increase the precision of AP generation twofold between P9/10 and P24–26. Thus these alterations produce neurons that are able to respond faster and more precisely to incoming excitatory signals. It should be noted that DNLL neurons are already very precise at age P9/10. Compared with cortical neurons, juvenile DNLL neurons are at least four times more precise (Fricker and Miles 2000; Rodriguez-Molina et al. 2007). Mature DNLL neurons with an AP jitter of $\sim 185 \mu\text{s}$ match the high AP precision of other auditory brain stem nuclei. In vitro recordings of bushy cells in the anterior ventral cochlear nucleus showed that AP generation jitters of $\sim 140 \mu\text{s}$ near threshold (Chanda and Xu-Friedman 2010). In vivo recordings of neurons in the medial nucleus of the trapezoid body and the MSO report a jitter of first spike latencies between 100 and 900 μs (Kopp-Scheinflug et al. 2003; Lorteije and Borst 2011; Yin and Chan 1990). Together these findings demonstrate that auditory neurons throughout the interaural time and level difference circuits up to the DNLL are of exquisite temporal precision.

ACKNOWLEDGMENTS

We thank Claudia Aerdker for technical support with the immunohistochemistry. J. J. Ammer is a member of the Graduate School for Systemic Neurosciences at the Ludwig Maximilians University.

GRANTS

This study and J. J. Ammer were supported by the Deutsche Forschungsgemeinschaft (FE789/2-1).

DISCLOSURES

No conflicts of interest, financial or otherwise, are declared by the author(s).

AUTHOR CONTRIBUTIONS

Author contributions: J.J.A., B.G., and F.F. conception and design of research; J.J.A. and F.F. performed experiments; J.J.A. and F.F. analyzed data; J.J.A., B.G., and F.F. interpreted results of experiments; J.J.A. and F.F. prepared figures; J.J.A. and F.F. drafted manuscript; J.J.A., B.G., and F.F. edited and revised manuscript; J.J.A., B.G., and F.F. approved final version of manuscript.

REFERENCES

- Adams JC. Ascending projections to the inferior colliculus. *J Comp Neurol* 183: 519–538, 1979.
- Adams JC, Mugnaini E. Dorsal nucleus of the lateral lemniscus: a nucleus of GABAergic projection neurons. *Brain Res Bull* 13: 585–590, 1984.
- Ahuja TK, Wu SH. Developmental changes in physiological properties in the rat's dorsal nucleus of the lateral lemniscus. *Hear Res* 149: 33–45, 2000.
- Bajo VM, Merchan MA, Lopez DE, Rouiller EM. Neuronal morphology and efferent projections of the dorsal nucleus of the lateral lemniscus in the rat. *J Comp Neurol* 334: 241–262, 1993.
- Balakrishnan V, Kuo SP, Roberts PD, Trussell LO. Slow glycinergic transmission mediated by transmitter pooling. *Nat Neurosci* 12: 286–294, 2009.
- Blauert J. *Spatial Hearing with Multiple Sound Sources and in Enclosed Spaces*. Cambridge, MA: MIT, 1997, p. 201–287.
- Brand A, Behrend O, Marquardt T, McAlpine D, Grothe B. Precise inhibition is essential for microsecond interaural time difference coding. *Nature* 417: 543–547, 2002.
- Brugge JF, Anderson DJ, Aitkin LM. Responses of neurons in the dorsal nucleus of the lateral lemniscus of cat to binaural tonal stimulation. *J Neurophysiol* 33: 441–458, 1970.
- Burger RM, Pollak GD. Reversible inactivation of the dorsal nucleus of the lateral lemniscus reveals its role in the processing of multiple sound sources in the inferior colliculus of bats. *J Neurosci* 21: 4830–4843, 2001.
- Caicedo A, d'Aldin C, Puel JL, Eybalin M. Distribution of calcium-binding protein immunoreactivities in the guinea pig auditory brainstem. *Anat Embryol (Berl)* 194: 465–487, 1996.
- Cathala L, Brickley S, Cull-Candy S, Farrant M. Maturation of EPSCs and intrinsic membrane properties enhances precision at a cerebellar synapse. *J Neurosci* 23: 6074–6085, 2003.
- Chanda S, Xu-Friedman MA. Neuromodulation by GABA converts a relay into a coincidence detector. *J Neurophysiol* 104: 2063–2074, 2010.
- Chirila FV, Rowland KC, Thompson JM, Spirou GA. Development of gerbil medial superior olive: integration of temporally delayed excitation and inhibition at physiological temperature. *J Physiol* 584: 167–190, 2007.
- Couchman K, Grothe B, Felmy F. Medial superior olivary neurons receive surprisingly few excitatory and inhibitory inputs with balanced strength and short-term dynamics. *J Neurosci* 30: 17111–17121, 2010.
- Faingold CL, Anderson CA, Randall ME. Stimulation or blockade of the dorsal nucleus of the lateral lemniscus alters binaural and tonic inhibition in contralateral inferior colliculus neurons. *Hear Res* 69: 98–106, 1993.
- Farrant M, Nusser Z. Variations on an inhibitory theme: phasic and tonic activation of GABA_A receptors. *Nat Rev Neurosci* 6: 215–229, 2005.
- Felmy F, Schneggenburger R. Developmental expression of the Ca²⁺-binding proteins calretinin and parvalbumin at the calyx of Held of rats and mice. *Eur J Neurosci* 20: 1473–1482, 2004.
- Finck A, Schneck CD, Hartman AF. Development of cochlear function in the neonate Mongolian gerbil (*Meriones unguiculatus*). *J Comp Physiol Psychol* 78: 375–380, 1972.
- Fricker D, Miles R. EPSP amplification and the precision of spike timing in hippocampal neurons. *Neuron* 28: 559–569, 2000.
- Fu XW, Brezden BL, Kelly JB, Wu SH. Synaptic excitation in the dorsal nucleus of the lateral lemniscus: whole-cell patch-clamp recordings from rat brain slice. *Neuroscience* 78: 815–827, 1997.
- Gao H, Lu Y. Early development of intrinsic and synaptic properties of chicken nucleus laminaris neurons. *Neuroscience* 153: 131–143, 2008.
- Glendenning KK, Brunso-Bechtold JK, Thompson GC, Masterton RB. Ascending auditory afferents to the nuclei of the lateral lemniscus. *J Comp Neurol* 197: 673–703, 1981.
- Gonzalez-Hernandez T, Mantolan-Sarmiento B, Gonzalez-Gonzalez B, Perez-Gonzalez H. Sources of GABAergic input to the inferior colliculus of the rat. *J Comp Neurol* 372: 309–326, 1996.
- Houston CM, Bright DP, Sivilotti LG, Beato M, Smart TG. Intracellular chloride ions regulate the time course of GABA-mediated inhibitory synaptic transmission. *J Neurosci* 29: 10416–10423, 2009.
- Iwahori N. A Golgi study on the dorsal nucleus of the lateral lemniscus in the mouse. *Neurosci Res* 3: 196–212, 1986.
- Jones MV, Westbrook GL. Desensitized states prolong GABA_A channel responses to brief agonist pulses. *Neuron* 15: 181–191, 1995.
- Joshi I, Wang LY. Developmental profiles of glutamate receptors and synaptic transmission at a single synapse in the mouse auditory brainstem. *J Physiol* 540: 861–873, 2002.
- Kandler K, Friauf E. Development of glycinergic and glutamatergic synaptic transmission in the auditory brainstem of perinatal rats. *J Neurosci* 15: 6890–6904, 1995.
- Kane ES, Barone LM. The dorsal nucleus of the lateral lemniscus in the cat: neuronal types and their distributions. *J Comp Neurol* 192: 797–826, 1980.
- Kelly JB, Buckthought AD, Kidd SA. Monoaural and binaural response properties of single neurons in the rat's dorsal nucleus of the lateral lemniscus. *Hear Res* 122: 25–40, 1998.
- Kelly JB, Potash M. Directional responses to sounds in young gerbils (*Meriones unguiculatus*). *J Comp Psychol* 100: 37–45, 1986.
- Kelly JB, van Adel BA, Ito M. Anatomical projections of the nuclei of the lateral lemniscus in the albino rat (*Rattus norvegicus*). *J Comp Neurol* 512: 573–593, 2009.
- Koike-Tani M, Saitoh N, Takahashi T. Mechanisms underlying developmental speeding in AMPA-EPSC decay time at the calyx of Held. *J Neurosci* 25: 199–207, 2005.
- Kopp-Scheinflug C, Fuchs K, Lippe WR, Tempel BL, Rubsamen R. Decreased temporal precision of auditory signaling in Kcna1-null mice: an electrophysiological study in vivo. *J Neurosci* 23: 9199–9207, 2003.

- Kuwada S, Fitzpatrick DC, Batra R, Ostapoff EM.** Sensitivity to interaural time differences in the dorsal nucleus of the lateral lemniscus of the unanesthetized rabbit: comparison with other structures. *J Neurophysiol* 95: 1309–1322, 2006.
- Litovsky RY, Colburn HS, Yost WA, Guzman SJ.** The precedence effect. *J Acoust Soc Am* 106: 1633–1654, 1999.
- Lohmann C, Friauf E.** Distribution of the calcium-binding proteins parvalbumin and calretinin in the auditory brainstem of adult and developing rats. *J Comp Neurol* 367: 90–109, 1996.
- Lorteije JA, Borst JG.** Contribution of the mouse calyx of Held synapse to tone adaptation. *Eur J Neurosci* 33: 251–258, 2011.
- Lu T, Trussell LO.** Inhibitory transmission mediated by asynchronous transmitter release. *Neuron* 26: 683–694, 2000.
- Magnusson AK, Kapfer C, Grothe B, Koch U.** Maturation of glycinergic inhibition in the gerbil medial superior olive after hearing onset. *J Physiol* 568: 497–512, 2005.
- Markovitz NS, Pollak GD.** Binaural processing in the dorsal nucleus of the lateral lemniscus. *Hear Res* 73: 121–140, 1994.
- Meffin H, Grothe B.** Selective filtering to spurious localization cues in the mammalian auditory brainstem. *J Acoust Soc Am* 126: 2437–2454, 2009.
- Oliver DL.** Ascending efferent projections of the superior olivary complex. *Microsc Res Tech* 51: 355–363, 2000.
- Oliver DL, Shneiderman A.** An EM study of the dorsal nucleus of the lateral lemniscus: inhibitory, commissural, synaptic connections between ascending auditory pathways. *J Neurosci* 9: 967–982, 1989.
- Pecka M, Brand A, Behrend O, Grothe B.** Interaural time difference processing in the mammalian medial superior olive: the role of glycinergic inhibition. *J Neurosci* 28: 6914–6925, 2008.
- Pecka M, Siveke I, Grothe B, Lesica NA.** Enhancement of ITD coding within the initial stages of the auditory pathway. *J Neurophysiol* 103: 38–46, 2010.
- Pecka M, Zahn TP, Saunier-Rebori B, Siveke I, Felmy F, Wiegube L, Klug A, Pollak GD, Grothe B.** Inhibiting the inhibition: a neuronal network for sound localization in reverberant environments. *J Neurosci* 27: 1782–1790, 2007.
- Porres CP, Meyer EM, Grothe B, Felmy F.** NMDA currents modulate the synaptic input-output functions of neurons in the dorsal nucleus of the lateral lemniscus in Mongolian gerbils. *J Neurosci* 31: 4511–4523, 2011.
- Rautenberg PL, Grothe B, Felmy F.** Quantification of the three-dimensional morphology of coincidence detector neurons in the medial superior olive of gerbils during late postnatal development. *J Comp Neurol* 517: 385–396, 2009.
- Rietzel HJ, Friauf E.** Neuron types in the rat lateral superior olive and developmental changes in the complexity of their dendritic arbors. *J Comp Neurol* 390: 20–40, 1998.
- Roberts RC, Ribak CE.** GABAergic neurons and axon terminals in the brainstem auditory nuclei of the gerbil. *J Comp Neurol* 258: 267–280, 1987.
- Rodriguez-Molina VM, Aertsen A, Heck DH.** Spike timing and reliability in cortical pyramidal neurons: effects of EPSC kinetics, input synchronization and background noise on spike timing. *PLoS One* 2: e319, 2007.
- Rogowski BA, Feng AS.** Normal postnatal development of medial superior olivary neurons in the albino rat: a Golgi and Nissl study. *J Comp Neurol* 196: 85–97, 1981.
- Ryan AF, Woolf NK, Sharp FR.** Functional ontogeny in the central auditory pathway of the Mongolian gerbil. A 2-deoxyglucose study. *Exp Brain Res* 47: 428–436, 1982a.
- Ryan AF, Woolf NK, Sharp FR.** Tonotopic organization in the central auditory pathway of the Mongolian gerbil: a 2-deoxyglucose study. *J Comp Neurol* 207: 369–380, 1982b.
- Saint Marie RL, Shneiderman A, Stanforth DA.** Patterns of gamma-aminobutyric acid and glycine immunoreactivities reflect structural and functional differences of the cat lateral lemniscal nuclei. *J Comp Neurol* 389: 264–276, 1997.
- Sanes DH, Song J, Tyson J.** Refinement of dendritic arbors along the tonotopic axis of the gerbil lateral superior olive. *Brain Res Dev Brain Res* 67: 47–55, 1992.
- Scott LL, Mathews PJ, Golding NL.** Posthearing developmental refinement of temporal processing in principal neurons of the medial superior olive. *J Neurosci* 25: 7887–7895, 2005.
- Seidl AH, Grothe B.** Development of sound localization mechanisms in the mongolian gerbil is shaped by early acoustic experience. *J Neurophysiol* 94: 1028–1036, 2005.
- Shneiderman A, Oliver DL, Henkel CK.** Connections of the dorsal nucleus of the lateral lemniscus: an inhibitory parallel pathway in the ascending auditory system? *J Comp Neurol* 276: 188–208, 1988.
- Shneiderman A, Stanforth DA, Henkel CK, Saint Marie RL.** Input-output relationships of the dorsal nucleus of the lateral lemniscus: possible substrate for the processing of dynamic spatial cues. *J Comp Neurol* 410: 265–276, 1999.
- Siveke I, Pecka M, Seidl AH, Baudoux S, Grothe B.** Binaural response properties of low-frequency neurons in the gerbil dorsal nucleus of the lateral lemniscus. *J Neurophysiol* 96: 1425–1440, 2006.
- Smith DI, Kraus N.** Postnatal development of the auditory brainstem response (ABR) in the unanesthetized gerbil. *Hear Res* 27: 157–164, 1987.
- Smith PH, Joris PX, Yin TC.** Anatomy and physiology of principal cells of the medial nucleus of the trapezoid body (MNTB) of the cat. *J Neurophysiol* 79: 3127–3142, 1998.
- Taschenberger H, von Gersdorff H.** Fine-tuning an auditory synapse for speed and fidelity: developmental changes in presynaptic waveform, EPSC kinetics, and synaptic plasticity. *J Neurosci* 20: 9162–9173, 2000.
- Tollin DJ, Yin TC.** Interaural phase and level difference sensitivity in low-frequency neurons in the lateral superior olive. *J Neurosci* 25: 10648–10657, 2005.
- Vater M, Braun K.** Parvalbumin, calbindin D-28k, and calretinin immunoreactivity in the ascending auditory pathway of horseshoe bats. *J Comp Neurol* 341: 534–558, 1994.
- Vater M, Covey E, Casseday JH.** The columnar region of the ventral nucleus of the lateral lemniscus in the big brown bat (*Eptesicus fuscus*): synaptic arrangements and structural correlates of feedforward inhibitory function. *Cell Tissue Res* 289: 223–233, 1997.
- Winer JA, Larue DT, Pollak GD.** GABA and glycine in the central auditory system of the mustache bat: structural substrates for inhibitory neuronal organization. *J Comp Neurol* 355: 317–353, 1995.
- Wu SH, Kelly JB.** In vitro brain slice studies of the rat's dorsal nucleus of the lateral lemniscus. II. Physiological properties of biocytin-labeled neurons. *J Neurophysiol* 73: 794–809, 1995.
- Yang L, Pollak GD.** The roles of GABAergic and glycinergic inhibition on binaural processing in the dorsal nucleus of the lateral lemniscus of the mustache bat. *J Neurophysiol* 71: 1999–2013, 1994.
- Yin TC, Chan JC.** Interaural time sensitivity in medial superior olive of cat. *J Neurophysiol* 64: 465–488, 1990.
- Zurek PM.** *The Precedence Effect*. New York: Springer, 1987, p. 85–105.

3 Long lasting inhibition in the DNLL

Contributions

Julian Ammer (J.J.A.) and Felix Felmy (F.F.) conception and design of research; J.J.A. performed experiments; J.J.A. analyzed data; J.J.A. and F.F. interpreted results of experiments; J.J.A. prepared figures; J.J.A. and F.F. drafted manuscript; J.J.A. and F.F. edited and revised manuscript.

Acknowledgements

We thank Benedikt Grothe for generous support and helpful discussions, Martin Stemmler for helpful discussions and George Pollak for comments on the manuscript. This work was funded by DFG FE789/2-1 and the Elisabeth and Helmut Uhl Foundation.

Activity-dependent inhibition gates information in an echo processing circuit

Ammer J.J.^{1,2}, Felmy F.^{1,3}

¹ Division of Neurobiology, Department for Biology II, Ludwig-Maximilians University Munich, Großhaderner Straße 2 2, D-82152 Planegg-Martinsried, Germany

² Graduate School of Systemic Neuroscience Munich D-82152 Planegg-Martinsried, Germany

³ Bioimaging Center, D-82152 Planegg-Martinsried, Germany

Abstract

The auditory system selectively suppresses the directional information of echoes to achieve accurate sound localization in reverberant environments. The initial step in this process is mediated by persistent GABAergic inhibition in the dorsal nucleus of the lateral lemniscus (DNLL) that suppresses responses to trailing sounds for tens of milliseconds. Here, we identify the cellular mechanisms in Mongolian gerbils that flexibly control the duration of inhibition in the DNLL depending on presynaptic activity. Activity-dependent GABA spillover and asynchronous release translate high presynaptic firing rates into a prolongation of GABAergic IPSCs. Passive integration of hyperpolarizing inhibition additionally prolongs IPSPs depending on the conductance amplitude, due to the non-linear membrane relaxation between GABA-reversal and resting potential. The resulting IPSP efficiently suppresses action potential generation for a duration matching *in vivo* findings. Thus, these cellular mechanisms work in synergy to achieve an activity-dependent control of inhibition that gates information during the categorization of echoes.

Introduction

In reverberant environments, the auditory system suppresses the directional information of echoes to localize primary sound sources faithfully. Psychophysically, this selective filtering is known as the precedence effect¹. The initial step in the physiological implementation of this process is thought to take place in the circuitry of the dorsal nucleus of the lateral lemniscus (DNLL)²⁻⁵. The DNLL generates a GABA_A-receptor mediated persistent inhibition (PI) that outlasts a leading sound stimulus long enough to inhibit responses to lagging reverberant sounds in the contralateral DNLL²⁻⁵. Depending on the intensity of the leading sound, the duration of PI is dynamically adjusted acting like a variable gate to suppress activity in the DNLL for up to 60 ms³⁻⁵. However, how this PI is generated on a cellular level is still unclear. As there is no prolonged activity after a sound stimulus in the presynaptic DNLL^{2,3,5}, there is no continuous inhibitory input that could cause the PI. Rather, the GABA_A-receptor mediated inhibition has to be effective for tens of millisecond after the last presynaptic action potential (AP).

Generally, duration and effectiveness of neuronal inhibition depend on synaptic as well as on intrinsic membrane properties. Binding of transmitter to an inhibitory receptor channel shunts excitation by increasing the conductance of the cell membrane for the open time of the receptor^{6,7}. The duration of transmitter action can be prolonged by activity-dependent processes such as transmitter spillover⁸⁻¹² and asynchronous release¹²⁻¹⁵. If inhibition is hyperpolarizing, the intrinsic filter properties of the membrane can lead to an inhibitory postsynaptic potential (IPSP) that lasts longer than the receptor opening^{7,16,17}.

In adult DNLL neurons, both synaptic and membrane time constants are too fast to explain the *in vivo* duration of PI¹⁸. This discrepancy raises the general question, how efficient long lasting inhibition is achieved in a fast spiking neuron with a fast synaptic input. As one possible solution, activity-dependent synaptic mechanisms

have been proposed in juvenile gerbils to translate the high firing rates in DNLL neurons into a prolonged inhibitory output signal¹⁹.

Here, we identify several factors that are essential to generate long lasting inhibition in mature DNLL neurons. First, transmitter spillover and asynchronous release prolong the decay of GABAergic IPSCs in a graded and activity-dependent manner. Second, passive integration prolongs IPSPs preferentially for slow IPSCs in an amplitude dependent manner, indicating that a recruitment of more GABAergic inputs automatically leads to longer lasting inhibition. And finally, the negative GABA reversal potential leads to hyperpolarizing IPSPs which are far more effective in suppressing action potentials than mere shunting inhibition.

Results

GABAergic inhibition is hyperpolarizing in DNLL neurons

PI *in vivo* is caused by GABAergic inhibition via the commissure of Probst (CP) that competes with incoming excitation from lower brainstem nuclei (Fig. 1a). As the reversal potential of an inhibitory synapse influences how inhibition affects the computations in the postsynaptic neuron²⁰, we first determined the GABAergic reversal potential (E_{GABA}) in the DNLL (Fig. 1d-f). To get electrical access to the neuron without altering the internal chloride concentration ($[Cl_i]$) we used Gramicidin perforated-patch recordings and altered the holding potential in current-clamp. GABAergic IPSPs evoked via the CP (Fig. 1b,c) had an E_{GABA} of -91.3 ± 2.4 mV ($n = 8$, Fig. 1d), which is about 15 mV lower than the average membrane potential of -76.2 ± 0.8 mV ($n = 47$). Thus, in line with the generally negative reversal potentials for inhibition in the auditory brainstem and midbrain²¹, GABAergic inhibition is hyperpolarizing in the DNLL. As $[Cl_i]$ at GABAergic synapses not only controls E_{GABA} , but additionally influences the kinetics of the receptor and thus the duration

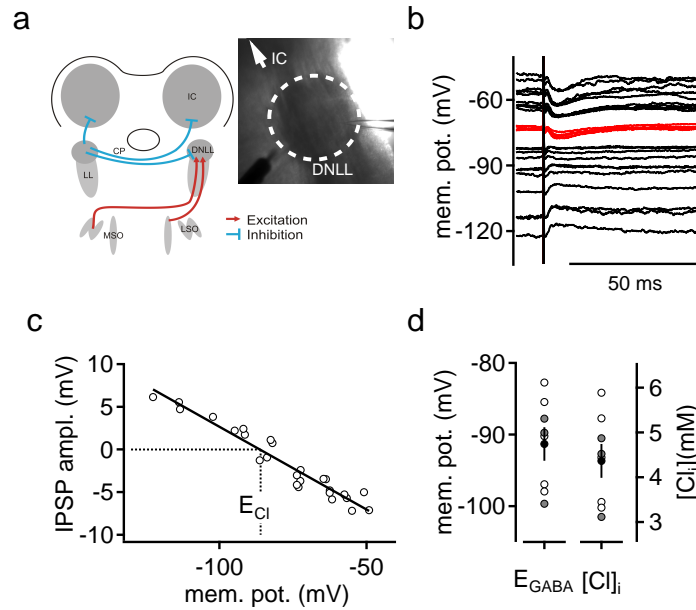


Figure 1: The GABA reversal potential in DNLL neurons is hyperpolarizing. **(a)** Simplified DNLL circuit with main glutamatergic and GABAergic connections in red and blue. Other projections were omitted for clarity. CP = commissure of Probst, LL = lateral lemniscus, LSO/MSO = lateral/medial superior olive, IC = inferior colliculus. Inset: Recording configuration with patch electrode in the DNLL and stimulation electrode in the CP. **(b)** Perforated-patch recording of a P25 neuron. The membrane potential was altered with constant current injections and IPSPs were stimulated via the CP. Traces at resting membrane potential in red. **(c)** IPSP amplitudes were fitted with a linear function versus the holding potential to calculate the GABA reversal potential (E_{GABA}). **(d)** Pooled data of measured reversal potential and corresponding estimated chloride concentration. Open symbols P18/19 $n = 5$, gray closed symbols P25 - 32 $n = 3$, average black closed symbols. Data are given as mean \pm sem.

of inhibition²², all subsequent recordings were performed with the estimated $[Cl]_i$ of 4.5 mM (Fig. 1d).

IPSC decay depends on presynaptic activity

The duration of PI *in vivo* depends on the intensity of the leading sound representing the primary sound source. One possible mechanism for this dependency would be a prolongation of the GABAergic inhibitory postsynaptic current (IPSC) decay after increased presynaptic activity. Accordingly, we asked whether presynaptic activity adjusts GABAergic decay kinetics in the DNLL at P30 - 35 where *in vivo* physiology is fully developed²³ by using *in vivo*-like stimulation frequencies of 10 – 400

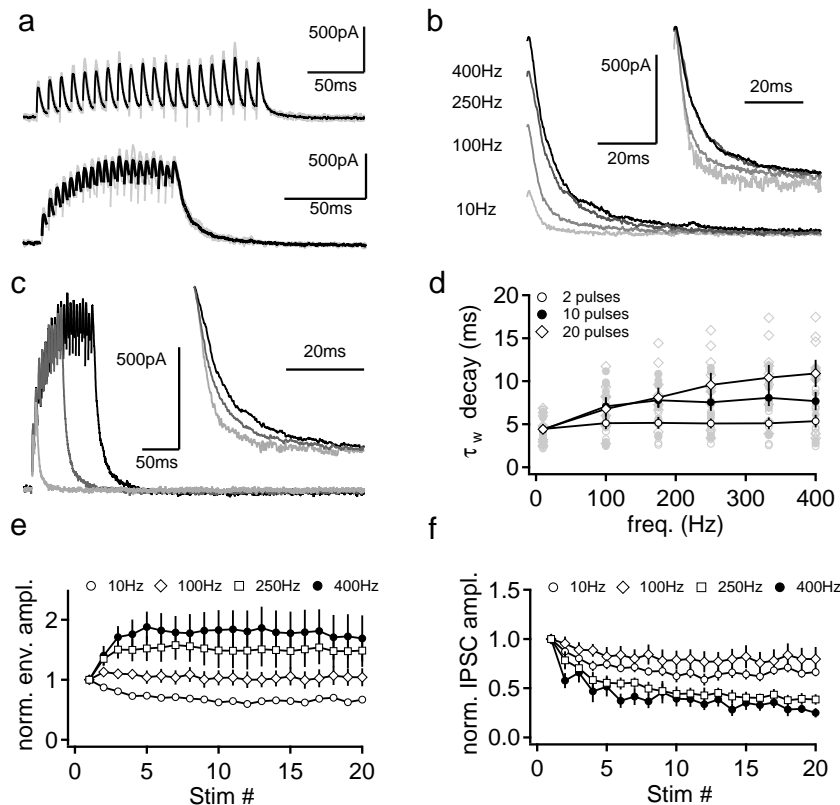


Figure 2: GABA decay kinetics are modulated by presynaptic activity. (a) IPSCs were evoked at stimulation frequencies of 10 - 400 Hz with 2 - 20 stimuli. Shown are responses to 20 pulses at 100 (top) and 250 Hz (bottom). Black traces are averages of the 4 single trials in gray. Artifacts are removed for clarity. (b) Aligned average decays after 20 pulses at different frequencies depict increased summation and prolonged decays for higher frequencies. Traces are averages of 4 repetitions. Inset shows last amplitude normalized traces. (c) IPSCs in response to 2, 10 and 20 pulses at 250 Hz. The inset shows last amplitude normalized traces. (d) Summary plot of decay time constants vs. stimulation frequency. The decays of the IPSCs after the stimulation trains were fitted with a bi-exponential function and a weighted decay time (τ_w) constant was computed. Single cells gray symbols ($n = 9$), averages black. (e) For the 20 pulse trains, the envelope amplitude was analyzed as total peak current after each individual stimulation pulse normalized to the first IPSC peak. (f) To estimate the synaptic depression during the train, the amplitude of the individual IPSCs was analyzed and normalized to the first IPSC amplitude. Data are given as mean \pm sem.

Hz (Fig. a,b) applied with 2, 10 or 20 pulses (Fig. 2c). The IPSC decay was similar for 2 pulses across all frequencies (4.4 ± 0.6 ms at 10 Hz to 5.5 ± 0.7 ms at 400 Hz, ANOVA $p = 0.95$, $n = 9$, Fig. 2d) as well as for all pulse numbers tested at 10 Hz (4.4 ± 0.6 ms for 2 and 20 pulses at 10 Hz, ANOVA $p = 0.995$, $n = 9$). However, an activity-dependent IPSC prolongation was observed with increasing pulse number at higher frequencies. At 400 Hz the IPSC decay increased twofold from 2 to 20

pulses (ANOVA $p = 0.004$, $n = 9$). This effect is even stronger with 2 mM extracellular calcium ($[Ca_o^{2+}]$, Fig. S1). Thus, even if the synaptic kinetics alone can not directly explain the whole range of PI duration *in vivo*^{3,5}, the activity-dependent prolongation of the GABAergic IPSCs might contribute to the generation of long lasting inhibition in the DNLL. At other inhibitory synapses, such a prolongation has been attributed to transmitter spillover, asynchronous release and desensitization with subsequent reopening of receptors^{11–15,24}.

Parallel to the IPSC prolongation, summation of IPSCs progressed during trains and increased with frequency. IPSCs did not sum at 10 Hz but displayed a 1.7 fold build-up during a 400 Hz train (Fig. 2e) even though individual IPSC amplitudes showed depression during the stimulation trains (Fig. 2f). Thus, repetitive stimulation leads to IPSC summation and prolongation in an activity-dependent manner, thereby enhancing the inhibitory power at higher frequencies.

Spillover and asynchronous release prolong the IPSC during high activity

If transmitter spillover between GABAergic synapses in the DNLL contributes to the IPSC prolongation, recruiting more presynaptic fibres should prolong the IPSC decay¹¹. To test this prediction, we evoked IPSCs of different amplitudes within the same cells (Fig. 3a). The decay after single stimuli was unaffected by the increase in amplitude (Fig. 3b, linear correlation coefficient $r = 0.09$, $p = 0.54$, $n = 50$ IPSCS from 18 cells). In contrast, IPSC decays after 400 Hz trains were prolonged with increasing final amplitude (Fig. 3b, linear correlation coefficient $r = 0.59$, $p = 0.00002$, $n = 57$ IPSCs from $n = 18$ cells), indicating an activity-dependent induction of spillover.

In case of spillover, transmitter still binds to receptors during the decaying phase of the IPSCs. This late binding should be reduced in the presence of a low-affinity GABA_A antagonist, like TPMPA, as such antagonists compete more efficiently for

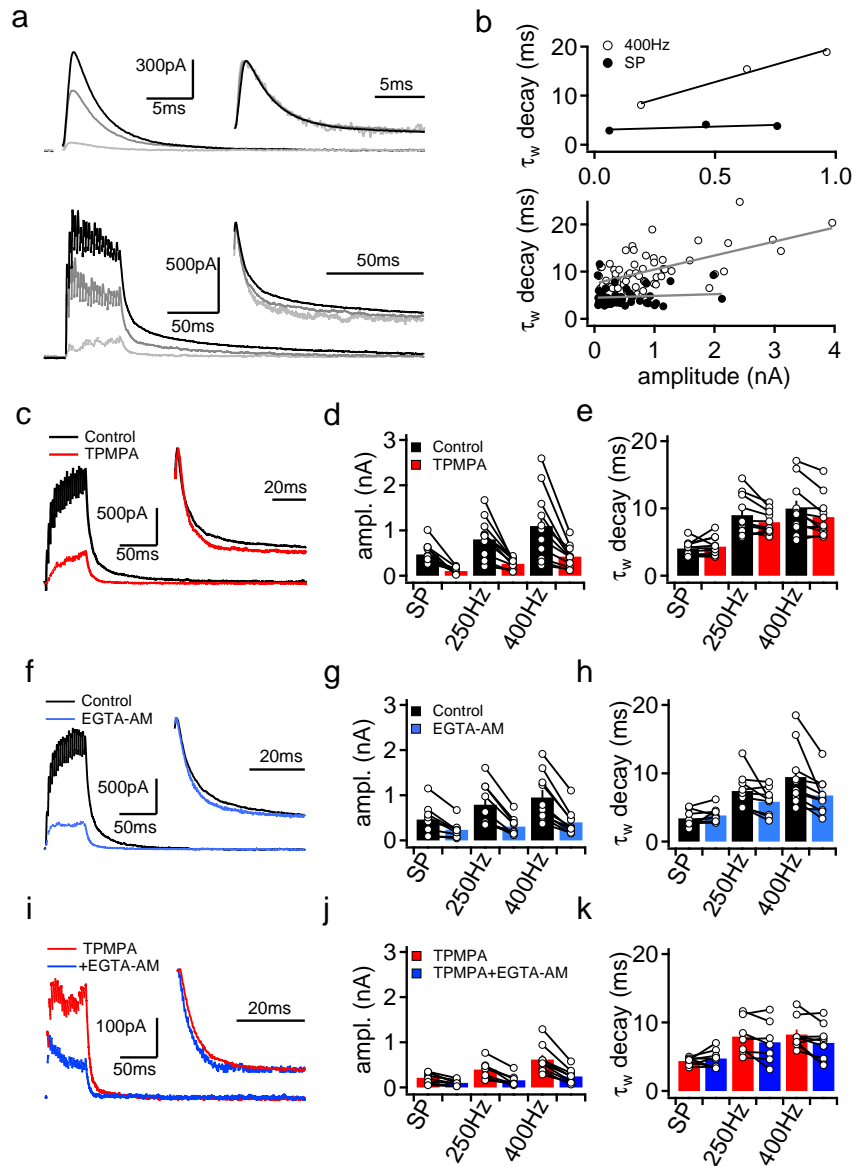


Figure 3: Spillover and asynchronous release contribute to activity-dependent IPSC prolongation. (a) GABAergic IPSCs evoked with different stimulation intensities in response to 1 (top) and 20 pulses at 400 Hz (bottom). Traces are averages of 2 - 5 repetitions. Different gray values signify different intensities. Insets: Amplitude normalized IPSCs. (b) Top: IPSC decays of the cell in (a) vs. IPSC amplitude. Bottom: IPSC decay vs. amplitude for pooled data (SP: 50 IPSCs in 17 cells correlation coefficient $r = 0.088$ $p = 0.54$; 400 Hz: 57 IPSCs in 18 cells, correlation coefficient $r = 0.59$, $p = 0.00002$) (c) IPSC before (black) and after (red) bath application of $200 \mu\text{M}$ TPMPA in response to 400 Hz stimulation. Traces are averages of 2 repetitions. Inset shows last amplitude normalized traces. (d) Effect of TPMPA on IPSC amplitudes of single (SP) and 20 pulses at 250 Hz and 400 Hz. Bars represent average values, open symbols single cells ($n = 11$, paired t-tests SP $p = 0.0003$, 250 Hz $p = 0.0009$, 400 Hz $p = 0.002$) (e) Effect of TPMPA on IPSC decay (paired t-tests SP $p = 0.43$, 250 Hz $p = 0.040$, 400 Hz $p = 0.016$). (f) IPSCs before (black) and after bath application of $200 \mu\text{M}$ EGTA-AM (blue). Traces are averages of 4 repetitions. (g) Effect of EGTA-AM on IPSC amplitude ($n = 9 - 10$, paired t-tests SP $p = 0.004$, 250 Hz $p = 0.0009$, 400 Hz $p = 0.0002$) and (h) IPSC decay (paired t-tests SP $p = 0.23$, 250 Hz $p = 0.054$, 400 Hz $p = 0.011$). (i) IPSCs recorded in $200 \mu\text{M}$ TPMPA (red) and after additional application of $200 \mu\text{M}$ EGTA-AM (blue). Traces are averages of 4 repetitions. (j) Effect of EGTA-AM on IPSC amplitude after pre-application of $200 \mu\text{M}$ TPMPA ($n = 7 - 9$, paired t-tests SP $p = 0.006$, 250 Hz $p = 0.001$, 400 Hz $p = 0.0002$) and (k) decay ($n = 7 - 9$, paired t-tests SP $p = 0.39$, 250 Hz $p = 0.13$ 400 Hz $p = 0.04$). Data are given as mean \pm sem.

binding sites when transmitter concentration is low^{11,12,25}. Thus, we tested whether TPMPA application accelerated IPSC decay (Fig. 3c-e). 200 μ M TPMPA reduced the IPSC amplitude of single pulses (to 20% of control) and after train stimulation (to 40% of control, Fig. 3d). In contrast to single pulses, the decay after train stimuli was significantly accelerated (from 10.0 ± 1.1 to 8.7 ± 0.9 ms at 400 Hz paired t-test $p = 0.016$, 9.0 ± 0.9 to 7.9 ± 0.6 ms at 250 Hz, $p = 0.04$, Fig. 3e). Additionally, TPMPA also reduced depression or even revealed facilitation (Fig. S2). This change in short-term plasticity might reflect relief from saturation or desensitization²⁶, but in any case reveals strong maintained transmitter release during trains. This strong release increases the probability of spillover of excess transmitter from the synaptic cleft during times of high presynaptic activity^{11,27}.

Having established the contribution of spillover, we next tested the role of asynchronous release during the activity-dependent IPSC prolongation. The presence of asynchronous release was assessed with application of the calcium chelator EGTA-AM to reduce the intracellular accumulation of calcium during trains²⁸. 200 μ M EGTA-AM effectively reduced IPSC amplitudes (to 50% for SP paired t-test $p = 0.004$; 39% for 250 Hz, $p = 0.0008$; 42% for 400 Hz, $p = 0.0002$, Fig. 3f,g), suggesting micro-domain coupling of synaptic release at GABAergic synapses in the DNLL²⁹. Additionally, EGTA-AM accelerated IPSC decays after train stimulation (Fig. 3h, from 7.4 ± 0.9 to 5.8 ± 0.7 ms at 250 Hz, paired t-test $p = 0.054$ and from 9.5 ± 1.4 to 6.7 ± 0.9 ms at 400 Hz, $p = 0.011$). As buffering calcium by EGTA-AM also reduces overall transmitter release and thus reduces spillover at the same time as asynchronous release, we repeated the application of EGTA-AM with prior block of the spillover component by TPMPA (Fig. 3i-k). Again, EGTA-AM decreased IPSC amplitude (Fig. 3l, SP to 47%, paired t-test $p = 0.0060$; 250 Hz to 40%, $p = 0.0014$; 400 Hz to 40%, $p = 0.0002$) and lead to a small acceleration in IPSC decay after train stimulations (Fig. 3m, from 7.9 ± 1.0 to 7.1 ± 1.2 ms at

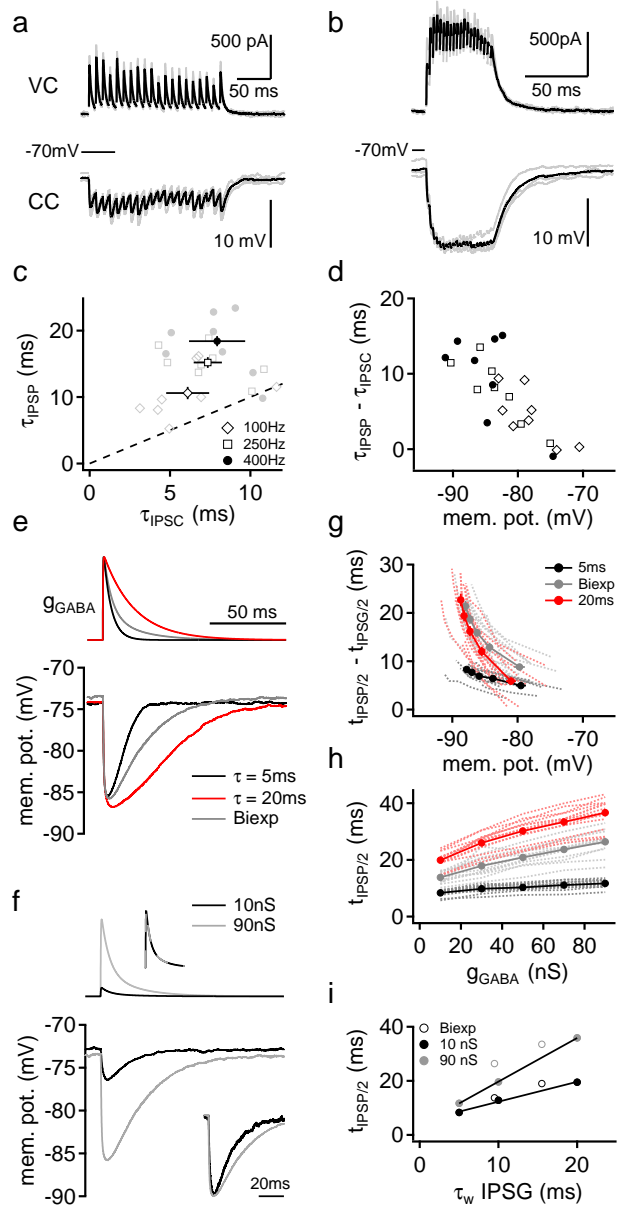
250 Hz, paired t-test $p = 0.13$; 8.2 ± 0.7 to 7.0 ± 0.9 at 400 Hz, paired t-test $p = 0.04$). From this additive action of TPMPA and EGTA-AM we conclude that both spillover and asynchronous release prolong the IPSC decay during increased presynaptic activity. Although the pharmacological alterations in the decay time constant described here appear small, their contribution to the PI will in the following be shown to be substantial.

Passive integration prolongs inhibition

How synaptic inputs influence the output of a neuron depends on how synaptic currents are converted into postsynaptic potentials. To investigate this conversion, the same GABAergic input was recorded in voltage- and current-clamp in a given DNLL neuron. These recordings allow to directly compare the decay time constants of IPSCs and IPSPs (Fig. 4a,b). IPSPs were generally slower than corresponding IPSCs (Fig. 4c, paired t-tests for 100 Hz $p = 0.009$, 250 Hz $p = 0.001$, 400 Hz $p = 0.002$). Yet, the prolongation was not equal for all stimuli, but seemed to be stronger for higher stimulation frequencies (Fig. 4c). Interestingly, the difference between IPSP and IPSC decay correlated with the peak membrane potential of the IPSPs (Fig. 4d, linear correlation $r = -0.79$, $p = 0.000005$). Thus, stronger hyperpolarization causes longer lasting IPSPs, an effect not explained by the intrinsic membrane properties of DNLL neurons (Fig. S3).

To investigate the dependence of IPSP duration on the membrane potential more systematically, we injected artificial conductances (IPSGs) with different amplitudes and decay time constants spanning the physiological parameter space. For the same maximal conductance, more slowly decaying conductance waveforms caused slower IPSPs (Fig. 4e). Strikingly, increasing the maximal conductance for IPSGs with the same decay time constant also prolonged the resulting IPSP (Fig. 4f) thereby leading to an equivalent relationship between IPSP time course

Figure 4: Integration of GABAergic IPSCs prolongs inhibition. **(a+b)** GABAergic inputs recorded in voltage- and current-clamp (VC, CC) in the same neuron. Traces show responses to 20 pulses at 100 Hz (a) and 400 Hz (b). Top: IPSCs, Bottom: IPSPs. Single trials in gray, averages in black. **(c)** IPSP vs. IPSC decay. Gray symbols represent single values, black symbols averages across $n = 8$ cells (paired t-tests IPSPs vs. IPSCs for 100 Hz $p = 0.009$, 250 Hz $p = 0.001$, 400 Hz $p = 0.002$). **(d)** The τ_w difference between IPSP and IPSC vs. membrane potential, linear correlation coefficient $r = -0.79$, $p = 0.000005$, fit not shown. **(e)** IPSPs in response to IPSGs (g_{GABA}) with different decay kinetics. Voltage traces are averages of 5 sweeps. The bi-exponential decay consists of $\tau_{fast} = 5$ ms, $\tau_{slow} = 20$ ms fractionfast = 0.7 ($\tau_w = 9.5$ ms) **(f)** IPSPs in response to the bi-exponentially decaying conductance with amplitudes of 10 and 90 nS. Inset shows amplitude normalized traces. **(g)** The difference in half-decay times of IPSPs/IPSGs ($t_{IPSP/2} - t_{IPSG/2}$) vs. membrane potential. Dotted lines represent single cells, solid lines and closed circles average data of $n = 14$ cells. **(h)** $t_{IPSP/2}$ vs. conductance amplitude, same data as in (g). **(i)** Average $t_{IPSP/2}$ vs. conductance decay (τ_w IPSG) for the 10 and 90 nS conductance, $n = 14$. Data are given as mean \pm sem.



and membrane potential as for the synaptic events (Fig. 4d,g). Thus, the correlation between IPSP prolongation and membrane potential is caused by a conductance amplitude dependent mechanism (Fig. 4h). This amplitude dependence was stronger for slower IPSGs (for $\tau = 5$ ms from 8.4 ± 0.3 ms at 10 nS to 11.7 ± 0.3 ms at 90 nS,

Kruskall-Wallis $p = 2e-08$; for $\tau = 20$ ms from 19.9 ± 0.8 ms at 10 nS to 36.7 ± 1.3 ms at 90 nS, Kruskal-Wallis $p = 2e-15$, $n = 14$). Thus, small differences in synaptic kinetics result in large differences in IPSP duration, at least for large conductance amplitudes (Fig. 4i). As IPSCs in the DNLL usually have bi-exponential decays, we also injected bi-exponentially decaying IPSPs. The resulting IPSPs are slower than expected from the linear relationship between mono-exponential IPSP and IPSP decays. Thus bi-exponentially decaying IPSCs might constitute an efficient way of prolonging the resulting IPSP.

To understand the mechanism underlying the conductance amplitude dependent IPSP prolongation we simulated a passive cell membrane with a capacitance, a leak conductance (g_{leak}) and a GABA conductance (g_{GABA}). Applying the same IPSP waveforms as in the conductance clamp measurements to this simple model (Fig. 5a) reproduced the experimental results unexpectedly well (Fig. 5b). This similarity implies that DNLL neurons integrate inhibition passively, which is in accord with the largely passive membrane dynamics between E_{GABA} and the resting membrane potential (Fig. S3). Therefore, active membrane properties are not required to cause the IPSP prolongation. The mechanism that underlies the IPSP prolongation is the non-linearity in the equilibrium potential between g_{GABA} and g_{leak} for increasing g_{GABA} (Fig. 5c). This relationship leads to a saturation of IPSP amplitude when increasing g_{GABA} and also influences IPSP dynamics. Because of the non-linearity, an equal change in g_{GABA} causes a smaller change in the equilibrium potential when initial g_{GABA} is high than when initial g_{GABA} is low. Even if the responses to the IPSPs are solely computed on the basis of the equilibrium potential, IPSPs are prolonged for larger g_{GABA} (Fig. 5d).

Experimentally, the non-linearity in the equilibrium potential can be demonstrated by applying slowly decaying linear conductance ramps (Fig. 5e). Here, an acceleration in the voltage response during the linearly decreasing g_{GABA} would

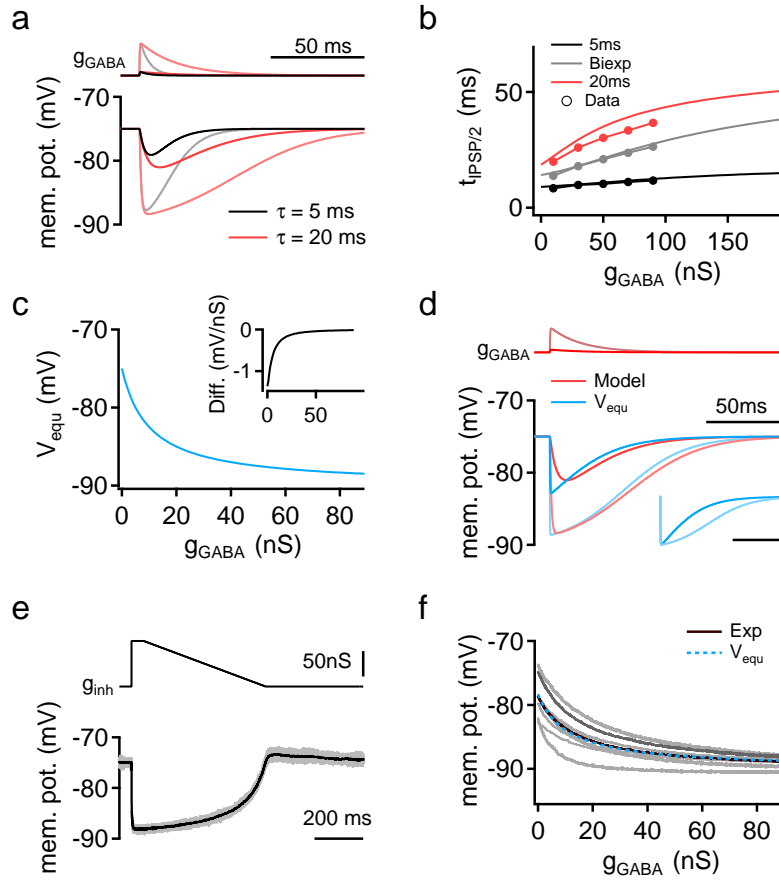


Figure 5: The equilibrium potential between resting and GABA conductance influences the IPSP shape **(a)** Simulations were performed with a simple circuit representing the passive membrane with capacitance $C_m = 80$ pF, $g_{leak} = 9.1$ nS, $E_{leak} = -75$ mV and a GABAergic conductance with $E_{GABA} = -90$ mV and variable g_{GABA} . Voltage traces are model responses to IPSPs with decay time constants of 5 (black and gray) and 20 ms (red and light red) and amplitudes of 10 and 90 nS. **(b)** The half-decay ($t_{IPSP/2}$) of the IPSPs vs. conductance amplitude (g_{GABA}). Continuous lines represent model responses, connected symbols average values of DNLL data. **(c)** Equilibrium potential ($V_{equ} = (g_{leak} * E_{leak} + g_{GABA} * E_{GABA}) / (g_{leak} + g_{GABA})$) between g_{GABA} and g_{leak} as a function of g_{GABA} . The inset shows dV_{equ}/dg_{GABA} . **(d)** Comparison of model response with response computed with equilibrium potential. Inset shows amplitude normalized traces computed with the equilibrium potential. **(e)** Response of a DNLL neuron to a conductance that ramps linearly from 90 nS to 0 nS in 1 s. The black trace represents average of 10 single trials in gray. **(f)** The voltage response during the ramp in **(e)** vs. the conductance of the ramp stimulus. Black trace represents the average of $n = 8$ neurons in gray, the neuron in **(e)** is shown in dark gray, the dotted line is the prediction computed with V_{equ} with average $g_{leak} = 10.9$ nS and $V_m = -78.3$ of the 8 recorded neurons.

be predicted from the equilibrium potential. Indeed, the voltage responses were markedly non-linear in all cases (Fig. 5f) and followed the prediction of the equilibrium potential calculated with the measured input resistance and resting potential of these neurons. Thus, this non-linearity within the equilibrium under-

lies the conductance amplitude dependent IPSP prolongation. These results suggest that integration of inhibition in DNLL neurons is largely passive and depict a general mechanism by which IPSPs can be prolonged in neurons with fast membrane time constants.

Inhibition *in vitro* matches PI duration

In the DNLL, GABAergic inhibition after a leading tone suppresses the response to a lagging tone that is excitatory when played alone³⁻⁵. As the contralateral DNLL is not persistently active to provide continuous inhibitory input for the tens of milliseconds of PI^{5,30}, the inhibition has to be effective for a long time after the last presynaptic AP. Accordingly, we asked whether such a long lasting inhibitory action can be achieved by synaptically evoked inhibition in our slice preparation. Evoked GABAergic IPSPs were paired with an injection of an excitatory conductance train that was just supra-threshold when presented alone (Fig 6a). To determine the underlying GABAergic conductances, we recorded IPSCs to identical stimulation at different membrane potentials (Fig. 6b). Effectiveness of AP suppression was quantified as the time of 50% AP probability after the last stimulation pulse (Fig 6a). On average, APs were suppressed for 22 ± 3 ms by a conductance of 44.9 ± 6.5 nS with a τ_w of 8.8 ± 1.0 ms ($n = 9$). The range of AP suppression of 13 to 38 ms fits well to the PI *in vivo*³⁻⁵. Analysis of the stimulated conductances indicated that their decay and amplitude might determine AP suppression (Fig. 6c, linear correlation coefficient decay $r = 0.7$, $p = 0.005$, amplitude $r = 0.3$, $p = 0.3$). To systematically investigate the contributions of these conductance parameters on AP suppression, injections of artificial conductances resembling a typical IPSC train with variable decays were used (Fig. 6d). Increasing the conductance amplitude for a given decay caused longer and more effective AP suppression (Fig. 6d,e, eg. from 16.6 ± 2.7 at 10 nS to 56.7 ± 3.6 ms at 90 nS for $\tau = 20$ ms, $n =$

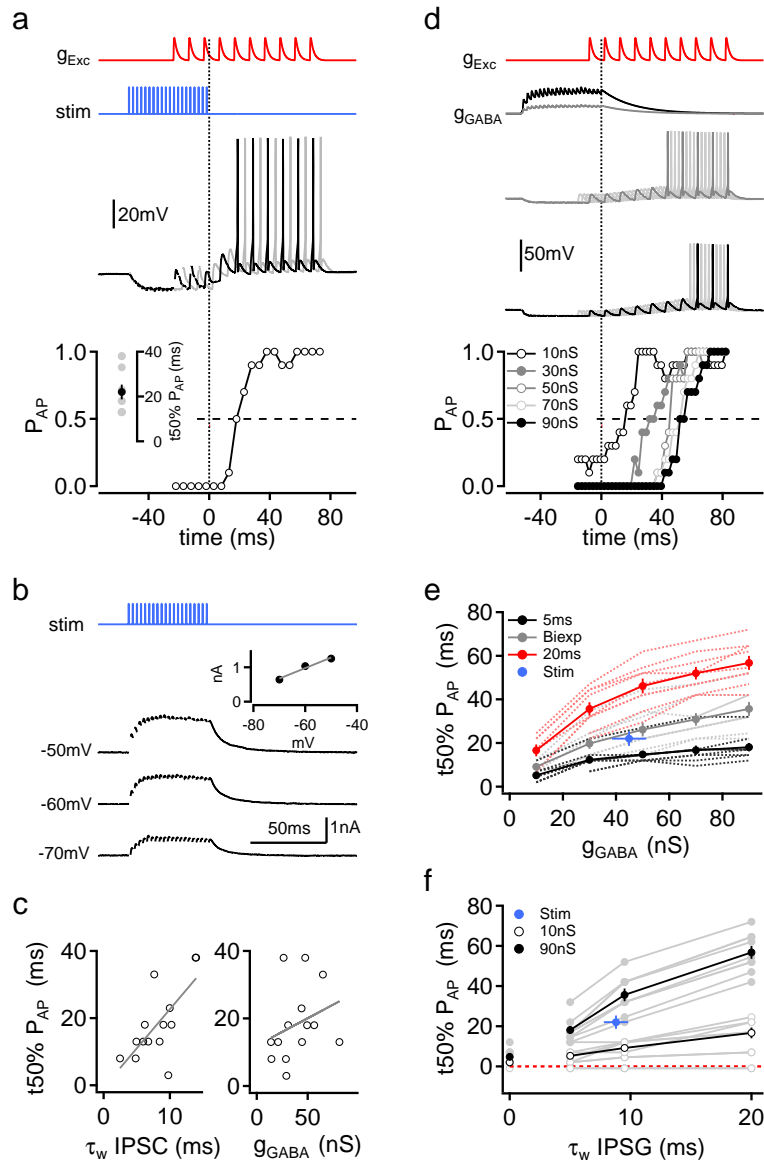


Figure 6: Suppression of APs by GABAergic inhibition in vitro matches PI in vivo. **(a)** The excitatory conductance (g_{exc}) was scaled to evoke APs with every EPSP pulse and shifted 5 ms relative to the GABAergic input stimulated with 20 pulses at 400 Hz (stim). AP probability (P_{AP}) was computed from 10 repetitions at each time shift. Inset: maximal time of 50% AP suppression ($t_{50\%P_{AP}}$) for $n = 10$ neurons. **(b)** g_{GABA} determined from a linear fit to IPSC amplitudes recorded at different holding potentials. Traces are averages of 4 repetitions. **(c)** $t_{50\%P_{AP}}$ vs. decay and g_{GABA} for 14 conditions in 10 neurons. **(d)** AP suppression by artificial g_{GABA} scaled to final amplitudes of 10 - 90 nS with decays time constants of 5 - 20 ms and $E_{GABA} = -90$ mV. Excitation was shifted relative to inhibition in 2.5 ms increments. Traces show AP suppression by 30 and 90 nS with $\tau = 20$ ms. P_{AP} for $\tau = 20$ ms and g_{GABA} from 10 to 90 nS. **(e)** $t_{50\%P_{AP}}$ for different decays vs. g_{GABA} . Dotted lines represent single cells, solid lines average data, $n = 9$. The blue circle represents average of stimulated GABA input, with $\tau_w = 8.8 \pm 1.0$ ms. **(f)** $t_{50\%P_{AP}}$ for 10 and 90 nS vs. conductance decay, $n = 10$ for 0 ms decay, $n = 9$ for all other decays. Kruskal-Wallis for 10 nS $p = 0.000004$, for 90 nS $p = 4 \times 10^{-15}$. Average stimulated value in blue with $g_{GABA} = 44.9 \pm 6.5$ nS. Data are given as mean \pm sem.

9, Kruskal-Wallis $p = 0.0000002$). Slower decays generally produced longer AP suppression (eg. 14.8 ± 1.6 for $\tau = 5$ ms vs. 46.2 ± 3.4 ms for $\tau = 20$ ms at 50 nS, Kruskal-Wallis $p = 0.00005$). The difference in duration of AP suppression between the different underlying conductance decays was enhanced for large conductance amplitudes (Fig. 6f). A conductance waveform with instantaneous decay caused only very short AP suppression (4.8 ± 1.1 ms at 90 nS) suggesting only a minor role for the membrane time constant in PI. From the comparison of AP suppression by synaptically stimulated and artificial inhibition (Fig. 6e,f) we propose that the conductance clamp technique is an adequate tool to study the integration of inhibition in DNLL neurons. Taken together, an AP suppression that matches PI *in vivo* can be achieved *in vitro*. Furthermore, these experiments suggest that the amplitude and the decay time constants of the inhibitory conductance, which we have shown to influence the IPSP shape, also determine the duration of AP suppression.

Given the large variability of IPSC decays in the DNLL ($\tau_w = 3 - 25$ ms), we tested the range of possible AP suppression using conductances with the fastest and the slowest decaying phase (Fig. 7a,b). The slow decay produced a suppression of more than the sampled interval of 82 ms at 90 nS in 7 of 10 neurons. The fastest decay suppressed APs for only 15 ± 1 ms. Hence, prolonging synaptic mechanisms are crucial to generate an inhibitory conductance that can suppress APs for a physiologically relevant duration. To assess the effect of spillover and asynchronous release on PI *in vitro*, we compared the effect of conductance waveforms reflecting the IPSC kinetics under control conditions and after treatment of TPMPA and EGTA-AM (Control $\tau_w = 10.1$ ms, TPMPA $\tau_w = 8.9$ ms, EGTA-AM $\tau_w = 6.9$ ms, Fig. 7c). The different waveforms produced similar AP suppression for a 10 nS conductance (siControl 5.6 ± 1.0 ms; siTPMPA 5.1 ± 1.0 ms; siEGTA 5.1 ± 1.0 ms, Kruskal Wallis $p = 0.81$), consistent with the finding that decay has little effect on AP suppression for small conductances (Fig. 7d). For a 90 nS conductance AP

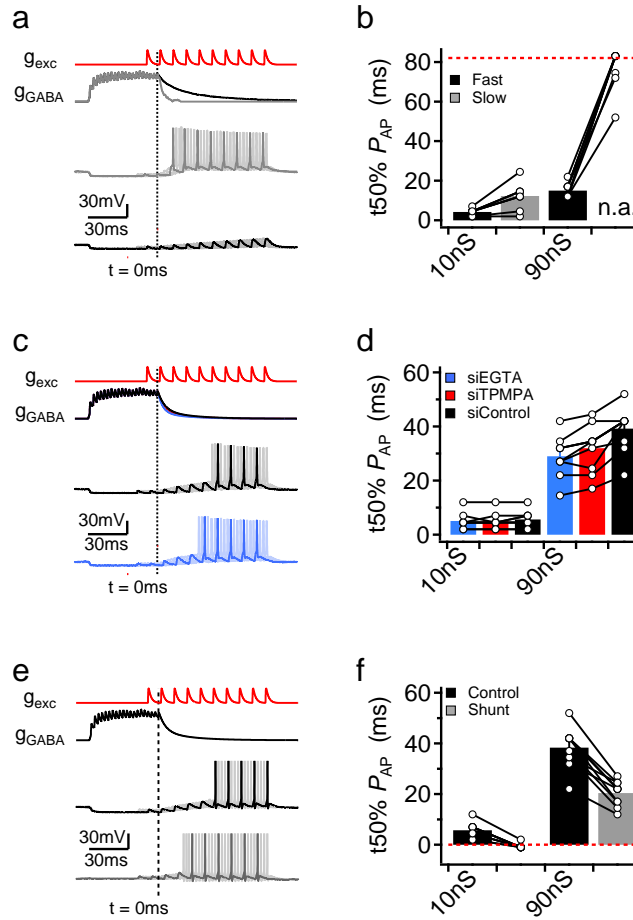


Figure 7: Interaction of synaptic and integrational properties determine the PI duration. **(a)** AP suppression by the fastest recorded IPSC decay in gray ($\tau_w = 3.4$ ms) and the slowest ($\tau_w = 24.8$) decay in black for $g_{GABA} = 90$ nS. **(b)** $t50\%P_{AP}$ for $n = 10$ neurons. $t50\%P_{AP}$ of the slow decay time constant was out of the sampled range (indicated by red dotted line) for 7 of 10 neurons. Therefore no average was computed. Bars represent average values, open circles single cells. **(c)** Bi-exponential conductances simulating mean effects of TPMPA in red (siTPMPA, $\tau_w = 8.4$ ms) and EGTA in blue (siEGTA, $\tau_w = 6.9$ ms) were compared with a decay simulating control conditions in black (siControl $\tau_w = 10.1$ ms). Traces show responses to siControl and siEGTA at $g_{GABA} = 90$ nS. **(d)** $t50\%P_{AP}$ for $n = 10$ neurons. Kruskal-Wallis for 10 nS data $p = 0.81$, for 90 nS data $p = 0.036$, Dunn-Holland-Wolfe significantly different pair siEGTA vs. siControl. **(e)** For siControl E_{GABA} was set to the resting potential of the neuron to produce shunting inhibition. Traces show responses to identical g_{GABA} (siControl, 90nS) with either hyperpolarizing (black) or shunting E_{GABA} (gray). **(f)** $t50\%P_{AP}$ for $n = 11$ neurons. The 10 nS g_{GABA} in shunting condition failed to reduce P_{AP} below 50% in 10 out of 11 neurons and made computation of $t50\%P_{AP}$ impossible (indicated by values below zero, red dotted line). Paired t-test for 90 nS data $p = 9e-07$. Data are given as mean \pm sem.

suppression differed significantly (siEGTA 29.0 ± 2.4 ms, siTPMPA 32.0 ± 2.7 ms, siControl 39.3 ± 2.5 ms, $n = 10$ Kruskal Wallis $p = 0.036$). The ~ 3 ms difference in decay times between siControl and siEGTA translated into a ~ 10 ms difference in

AP suppression. Thus, little differences in IPSC decay can have large effects on AP suppression. The activity-dependent prolongation of the IPSC is therefore ideally suited to adjust the AP suppression time in the DNLL.

Next, we asked whether hyperpolarization due to the low E_{GABA} in the DNLL is crucial for the PI. AP suppression by an identical GABA conductance (siControl) was assessed once with hyperpolarizing and once with shunting inhibition (Fig. 7e,f). For a 10 nS conductance, shunting inhibition failed to effectively suppress APs in 10 out of 11 cells. At 90 nS, shunting inhibition reduced AP suppression from 38.4 ± 1.3 ms to 20.4 ± 1.4 ms ($n = 11$, paired t-test $p = 9e-07$) compared with hyperpolarizing inhibition. Thus, the negative E_{GABA} works together with the passive integration mechanism to produce long lasting hyperpolarizing IPSPs that effectively suppresses APs for a duration matching PI *in vivo*.

Discussion

Synaptic and integrative properties of DNLL neurons *in vitro* lead to AP suppression in a graded, activity-dependent manner - matching the *in vivo* description of PI and therefore likely represent the cellular basis of the precedence effect¹⁻⁵. To achieve PI, the interplay between the activity-dependent IPSC prolongation by spillover and asynchronous release and the passive integration based on a hyperpolarizing inhibition are crucial. This interplay is required as the fast kinetics of a single IPSC and membrane time constants in the mature DNLL cannot explain the duration of PI *in vivo*¹⁸. Our mechanistic description furthermore explains the sound intensity dependence of PI³⁻⁵. In general, the interactions between different cellular mechanisms described here might be relevant for a dynamic control of inhibition in other fast spiking neurons.

Both spillover and asynchronous release contribute to the IPSC prolongation in an activity-dependent manner in the DNLL. Consistent with GABA spillover onto

neighboring or extra-synaptic receptors the IPSC decay depended on the stimulation frequency and amplitude and accelerated after application of the low-affinity antagonist TPMPA^{9,11,12,25,27,31–33}. Additionally, a facilitation of GABAergic IPSCs was revealed under TPMPA indicating saturation and/or desensitization of receptors^{11,12,26}. This facilitation of GABAergic IPSCs indicates a shift from low to high release probability during strong synaptic activity. It is safe to assume that the spillover-supporting facilitation is driven by accumulation of presynaptic calcium. This accumulation links the basis for spillover with the increase of asynchronous release during high frequency stimulation that was revealed by applying EGTA-AM. Buffering the internal calcium with EGTA-AM also reduced IPSC amplitudes in the DNLL. This finding indicates a rather loose micro-domain coupling between calcium influx and vesicle release²⁹. Loose micro-domain coupling is ideally suited to support calcium build-up and therefore facilitation as well as asynchronous release and is thus a basis for the generation of the activity-dependent prolongation of GABAergic IPSCs in DNLL neurons.

The duration of inhibitory action not only depends on IPSC kinetics but also on their integration. In contrast to other neurons in the auditory brainstem that express prominent I_h and/or low threshold calcium currents^{34–37}, the membrane properties of DNLL neurons are largely passive between the resting potential and E_{GABA} . Thus, in DNLL neurons, hyperpolarizing inhibition is passively integrated. If integration is passive and the membrane dynamics are slower than the synaptic kinetics, the difference between IPSC decay time constants is reduced resulting in slow IPSPs with little variation¹⁷. Conversely, IPSC kinetics dominate the IPSP shape if they are slower than the membrane dynamics and their temporal differences are maintained^{38,39}. Here, however, we find that IPSPs can decay more slowly than either membrane or synaptic decay time constants, and the temporal differences between underlying IPSCs are even enhanced. This dynamic prolongation is made

possible by the similarity between the IPSC decay and the membrane time constant and is caused by the non-linearity in the equilibrium potential between g_{leak} and g_{GABA} . During passive integration of strong hyperpolarizing inhibition this non-linearity influences the decay of the IPSP, given that the membrane time constant is not substantially slower than the synaptic conductance decay. On the circuit level this mechanism can be exploited in two ways. First, the number of simultaneously activated presynaptic inhibitory neurons defines the size of the compound inhibitory conductance and therefore influences the time course of the IPSP. Second, a frequency-dependent build-up in synaptic conductance of a single presynaptic neuron prolongs the IPSP. Therefore, an increase in sound intensity, which recruits more presynaptic neurons and leads to higher firing rates^{40,41} most efficiently exploits the passive integration to prolong the inhibitory action of the IPSP. As both the amplitude and the decay of g_{GABA} in the DNLL depend on the presynaptic activity level, an integration mechanism that is sensitive to exactly these parameters seems ideal to enable a graded encoding of stimulus strength.

The supra-threshold responses in the DNLL are, like the IPSP duration, affected by the decay and amplitude of g_{GABA} . The high variability in the activity-dependent IPSC decay in our data leads to a wide range of possible durations of AP suppression. This variability might constitute specific adaptations of synaptic properties in different cells, consistent with the large heterogeneity of PI duration *in vivo*³⁻⁵. To explain at least the upper 50% of *in vivo* PI durations the activity-dependent IPSC prolongation is required³⁻⁵. Spillover and asynchronous release add substantially to this activity-dependent AP suppression, despite their apparently small effects on the level of IPSC decays. Thus, these synaptic mechanisms play a crucial physiological role in generating PI. Furthermore, hyperpolarizing inhibition generates far longer and more effective AP suppression than mere shunting inhibition. Taken together, inhibition in the DNLL is adjusted to the physiologically relevant duration

by passive integration of hyperpolarizing inhibition with activity-dependent synaptic kinetics.

Together with previous work^{18,19}, our findings elucidate the cellular physiology of the neuronal circuitry generating PI. Incoming excitatory signals of ascending binaural pathways are amplified in an NMDA-dependent manner generating high firing rates in DNLL neurons^{18,19,42}. The high firing rates in turn prolong the synaptic output of these neurons by pre- and postsynaptic mechanisms, based on asynchronous release and spillover. This activity-dependent prolongation is enhanced by the passive integration of hyperpolarizing GABA_A-receptor mediated IPSCs in DNLL neurons. These interacting mechanisms allow to shift the sensory processing time scale from the microsecond to the millisecond level from the superior olivary complex to the DNLL and the inferior colliculus. Overall, the properties of this GABAergic input combined with the reciprocal inhibition between the two hemispheres implement a flexible, context-dependent gating mechanism for the categorization of echoes^{43,44}.

Methods

Preparation

Slice preparation followed the same procedure as described previously¹⁸. Mongolian gerbils (*Meriones unguiculatus*) of postnatal day (P) 18 - 32 (Fig. 1) or P 30 - 36 (all other recordings) were first anesthetized and then decapitated and the brains were removed in cold dissection solution containing (in mM) 50 - 120 sucrose, 25 NaCl, 25 NaHCO₃, 2.5 KCl, 1.25 Na₂HPO₄, 3 MgCl₂, 0.1 CaCl₂, 25 glucose, 0.4 ascorbic acid, 3 myo-inositol and 2 Na-pyruvate, pH 7.4 when bubbled with carbogen (95% O₂ and 5% CO₂). 200 μm thick transverse slices containing the DNLL were cut with a vibratome (VT1200S Leica, Wetzlar, Germany). Slices

were incubated for 45 minutes at 36°C in extracellular recording solution (same as dissection solution but with 125 mM NaCl, no sucrose, 1.2 mM CaCl₂ and 1 mM MgCl₂). All recordings were carried out at near physiological temperature (34-36°C). Cells were visualized and imaged with a microscope (BX50WI, Olympus, Hamburg, Germany) equipped with gradient contrast illumination (Luigs and Neumann, Ratingen, Germany) and a TILL Photonics system (Gräfelfing, Germany) composed of an Imago CCD-camera, a Poly-IV monochromator, and its control unit.

Electrophysiology

Recordings were performed using an EPC10/2 amplifier (HEKA Elektronik, Lambrecht, Germany). Data were acquired at 20-50 kHz and filtered at 3 kHz. In whole-cell or perforated-patch current-clamp, the bridge balance was set to 100% after estimation of the series resistance and was monitored repeatedly during recordings. Series resistance in whole-cell voltage-clamp was compensated to a residual 3 MΩ. For current-clamp and some voltage-clamp recordings the internal recording solution consisted of (in mM): 145 K-gluconate, 4.5 KCl, 15 HEPES, 2 Mg-ATP, 2 K-ATP, 0.3 Na₂-GTP, 7.5 Na₂-Phosphocreatine, 5 K-EGTA (pH 7.3). For all other voltage-clamp recordings the internal solution consisted of (in mM): 140 Cs-gluconate, 15 HEPES, 3 Mg-ATP, 0.3 Na₂-GTP, 5 Na₂-Phosphocreatine, 5 Cs-EGTA, 2.5 QX-Cl, 2 TEA-Cl (pH 7.3). A liquid junction potential of 17 mV was calculated and corrected for according to Barry (1994)⁴⁵, with a custom written IGOR Pro script on the basis of ion concentrations rather than their activity. 100 μM Alexa 488 or 568 were added to the internal solution to control for cell type and location. For perforated-patch recordings the pipette was tip-filled with a solution containing (in mM) 130 KCl, 10 HEPES, 5 NaCl, 3 MgCl₂, 0.5 K-EGTA and then back filled with the same solution containing 50 μg Gramicidin A (Merck, Darmstadt,

Germany) and 100 μ M Alexa 568. Fluorescence was monitored repeatedly to detect break-through of the membrane. Recordings were started usually 10 - 15 min after formation of the gigaseal when the access resistance decreased below 50 M Ω and canceled immediately when a breakthrough was detected by either fluorescence inside the cell or a sudden change in GABAergic current.

Synaptic GABAergic currents were stimulated using a concentric bipolar stimulation electrode (MCE-100X, Scientific Products or CBASD75, FHC) placed in the commissure of Probst with a biphasic voltage deflection of 200 μ s total duration triggered by the EPC10/2, conveyed and adjusted with a stimulator unit (model 2100, A-M Systems, Scientific Products) and isolated pharmacologically in the presence of 0.5 μ M Strychnine, 20 μ M DNQX and 10 μ M R-CPP. GABAergic currents were measured at holding potentials of -75 (Fig. 2c-h) or -50 mV (all other recordings unless otherwise stated). Simulated conductances were injected with an analogue conductance amplifier (SM-1, Cambridge Conductance, Royston, UK) and the reversal potential of inhibition and excitation were set to the measured -90 and estimated 0 mV respectively. Conductance waveforms were either constructed artificially in IGOR Pro (WaveMetrics, Lake Oswego, OR) or GABAergic currents were cut, scaled and re-sampled where necessary. Gaps in recorded IPSCs due to artifact removal (<1 ms) were filled with linear extrapolations. Constructed waveforms had decays with mono-exponential τ s of 5, 10 and 20 ms or bi-exponential decay time constants constructed from different contributions of τ s of 5 and 20 ms in Figures 4-6 and following the mean values after pharmacological manipulation (Fig. 3) in Figure 7. Excitatory conductances were constructed according to the AMPA kinetics in P23 - 26 animals¹⁸ with decay time constants of $\tau = 2$ ms. For AP suppression experiments the conductance amplitude was scaled to be just supra-threshold in evoking one AP with every EPSC waveform. If paired with synaptically evoked GABAergic input, AP probability was sampled every 5 ms with

10 repetitions at 2 time-shifts with an inter-trial interval of 15 s. If paired with injection of artificial inhibitory conductance AP probability was sampled every 2.5 ms with 10 repetitions at 4 time-shifts and inter-trial intervals of 2 s. All waveforms were scaled and saved as HEKA templates using a customary modified PPT script (Mendez and Würriehausen, Göttingen).

Data Analysis

Electrophysiological data were analyzed with custom written procedures in IGOR Pro. Time constant, input resistance and capacitance of the neurons were determined as described previously¹⁸ from the deflection of and an exponential fit to the voltage response response to small, hyperpolarizing current injections. The internal chloride concentration was calculated from the GABA reversal potential using the Nernst equation.

The voltage current relationship was measured for current injections from -250 to 800 pA in 50 pA increments. Peak and steady state values of the hyperpolarizing responses were analyzed and the off responses were fitted with a mono-exponential function. Firing rates are given as AP number/time. Adaptation was analyzed at half maximal frequency in the range of up to 800 pA as interspike interval (ISI) vs ISI number. The weighted decay time constant for the IPSC/Ps was derived from a bi-exponential function fit to the average data of 2-4 traces and calculated according to $\tau_w = \frac{\tau_1 \times \text{amplitude}(\tau_1)}{\text{amplitude}} + \frac{\tau_2 \times \text{amplitude}(\tau_2)}{\text{amplitude}}$. As IPSPs for very slow and large artificial conductances could not be fitted with an exponential function, the time from peak IPSP/G to their half maximal amplitude was analyzed. To investigate build-up during trains of stimulated IPSCs, the envelope amplitude was analyzed as total peak current after each individual stimulation pulse normalized to the first IPSC peak. To estimate the synaptic depression during the train, the amplitude of the individual IPSCs was analyzed and normalized to the first IPSC amplitude. AP probability was

computed from 10 repetitions at each time shift. To get a robust measure to for the duration of AP suppression, the time to 50% AP suppression ($t_{50\%P_{AP}}$) was measured from the peak of conductance injection or from 1 ms after the last stimulation pulse until P_{AP} crossed 0.5. According to Ohms law, conductance amplitude was estimated from the slope of a linear fit to the IPSC amplitudes recorded at different holding potentials.

Statistical Analysis

Data are presented as mean \pm sem. We used the Jarque- Bera test to test for normal distribution and the Bartlett's test to test for equal variances. Significance was determined with either paired or unpaired Student's t-test, Wilcoxon rank-sum test or for more than two groups of samples with either ANOVA or Kruskal-Wallis followed by a post-hoc Tukey-Kramer or Dunn-Holland-Wolfe test.

Model circuit

A passive circuit was modeled in Igor Pro according to $\frac{dV}{dt} = g_{GABA} \times (V - E_{GABA}) - g_{leak} \times (V - E_{leak}) / C_m$ with $C_m = 80$ pF, $g_{leak} = 9.1$ nS, $E_{leak} = -75$ MOhm, and variable g_{GABA} as indicated with $E_{GABA} = -90$ mV The equilibrium potential between g_{leak} and g_{GABA} was computed with $V_{equ} = (g_{leak} \times E_{leak} + g_{GABA} \times E_{GABA}) / (g_{leak} + g_{GABA})$.

References

- 1 Litovsky, R. Y., Colburn, H. S., Yost, W. A. & Guzman, S. J. : The precedence effect. *J Acoust Soc Am* **106**, 1633-1654 (1999)
- 2 Yang, L. & Pollak, G. D. : The roles of GABAergic and glycinergic inhibition on binaural processing in the dorsal nucleus of the lateral lemniscus of the mustache bat. *J Neurophysiol* **71**, 1999-2013 (1994)
- 3 Yang, L. & Pollak, G. D. : Features of ipsilaterally evoked inhibition in the dorsal nucleus of the lateral lemniscus. *Hear Res* **122**, 125-141 (1998)
- 4 Burger, R. M. & Pollak, G. D. : Reversible inactivation of the dorsal nucleus of the lateral lemniscus reveals its role in the processing of multiple sound sources in the inferior colliculus of bats. *J Neurosci* **21**, 4830-4843 (2001)
- 5 Pecka, M., Zahn, T. P., Saunier-Rebori, B., Siveke, I., Felmy, F., Wiegrebe, L., Klug, A., Pollak, G. D. & Grothe, B. : Inhibiting the inhibition: a neuronal network for sound localization in reverberant environments. *J Neurosci* **27**, 1782-1790 (2007)
- 6 Fatt P., P. & Katz, B. : The effect of inhibitory nerve impulses on a crustacean muscle fibre. *J Physiol* **121**, 374-389 (1953)
- 7 Coombs, J. S., Eccles, J. C. & Fatt, P. : The inhibitory suppression of reflex discharges from motoneurons. *J Physiol* **130**, 396-413 (1955)
- 8 Alger, B. E. & Nicoll, R. A. : Pharmacological evidence for two kinds of GABA receptor on rat hippocampal pyramidal cells studied in vitro. *J Physiol* **328**, 125-141 (1982)
- 9 Overstreet, L. S. & Westbrook, G. L. : Synapse density regulates independence at unitary inhibitory synapses. *J Neurosci* **23**, 2618-2626 (2003)
- 10 Farrant, M. & Nusser, Z. : Variations on an inhibitory theme: phasic and tonic activation of

GABA(A) receptors. *Nat Rev Neurosci* **6**, 215-229 (2005)

11 Balakrishnan, V., Kuo, S. P., Roberts, P. D. & Trussell, L. O. : Slow glycinergic transmission mediated by transmitter pooling. *Nat Neurosci* **12**, 286-294 (2009)

12 Tang, Z.-Q. & Lu, Y. : Two GABAA responses with distinct kinetics in a sound localization circuit. *J Physiol* **590**, 3787-3805 (2012)

13 Lu, T. & Trussell, L. O. : Inhibitory transmission mediated by asynchronous transmitter release. *Neuron* **26**, 683-694 (2000)

14 Hefft, S. & Jonas, P. : Asynchronous GABA release generates long-lasting inhibition at a hippocampal interneuron-principal neuron synapse. *Nat Neurosci* **8**, 1319-1328 (2005)

15 Best, A. R. & Regehr, W. G. : Inhibitory regulation of electrically coupled neurons in the inferior olive is mediated by asynchronous release of GABA. *Neuron* **62**, 555-565 (2009)

16 Eccles, J. C. : The Ferrier Lecture: The Nature of Central Inhibition. *Proceedings of the Royal Society of London* **153**, 445-476 (1961) 17 Hardie, J. B. & Pearce, R. A. : Active and passive membrane properties and intrinsic kinetics shape synaptic inhibition in hippocampal CA1 pyramidal neurons. *J Neurosci* **26**, 8559-8569 (2006)

18 Ammer, J. J., Grothe, B. & Felmy, F. : Late postnatal development of intrinsic and synaptic properties promotes fast and precise signaling in the dorsal nucleus of the lateral lemniscus. *J Neurophysiol* **107**, 1172-1185 (2012)

19 Porres, C. P., Meyer, E. M. M., Grothe, B. & Felmy, F. : NMDA currents modulate the synaptic input-output functions of neurons in the dorsal nucleus of the lateral lemniscus in Mongolian gerbils. *J Neurosci* **31**, 4511-4523 (2011)

20 Vida, I., Bartos, M. & Jonas, P. : Shunting inhibition improves robustness of gamma oscillations in hippocampal interneuron networks by homogenizing firing rates. *Neuron* **49**, 107-117 (2006)

-
- 21 Friauf, E., Rust, M. B., Schulenburg, T. & Hirtz, J. J. : Chloride cotransporters, chloride homeostasis, and synaptic inhibition in the developing auditory system. *Hear Res* **279**, 96-110 (2011)
- 22 Houston, C. M., Bright, D. P., Sivilotti, L. G., Beato, M. & Smart, T. G. : Intracellular chloride ions regulate the time course of GABA-mediated inhibitory synaptic transmission. *J Neurosci* **29**, 10416-10423 (2009)
- 23 Seidl, A. H. & Grothe, B. : Development of sound localization mechanisms in the mongolian gerbil is shaped by early acoustic experience. *J Neurophysiol* **94**, 1028-1036 (2005)
- 24 Jones, M. V. & Westbrook, G. L. : Desensitized states prolong GABAA channel responses to brief agonist pulses. *Neuron* **15**, 181-191 (1995)
- 25 Szabadics, J., Tamás, G. & Soltesz, I. : Different transmitter transients underlie presynaptic cell type specificity of GABAA,slow and GABAA,fast. *Proc Natl Acad Sci U S A* **104**, 14831-14836 (2007)
- 26 Chanda, S. & Xu-Friedman, M. A. : A low-affinity antagonist reveals saturation and desensitization in mature synapses in the auditory brain stem. *J Neurophysiol* **103**, 1915-1926 (2010)
- 27 Satake, S., Inoue, T. & Imoto, K. : Paired-pulse facilitation of multivesicular release and intersynaptic spillover of glutamate at rat cerebellar granule cell-interneurone synapses. *J Physiol* **590**, 5653-5675 (2012)
- 28 Atluri, P. P. & Regehr, W. G. : Delayed release of neurotransmitter from cerebellar granule cells. *J Neurosci* **18**, 8214-8227 (1998)
- 29 Eggermann, E., Bucurenciu, I., Goswami, S. P. & Jonas, P. : Nanodomain coupling between Ca²⁺ channels and sensors of exocytosis at fast mammalian synapses. *Nat Rev Neurosci* **13**, 7-21 (2012)
- 30 Siveke, I., Pecka, M., Seidl, A. H., Baudoux, S. & Grothe, B. : Binaural response properties of low-frequency neurons in the gerbil dorsal nucleus of the lateral lemniscus. *J Neurophysiol* **96**,

1425-1440 (2006)

31 Diamond, J. S. : Neuronal glutamate transporters limit activation of NMDA receptors by neurotransmitter spillover on CA1 pyramidal cells. *J Neurosci* **21**, 8328-8338 (2001)

32 DiGregorio, D. A., Nusser, Z. & Silver, R. A. : Spillover of glutamate onto synaptic AMPA receptors enhances fast transmission at a cerebellar synapse. *Neuron* **35**, 521-533 (2002)

33 Crowley, J. J., Fioravante, D. & Regehr, W. G. : Dynamics of fast and slow inhibition from cerebellar golgi cells allow flexible control of synaptic integration. *Neuron* **63**, 843-853 (2009)

34 Bal, R. & Oertel, D. : Hyperpolarization-activated, mixed-cation current (I_h) in octopus cells of the mammalian cochlear nucleus. *J Neurophysiol* **84**, 806-817 (2000)

35 Leao, K. E., Leao, R. N., Sun, H., Fyffe, R. E. W. & Walmsley, B. : Hyperpolarization-activated currents are differentially expressed in mice brainstem auditory nuclei. *J Physiol* **576**, 849-864 (2006)

36 Felix 2nd, R. A., Fridberger, A., Leijon, S., Berrebi, A. S. & Magnusson, A. K. : Sound rhythms are encoded by postinhibitory rebound spiking in the superior paraolivary nucleus. *J Neurosci* **31**, 12566-12578 (2011)

37 Kopp-Scheinflug, C., Tozer, A. J. B., Robinson, S. W., Tempel, B. L., Hennig, M. H. & Forsythe, I. D. : The sound of silence: ionic mechanisms encoding sound termination. *Neuron* **71**, 911-925 (2011)

38 Curtis, D. R. & Eccles, J. C. : The time courses of excitatory and inhibitory synaptic actions. *J Physiol* **145**, 529-546 (1959)

39 Xie, R. & Manis, P. B. : Target-Specific IPSC Kinetics Promote Temporal Processing in Auditory Parallel Pathways. *J Neurosci* **33**, 1598-1614 (2013)

40 Yang, L. & Pollak, G. D. : GABA and glycine have different effects on monaural response

properties in the dorsal nucleus of the lateral lemniscus of the mustache bat. *J Neurophysiol* **71**, 2014-2024 (1994)

41 Kelly, J. B., Buckthought, A. D. & Kidd, S. A. : Monaural and binaural response properties of single neurons in the rat's dorsal nucleus of the lateral lemniscus. *Hear Res* **122**, 25-40 (1998)

42 Kelly, J. B. & Kidd, S. A. : NMDA and AMPA receptors in the dorsal nucleus of the lateral lemniscus shape binaural responses in rat inferior colliculus. *J Neurophysiol* **83**, 1403-1414 (2000)

43 Meffin, H. & Grothe, B. : Selective filtering to spurious localization cues in the mammalian auditory brainstem. *J Acoust Soc Am* **126**, 2437-2454 (2009)

44 Mysore, S. P. & Knudsen, E. I. : Reciprocal inhibition of inhibition: a circuit motif for flexible categorization in stimulus selection. *Neuron* **73**, 193-205 (2012)

45 Barry, P. H. : JPCalc, a software package for calculating liquid junction potential corrections in patch-clamp, intracellular, epithelial and bilayer measurements and for correcting junction potential measurements. *J Neurosci Methods* **51**, 107-116 (1994)

Supplementary Figures

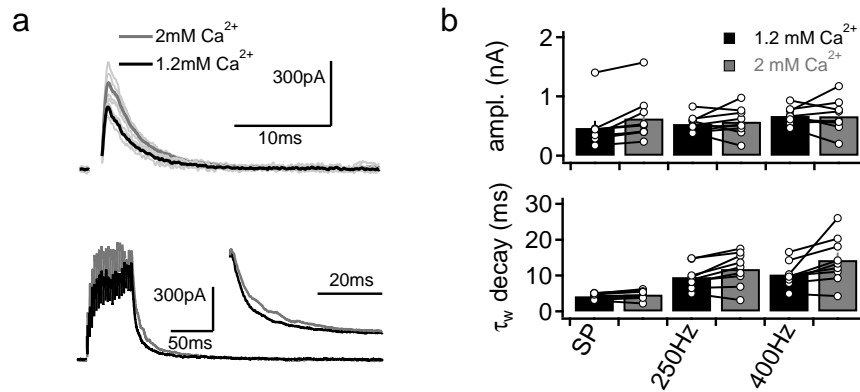


Figure S1: Effect of external calcium on IPSC prolongation (a) GABAergic IPSCs in response to a single pulse and 20 pulses at 400 Hz evoked in 2 mM (gray) and 1.2 mM Ca²⁺ (black). Train traces are averages of 4 repetitions. Artifacts are removed for clarity. Inset shows amplitude normalized traces. (b) Amplitudes (top) and decay time constants (bottom) for single pulses (SP), 250 Hz and 400 Hz trains in 1.2 mM and 2 mM Ca²⁺ (n = 9, Wilcoxon Rank Sum test for SP, p = 0.004, paired t-test for 250 Hz p = 0.56, 400 Hz p = 0.95, paired t-tests for decay SP: p = 0.06, 250 Hz p = 0.017, 400 Hz p = 0.022, n = 9).

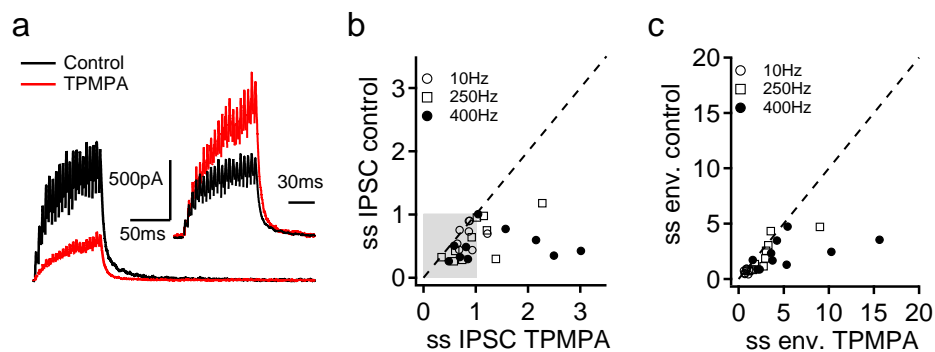


Figure S2: Short-term synaptic plasticity under TPMPA (a) GABAergic IPSCs in response to a 250 Hz train with 20 pulses before (black) and after (red) TPMPA application. Traces are averages of 2 - 4 repetitions. Inset: traces normalized to first IPSC amplitude to depict the difference in build-up between the two conditions. (b) Amplitudes of individual IPSCs to pulses 18 - 20 were averaged and normalized to the first IPSC amplitude to get a measure for the steady state depression during the stimulation trains (ssIPSC). Dashed line indicates unity. The data points fall below the unity line, indicating less depression or even facilitation under TPMPA treatment. Gray area indicates synaptic depression (ssIPSC < 1). (c) Envelope amplitude of pulses 18 - 20 normalized to the first IPSC amplitude. Dashed line indicates unity.

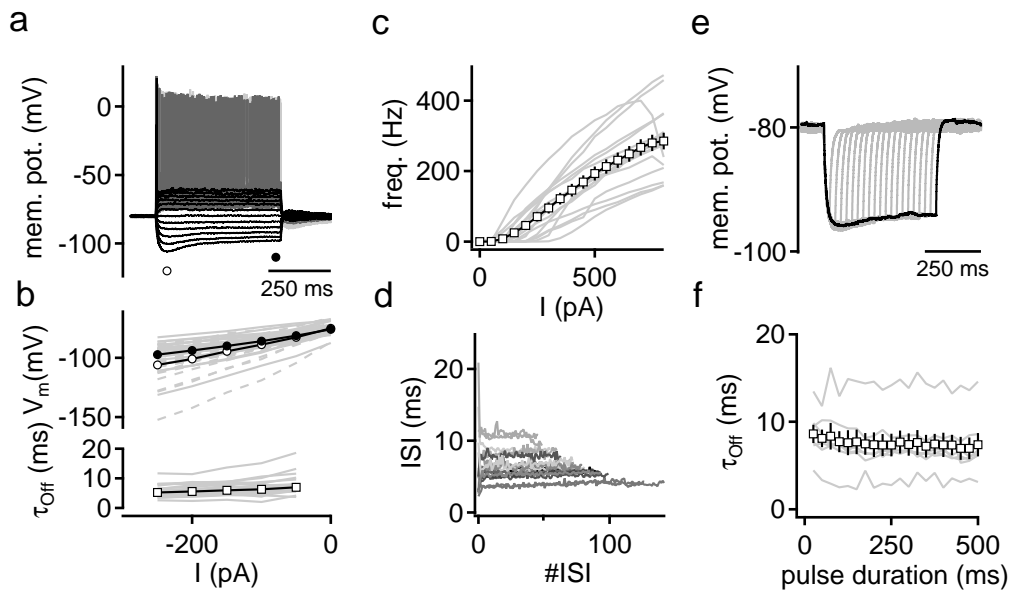


Figure S3: Intrinsic membrane properties of DNLL neurons **(a)** Voltage responses of a mature DNLL neuron to 500 ms pulses from -250 pA to 800 pA. Sub-threshold- and first spiking response black, half-maximal response dark gray. **(b)** For negative deflections peak (open circles) and steady state potentials (closed circles) were analyzed for $n = 22$ neuron (dashed and solid lines for peak and steady state) and the offset was fitted with an exponential function (τ_{off}). **(c)** Frequency-current relationship. The black symbols display average of $n = 16$ neurons in gray. **(d)** Inter spike intervals (ISI) analyzed at half maximal frequency versus ISI number for $n = 16$ cells. **(e)** Voltage responses to hyperpolarizing pulses between 25 and 500 ms. **(f)** The offset was fitted with an exponential function (τ_{off}) and plotted vs. pulse duration.

4 Discussion

During late postnatal developmental, DNLL neurons turn into fast spiking neurons that respond with very precisely timed APs to incoming signals. Importantly, this fast processing does not contradict the creation of PI. High presynaptic firing frequencies together with the activity-dependent properties of the GABAergic synaptic transmission and the postsynaptic integration produce a long lasting inhibition. These specific cellular properties enable DNLL neurons to take part in signal processing on very different time scales. On the one hand, they are able to transmit information fast and reliably. On the other hand, they display a prolonged filter property that adds context to the processing of binaural cues.

4.1 Implications of fast and precise signaling in the mature DNLL

The first study (section 2) revealed that both intrinsic and synaptic kinetics in DNLL neurons accelerate during late postnatal development. The APs become very narrow. Moreover, DNLL neurons develop into extremely fast spiking neurons with sustained firing rates of more than 400 Hz in some cases. Even at such high rates, DNLL neurons show little spike frequency adaptation. The fast AP generation together with the fast synaptic kinetics and membrane time constants leads to very precise AP responses upon just-suprathreshold stimuli. This high speed and pre-

cision is in line with the fast processing of stimuli in the DNLL *in vivo* (Siveke et al., 2006; Siveke et al., 2008), but is in contrast to the *in vitro* characterization of rat DNLL neurons that suggest slow excitation and moderate firing rates in DNLL neurons (Fu et al., 1997; Wu and Kelly, 1995a).

What is the role of the fast and precise processing to which DNLL neurons are tuned during development? Why create fast kinetics in neurons that serve to supply such a slow signal as the PI? One reason may be the increased flexibility related to the activity-dependent processes described in the second study (section 3) that will be discussed in detail in section 4.2. Another reason is that the efferent projections of the DNLL shape many response features in the IC. For this purpose reliable and fast signalling is essential. In the IC, the excitation from the MSO and LSO and the inhibition from the DNLL give the system a set of inputs with which various different and more complex response patterns can be built (Pollak et al., 2002). Some IC neurons, for instance, display what has been called a *de novo* ILD sensitivity (Li and Kelly, 1992; Burger and Pollak, 2001). In fact, the term *de novo* is misleading as these neurons do not perform a novel ILD comparison. Instead, the DNLL imprints its "negative" ILD selectivity as inhibition on monaural excitation from the CN (Park and Pollak, 1993; Burger and Pollak, 2001). Thus, the DNLL, which itself inherits its response properties from the LSO, imposes direction selectivity on the "*de novo*" cells. Other IC neurons have response functions that are shifted in a less drastic way by inhibitory DNLL inputs, or are entirely unaffected (Pollak et al., 2002).

Thus, the DNLL shapes the response properties in the IC not only for the processing of lagging sounds, but actively takes part in ITD and ILD processing on fast time scales. In the case of ITD sensitivity, it has been shown that the tuning curves in the DNLL are sharpened and mutual information is enhanced compared with the MSO (Kuwada et al., 2006; Pecka et al., 2010). For ITD functions with higher best

frequencies, the increase in information stems from an increase in dynamic range (Pecka et al., 2010). It has been hypothesized that the reciprocal inhibition through the commissure of Probst plays a part in reducing the trough response rates and thus increases the dynamic range, but this has been difficult to demonstrate *in vivo* (Siveke, 2007). Another possible mechanism to reduce trough rates may be the convergence of multiple MSO neurons onto one DNLL neuron. Here, the low rates during the troughs in the response curves may disappear through a postsynaptic thresholding effect. A specific role of the NMDA receptor mediated current could then be the selective amplification of supra-threshold responses. The non-linearity of the NMDA receptor activation may be ideally suited to increase the response at the peak of the response curve but leave the troughs unaffected. Whether this specific effect holds true needs further testing in *in vivo* experiments under application of NMDA receptor antagonists. An amplification of firing rate, as proposed in the first study here (section 2) and supported by Porres et al. (2011), can also be seen *in vivo* (Siveke, unpublished results).

For ITD functions of neurons with low preferred frequency, the enhanced representation in the DNLL is achieved through a reduction in the response rate variability from trial to trial compared to the MSO. In this case, the high fidelity of AP generation in DNLL neurons may play a role in combination with an NMDA receptor dependent effect. *In vivo* and *in vitro* data show that NMDA receptor mediated current plays a pivotal part at maintaining the firing rates and reducing the response variability (Siveke, unpublished results).

Taken together, the DNLL not only serves to slow down processing compared to signaling in the SOC, but is capable of operating on a fast time scale. This fast processing is a prerequisite to shape the processing of interaural disparity cues in the IC.

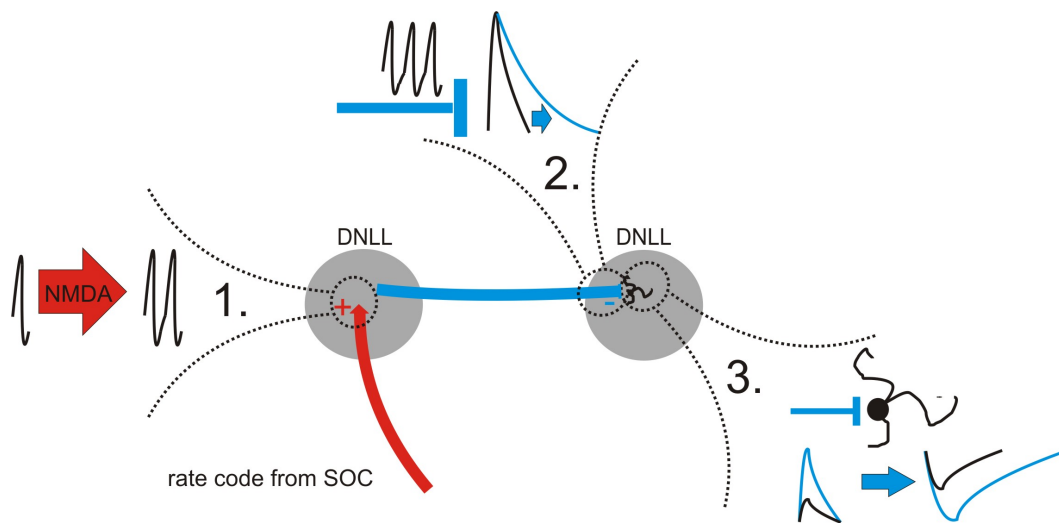


Figure 4.1: Circuit mechanisms that could create PI. 1. NMDA receptor mediated current amplifies the rate coded signal from the SOC. 2. The output of the GABAergic synapse in the contralateral DNLL is prolonged and increased in an activity-dependent manner. 3. The passive integration boosts IPSP for strong inputs.

4.2 Synergistic actions as cellular mechanism of persistent inhibition

The physiological hallmark of DNLL neurons is the persistent inhibition of activity mediated by the contralateral DNLL after an ipsilateral sound stimulus. Previously, slow kinetics of the GABAergic inhibition mediated by the DNLL projections via the commissure of Probst have been proposed to be the cellular mechanism of PI (Pecka et al., 2007).

Yet, the first study (section 2) shows that the GABAergic kinetics accelerate during development and become too fast to explain the PI. In addition, it has to be considered that the duration of the PI is not fixed, but depends on sound intensity (Yang and Pollak, 1998; Pecka et al., 2007). This variable duration speaks against a "hard coding" of synaptic kinetics to achieve the long lasting inhibition.

As a possible solution to this problem, this thesis together with the study of Por-

res et al. (2011) suggests that multiple cellular mechanisms in the DNLL circuitry interact to adjust the duration of inhibition in an activity-dependent manner (Figure 4.1). Specifically they are the following: High response rates in DNLL neurons supported by an NMDA receptor dependent input amplification (1), activity-dependent processes at the pre- and postsynaptic side of the GABAergic synapse (2) and an integration mechanism that is sensitive to the amplitude and kinetics of the inhibitory input (3).

4.2.1 NMDA receptor dependent input amplification

As described in section 4.1, NMDA receptor mediated current is able to boost response rates *in vivo* and *in vitro*. In line with these results, it has been shown previously in rats (Kelly and Kidd, 2000) that blockade of NMDA receptors in the DNLL reduces inhibition in the IC. Importantly, our data show that prolonged activity mediated by NMDA receptors in the DNLL after the offset of the sound stimulus is not necessary to produce PI (Wu and Kelly, 1996; Kelly and Kidd, 2000). Rather, the NMDA receptor component leads to sustained high firing rates (Porres et al., 2011). These high rates are one prerequisite to trigger the activity-dependent mechanisms at the GABAergic synapse in the DNLL. Whether the same holds true for the GABAergic synapse in the IC is speculative, but the data of Kelly and Kidd (2000) suggest that a similar mechanism is feasible. Not all DNLL neurons or at least not all excitatory synapses in our data of the first study (section 2) contain NMDA receptors. However, whether this heterogeneity constitutes a functional difference between different inputs from the SOC remains elusive.

4.2.2 Synaptic mechanisms

The high firing rates that DNLL neurons can sustain are translated into a prolongation of GABAergic IPSCs. We propose that spillover and asynchronous release contribute to this graded, activity-dependent prolongation. These mechanisms are not apparent after single stimulation pulses but build up during repetitive stimulation. As discussed in the second study (section 3), the frequency dependence of the IPSC decay, the amplitude dependence and the acceleration after application of the low-affinity antagonist TPMPA are in line with transmitter spillover (Diamond and Jahr, 1995; DiGregorio et al., 2002; Overstreet and Westbrook, 2003; Szabadics et al., 2007; Balakrishnan et al., 2009; Crowley et al., 2009; Satake et al., 2012; Tang and Lu, 2012).

Another possible explanation for the observed prolongation would be a progressing receptor desensitization during the stimulation train with subsequent re-opening of receptors during the late phase of the IPSC (Jones and Westbrook, 1995). Desensitization would also explain the facilitation of release revealed after TPMPA application (Chanda and Xu-Friedman, 2010). Yet, there are several arguments that support spillover over desensitization. First, desensitization fails to explain the slowing of the decay upon recruitment of multiple inputs, which suggests the involvement of transmitter pooling after spillover (Balakrishnan et al., 2009; Tang and Lu, 2012). Second, the fact that there is a build-up of IPSCs during stimulation trains rather than a depression under control conditions is better explained by saturation than by desensitization. In case of desensitization, a decreasing number of available receptors would be expected during the train which should lead to a decreasing amplitude. The strong transmitter release during the stimulation trains suggests an increased lifetime of transmitter in the cleft which could lead to late activation of receptors during the IPSC and spillover of transmitter (Clements, 1996; Nusser et al., 2001; Balakrishnan et al., 2009; Karayannis et al., 2010; Barberis et

al., 2011).

The facilitation of release during trains is probably driven by accumulation of intracellular calcium that also drives asynchronous release during high frequency stimulation. Buffering intracellular calcium with EGTA-AM reduced IPSC amplitudes as well as the decay time constants of IPSCs at high stimulation frequencies. This acceleration occurred even after the pre-application of TPMPA to block the spillover mediated current. This additive effect of the low affinity antagonist and the calcium buffer supports the hypothesis that asynchronous release contributes to the IPSC prolongation in the DNLL. Yet, the effect of asynchronous release on the decay is not as strong as described at other synapses (Lu and Trussell, 2000; Otsu et al., 2004; Hefft and Jonas, 2005; Maximov and Südhof, 2005; Best and Regehr, 2009; Tang and Lu, 2012).

Although the change in synaptic kinetics in our data is rather modest, the resulting prolongation of inhibition is substantial, as the synaptic decay can be shifted from being faster than the membrane time constant to being slower. This shift enables an effective prolongation of the IPSP with the mechanism discussed in section 4.2.3 and long lasting AP suppression. Thus, pre- and postsynaptic mechanisms seem to work in synergy to create a GABA_A receptor mediated IPSC, whose amplitude and decay depend on the firing rate of single presynaptic neurons as well as on the number of active presynaptic neurons.

4.2.3 Postsynaptic integration

As introduced in section 1.4, the influence of IPSC kinetics on the IPSP shape depends on passive and active membrane properties. In the DNLL, the hyperpolarizing inhibition is integrated largely passively. During passive integration, either the kinetics of the synaptic conductance or the membrane time constant can dominate the IPSP shape. The slower process controls the IPSP decay. When the membrane

time constant is slower than the conductance decay, the decay of the IPSP follows the membrane time constant. Thus, during conversion of IPSCs to IPSPs the difference between different synaptic time courses is reduced (Hardie and Pearce, 2006). On the other hand, IPSC kinetics dominate the IPSP shape if the synaptic decay time constant is larger than the membrane time constant (Curtis and Eccles, 1959; Xie and Manis, 2013). In this case, differences in synaptic kinetics are preserved on the level of the IPSP (Xie and Manis, 2013).

One interesting finding in our study is that IPSPs can decay more slowly than expected from either membrane or synaptic decay time constants. We tested this in more detail using artificial conductance injection and modeling and attributed it to a conductance amplitude dependent mechanism. The non-linearity in the equilibrium potential between leak and GABA conductance eventually leads to a saturation of IPSP amplitude (Koch, 1999) and in our case also influences the IPSP dynamics. A prerequisite for the influence of the equilibrium potential is that the membrane time constant is not substantially larger than the conductance decay time constant. Importantly, this mechanism becomes active before a saturation in IPSP amplitude is reached and is observed for realistic conductance kinetics and amplitudes.

The amplitude dependence might help neurons to obtain a good population read-out of presynaptic activity. Synchronous inputs would sum up and lead to an increased conductance amplitude, thereby causing a longer lasting IPSP. A requirement for this interaction are inhibitory inputs that target the soma or cells that are electrotonically compact enough to avoid a compartmentalization of synaptic charge (Williams, 2004). In the DNLL, neurons are electrotonically relatively compact (Ammer et al., 2012) and inhibitory inputs target mainly the soma and proximal dendrites (Iwahori, 1986; Oliver and Shneiderman, 1989). As both the amplitude and the decay of the GABA conductance in the DNLL depend on the level of presynaptic activity, an integration mechanism that is sensitive to exactly these parame-

ters seems an ideal way to enable a graded encoding of stimulus strength.

The AP suppression in the DNLL depends, like the IPSP duration, on the kinetics and amplitude of the GABA conductance. This result adds to the previously reported dependence of AP suppression on the kinetics of the IPSC (Balakrishnan et al., 2009; Tang and Lu, 2012).

As the IPSP shape seems largely dominated by the GABA conductance and a hyperpolarization alone leads to only a very short AP suppression, one might speculate that the inhibition exerts its AP suppressing action mainly through shunting the excitation. Yet, the shunting influence of the conductance alone is by far less effective as when it is combined with a hyperpolarizing GABA reversal potential. The low reversal potential in DNLL neurons is in line with the low inhibitory reversal potential throughout the auditory brainstem (Ehrlich et al., 1999; Löhrike et al., 2005; Magnusson et al., 2005; Milenkovic et al., 2007; Kopp-Scheinflug et al., 2011), which is often achieved by strong expression of KCC2 transporters (for review see Friauf et al., 2011). *In vivo*, the contribution of the negative GABA reversal potential to AP suppression might be even more prominent, as hyperpolarization effectively reduces activation of NMDA receptors that contribute to AP generation in the DNLL (Wu and Kelly, 1996; Kelly and Kidd, 2000; Porres et al., 2011).

Taken together, interacting cellular mechanisms can explain the duration and the activity-dependence of PI *in vivo* on the basis of the synaptic and intrinsic properties of DNLL neurons. Thus, no sustained activity in the DNLL or lower nuclei is necessary to explain PI. However, whether this mechanism is indeed used by the DNLL circuit *in vivo* remains an open question. *In vivo* whole-cell recordings would be necessary to get a definite answer. The most straightforward experiment would be to record from a DNLL neuron while simultaneously increasing the intensity on the ipsilateral ear. The prediction from our data would be that increased intensity on

the ipsilateral ear would recruit more presynaptic neurons that additionally respond with increased firing rates in the contralateral DNLL. Thus, presynaptic neurons would sum their conductance in the ipsilateral postsynaptic DNLL neuron and cause an increasingly stronger hyperpolarization. Along with this hyperpolarization, a longer decay of the IPSP would be expected. It remains possible that *in vivo* the underlying mechanism is a prolonged activity in the contralateral DNLL. In this case, an ongoing hyperpolarization that is continuously prolonged with sound intensity would be expected.

4.3 Persistent inhibition and the precedence effect

The activity-dependence of inhibition in our *in vitro* data is in line with the *in vivo* data in which a louder monaural sound or larger ILD on the ipsilateral ear leads to longer PI (Yang and Pollak, 1998; Pecka et al., 2007). Therefore, why is the PI activity-dependent at all? Would it not be better to have a constant delay for echo suppression? One reasonable explanation for the intensity dependence would be that louder sounds can also lead to stronger reflections. Thus, more inhibitory power is needed to suppress those reflections. In the AP suppression experiments in section 3 as well as in *in vivo* experiments in gerbils (Pecka et al., 2007), the testing stimulus that represents the lagging sound is kept constant while the leading stimulus is increased. This is of course not a naturalistic experiment, as in a natural scene both stimuli are interdependent. In psychophysical experiments, higher overall sound intensity even causes lower echo thresholds, meaning that the lagging sound can be localized earlier at higher overall sound levels (Shinn-Cunningham et al., 1993; Litovsky et al., 1999). Even if many processing stages follow the DNLL and thus these behavioral results cannot be linked directly to the DNLL physiology, it is tempting to speculate why this could happen. One possibility is that inhibition sat-

urates prior to excitation. This imbalance would lead to shorter PI at high sound intensity and thus maybe to a shorter echo threshold.

When the sound intensity on one ear is increased, the ILD is changed simultaneously. Higher ILDs and thus more lateral stimuli cause a longer PI and should - if the percept was only based on the DNLL response - have a longer echo threshold. The echo threshold should then decrease when the tone would arrive from a more frontal position. This scenario does not hold true in behavioral experiments. The echo threshold is equivalent even for echoes in the vertical midline and azimuth (Litovsky and Yin, 1998a). This result lead the authors to speculate that a spectral, maybe monaural component contributes to the precedence effect (Litovsky and Yin, 1998a; Litovsky and Yin, 1998b). Zahn (2003), however, suggested in a modelling study that the DNLL circuit is able to suppress responses to echoes even in the midline, as long as the two hemispheric response curves of the LSO populations sufficiently overlap.

Alternatively, one can argue that the long PI for lateral sounds makes sense as this would just strongly suppress responses to echoes that come from the contralateral hemifield. Such a sequence of sounds is likely caused by a reflection or interference of sound sources and not, for instance, by a naturally occurring movement (Meffin and Grothe, 2009). If the sound source moves gradually along the azimuthal axis, it will cause slowly changing binaural cues that should not be suppressed. In addition, directional information that comes from the opposite hemifield would be more distracting than directional cues from the vicinity of the primary sound source. Yet, as there is no indication of horizontal position on echo threshold, it is unclear how this property relates to behavior. One concept to consider is the complex effect the inhibition in the DNLL has on the response functions in the IC. As already described in section 4.1, the DNLL shapes response features in various ways in the IC. All neurons that are affected by the inhibitory

input from the DNLL will change their response properties upon DNLL inactivation by a prior tone stimulus. The most drastic change is seen as a full disinhibition or full inhibition of IC neurons by a preceding stimulus (Bauer et al., 2000; Burger and Pollak, 2001). As described previously (section 1.1.4.1), the disinhibition leads to additional activity in response to the lagging sound in a population of IC neurons, which could be used as an identification signal for echoes in higher centers. Other IC neurons are expected to show a shift in their response function as they are only gradually affected by the inhibition from the DNLL (Pollak et al., 2002; Li and Pollak, 2013). How, and at which level this change in response features is then finally read out and interpreted are open questions.

To demonstrate the involvement of the DNLL in the precedence effect, it would be ideal to conduct behavioral experiments while controlling the DNLL activity. For this purpose, viral expression of halorhodopsin would constitute a suitable tool. Compared to classical tools such as lesioning and injections of kynurenic acid, expression of halorhodopsin has several advantages: First, DNLL neurons could be repeatedly switched on and off by light. Second, this method is more selective and does not interfere with information that is transmitted through fibers of passage. However, lesioning the commissure of Probst in rats severely impaired the ability to localize sounds with an increase of 22° in the minimal audible angle (Ito et al., 1996). This result is promising and suggests that switching off the input from the DNLL indeed hampers sound localization. Yet, the specific role of the DNLL in echo suppression has yet to be demonstrated. Two possible experiments could be conducted with the help of optogenetics. In the first experiment, the sound localization performance of gerbils could be tested with and without optically silencing the DNLL contralateral to the sound source. The light pulse would mimic the PI that would have been caused by a preceding ipsilateral sound stimulus. If our hypothesis about the role of the DNLL is correct, the optically silenced trials would

correspond to simulated echoes and the localization performance should be hampered. The second experiment could use the standard paradigm with a leading and a lagging tone with ILDs favoring opposite hemifields. Here, the localization performance for the lagging tone could be tested with or without optically silencing the excitatory DNLL response to the first stimulus. This silencing would abolish the PI in the contralateral DNLL, which would then be responsive to the trailing sound and inhibit neurons in the IC. If our hypothesis is correct, localization performance of the lagging sound should be enhanced in this scenario.

Another open question in this neural circuit is the role of glycinergic inhibition from the LSO to both DNLL and IC (Glendenning et al., 1992; Saint Marie et al., 1989; Oliver, 2000). The DNLL may be used as a model system to investigate how two different inhibitory transmitter systems interact in one cell type, and the potentially distinct physiological functions they serve. Yang and Pollak (1994) showed in bats that the glycinergic inputs in the DNLL contribute to the inhibition primarily during the tone and only little to PI. This fact is intriguing, especially as the inhibition arrives during times when little incoming excitation is expected anyway as the inhibition stems from the ipsilateral LSO. It might serve to enhance the representation of ILDs in the DNLL by reducing the firing rates for stimuli from the ipsilateral hemifield. Alternatively, glycinergic inhibition could reset the DNLL activity in case of a strong lagging stimulus. In this way the glycinergic inhibition could constitute an additional switch with which the ipsilateral DNLL could be silenced rapidly. This silencing would deprive the contralateral DNLL from its inhibition and allow the new signal to be passed. The presence of this glycinergic inhibition is especially interesting considering that it only exists for the LSO projections to the DNLL and not for the MSO projections to the DNLL (Glendenning et al., 1992; Oliver, 2000). An equivalent functional connection from the MSO would be inhibitory projections targeting the DNLL on the contralateral side. Yet, projections

from the MSO to the DNLL seem to be predominantly ipsilateral (Kelly et al., 1998; Siveke et al., 2006). By comparing the processing that takes place between MSO and DNLL with that between LSO and DNLL, the role of this additional glycinergic inhibitory input to the DNLL may become apparent.

Bibliography

- Adams JC, Mugnaini E (1984) Dorsal nucleus of the lateral lemniscus: a nucleus of GABAergic projection neurons. *Brain Res Bull* 13:585–590.
- Ahuja TK, Wu SH (2000) Developmental changes in physiological properties in the rat's dorsal nucleus of the lateral lemniscus. *Hear Res* 149:33–45.
- Aitkin LM, Anderson DJ, Brugge JF (1970) Tonotopic organization and discharge characteristics of single neurons in nuclei of the lateral lemniscus of the cat. *J Neurophysiol* 33:421–440.
- Alger BE, Nicoll RA (1982) Pharmacological evidence for two kinds of GABA receptor on rat hippocampal pyramidal cells studied in vitro. *J Physiol* 328:125–141.
- Ammer JJ, Grothe B, Felmy F (2012) Late postnatal development of intrinsic and synaptic properties promotes fast and precise signaling in the dorsal nucleus of the lateral lemniscus. *J Neurophysiol* 107:1172–1185.
- Ashida G, Carr CE (2011) Sound localization: Jeffress and beyond. *Curr Opin Neurobiol* 21:745–751.
- Atluri PP, Regehr WG (1998) Delayed release of neurotransmitter from cerebellar granule cells. *J Neurosci* 18:8214–8227.
- Bajo VM, Merchán MA, López DE, Rouiller EM (1993) Neuronal morphology and efferent projections of the dorsal nucleus of the lateral lemniscus in the rat. *J Comp Neurol* 334:241–262.
- Bal R, Oertel D (2000) Hyperpolarization-activated, mixed-cation current (I_h) in octopus cells of the mammalian cochlear nucleus. *J Neurophysiol* 84:806–817.
- Balakrishnan V, Becker M, Löhrike S, Nothwang HG, Güresir E, Friauf E (2003) Expression and function of chloride transporters during development of inhibitory neurotransmission in the auditory brainstem. *J Neurosci* 23:4134–4145.

- Balakrishnan V, Kuo SP, Roberts PD, Trussell LO (2009) Slow glycinergic transmission mediated by transmitter pooling. *Nat Neurosci* 12:286–294.
- Barberis A, Petrini EM, Mozrzymas JW (2011) Impact of synaptic neurotransmitter concentration time course on the kinetics and pharmacological modulation of inhibitory synaptic currents. *Front Cell Neurosci* 5:6.
- Bauer EE, Klug A, Pollak GD (2000) Features of contralaterally evoked inhibition in the inferior colliculus. *Hear Res* 141:80–96.
- Ben-Ari Y (2002) Excitatory actions of gaba during development: the nature of the nurture. *Nat Rev Neurosci* 3:728–739.
- Best AR, Regehr WG (2009) Inhibitory regulation of electrically coupled neurons in the inferior olive is mediated by asynchronous release of GABA. *Neuron* 62:555–565.
- Blaesse P, Airaksinen MS, Rivera C, Kaila K (2009) Cation-chloride cotransporters and neuronal function. *Neuron* 61:820–838.
- Blauert (1997) *Spatial hearing: the psychophysics of human sound localization* MIT Press.
- Blauert J, Braasch J (2005) Acoustic Communication: The Precedence Effect. *Forum Acousticum* .
- Boudreau JC, Tsuchitani C (1968) Binaural interaction in the cat superior olive S segment. *J Neurophysiol* 31:442–454.
- Brand A, Behrend O, Marquardt T, McAlpine D, Grothe B (2002) Precise inhibition is essential for microsecond interaural time difference coding. *Nature* 417:543–547.
- Brugge JF, Anderson DJ, Aitkin LM (1970) Responses of neurons in the dorsal nucleus of the lateral lemniscus of cat to binaural tonal stimulation. *J Neurophysiol* 33:441–458.
- Burger RM, Pollak GD (2001) Reversible inactivation of the dorsal nucleus of the lateral lemniscus reveals its role in the processing of multiple sound sources in the inferior colliculus of bats. *J Neurosci* 21:4830–4843.
- Campos ML, de Cabo C, Wisden W, Juiz JM, Merlo D (2001) Expression of GABA(A) receptor subunits in rat brainstem auditory pathways: cochlear nuclei, superior olivary complex and nucleus of the lateral lemniscus. *Neuroscience* 102:625–638.
- Cant NB, Casseday JH (1986) Projections from the anteroventral cochlear nucleus to the lateral and medial superior olivary nuclei. *J Comp Neurol* 247:457–476.

- Cathala L, Misra C, Cull-Candy S (2000) Developmental profile of the changing properties of NMDA receptors at cerebellar mossy fiber-granule cell synapses. *J Neurosci* 20:5899–5905.
- Cathala L, Brickley S, Cull-Candy S, Farrant M (2003) Maturation of EPSCs and intrinsic membrane properties enhances precision at a cerebellar synapse. *J Neurosci* 23:6074–6085.
- Cathala L, Holderith NB, Nusser Z, DiGregorio DA, Cull-Candy SG (2005) Changes in synaptic structure underlie the developmental speeding of AMPA receptor-mediated EPSCs. *Nat Neurosci* 8:1310–1318.
- Chance FS, Abbott LF, Reyes AD (2002) Gain modulation from background synaptic input. *Neuron* 35:773–782.
- Chanda S, Xu-Friedman MA (2010) A low-affinity antagonist reveals saturation and desensitization in mature synapses in the auditory brain stem. *J Neurophysiol* 103:1915–1926.
- Chen L, Kelly JB, Wu SH (1999) The commissure of probst as a source of GABAergic inhibition. *Hear Res* 138:106–114.
- Chiu CQ, Lur G, Morse TM, Carnevale NT, Ellis-Davies GCR, Higley MJ (2013) Compartmentalization of GABAergic inhibition by dendritic spines. *Science* 340:759–762.
- Clements JD (1996) Transmitter timecourse in the synaptic cleft: its role in central synaptic function. *Trends Neurosci* 19:163–171.
- Clifton RK (1987) Breakdown of echo suppression in the precedence effect. *J Acoust Soc Am* 82:1834–1835.
- Coombs JS, Eccles JC, Fatt P (1955) The inhibitory suppression of reflex discharges from motoneurons. *J Physiol* 130:396–413.
- Crowley JJ, Fioravante D, Regehr WG (2009) Dynamics of fast and slow inhibition from cerebellar golgi cells allow flexible control of synaptic integration. *Neuron* 63:843–853.
- Curtis DR, Eccles JC (1959) The time courses of excitatory and inhibitory synaptic actions. *J Physiol* 145:529–546.
- Diamond JS, Jahr CE (1995) Asynchronous release of synaptic vesicles determines the time course of the AMPA receptor-mediated EPSC. *Neuron* 15:1097–1107.
- DiGregorio DA, Nusser Z, Silver RA (2002) Spillover of glutamate onto synaptic AMPA receptors enhances fast transmission at a cerebellar synapse. *Neuron* 35:521–533.

- Eccles JC (1961) Membrane time constants of cat motoneurons and time courses of synaptic action. *Exp Neurol* 4:1–22.
- Ehrlich I, Lohrke S, Friauf E (1999) Shift from depolarizing to hyperpolarizing glycine action in rat auditory neurones is due to age-dependent Cl⁻ regulation. *J Physiol* 520 Pt 1:121–137.
- Etherington SJ, Williams SR (2011) Postnatal development of intrinsic and synaptic properties transforms signaling in the layer 5 excitatory neural network of the visual cortex. *J Neurosci* 31:9526–9537.
- Farrant M, Nusser Z (2005) Variations on an inhibitory theme: phasic and tonic activation of GABA(A) receptors. *Nat Rev Neurosci* 6:215–229.
- Fatt P P, Katz B (1953) The effect of inhibitory nerve impulses on a crustacean muscle fibre. *J Physiol* 121:374–389.
- Felix n RA, Fridberger A, Leijon S, Berrebi AS, Magnusson AK (2011) Sound rhythms are encoded by postinhibitory rebound spiking in the superior paraolivary nucleus. *J Neurosci* 31:12566–12578.
- Ford MC, Grothe B, Klug A (2009) Fenestration of the calyx of Held occurs sequentially along the tonotopic axis, is influenced by afferent activity, and facilitates glutamate clearance. *J Comp Neurol* 514:92–106.
- Franks KM, Isaacson JS (2005) Synapse-specific downregulation of NMDA receptors by early experience: a critical period for plasticity of sensory input to olfactory cortex. *Neuron* 47:101–114.
- Friauf E, Rust MB, Schulenburg T, Hirtz JJ (2011) Chloride cotransporters, chloride homeostasis, and synaptic inhibition in the developing auditory system. *Hear Res* 279:96–110.
- Fu XW, Brezden BL, Kelly JB, Wu SH (1997) Synaptic excitation in the dorsal nucleus of the lateral lemniscus: whole-cell patch-clamp recordings from rat brain slice. *Neuroscience* 78:815–827.
- Fu XW, Brezden BL, Wu SH (1997) Hyperpolarization-activated inward current in neurons of the rat's dorsal nucleus of the lateral lemniscus in vitro. *J Neurophysiol* 78:2235–2245.
- Futai K, Okada M, Matsuyama K, Takahashi T (2001) High-fidelity transmission acquired via a developmental decrease in NMDA receptor expression at an auditory synapse. *J Neurosci* 21:3342–3349.
- Glendenning KK, Baker BN, Hutson KA, Masterton RB (1992) Acoustic chiasm V: inhibition and excitation in the ipsilateral and contralateral projections of LSO. *J Comp Neurol* 319:100–122.

- Glendenning KK, Brunso-Bechtold JK, Thompson GC, Masterton RB (1981) Ascending auditory afferents to the nuclei of the lateral lemniscus. *J Comp Neurol* 197:673–703.
- Goda Y, Stevens CF (1994) Two components of transmitter release at a central synapse. *Proc Natl Acad Sci U S A* 91:12942–12946.
- Grothe B (2003) New roles for synaptic inhibition in sound localization. *Nat Rev Neurosci* 4:540–550.
- Grothe B, Pecka M, McAlpine D (2010) Mechanisms of sound localization in mammals. *Physiol Rev* 90:983–1012.
- Hardie JB, Pearce RA (2006) Active and passive membrane properties and intrinsic kinetics shape synaptic inhibition in hippocampal CA1 pyramidal neurons. *J Neurosci* 26:8559–8569.
- Hefft S, Jonas P (2005) Asynchronous GABA release generates long-lasting inhibition at a hippocampal interneuron-principal neuron synapse. *Nat Neurosci* 8:1319–1328.
- Hirtz JJ, Boesen M, Braun N, Deitmer JW, Kramer F, Lohr C, Müller B, Nothwang HG, Striessnig J, Löhrike S, Friauf E (2011) Cav1.3 calcium channels are required for normal development of the auditory brainstem. *J Neurosci* 31:8280–8294.
- Hirtz JJ, Braun N, Griesemer D, Hannes C, Janz K, Löhrike S, Müller B, Friauf E (2012) Synaptic refinement of an inhibitory topographic map in the auditory brainstem requires functional Cav1.3 calcium channels. *J Neurosci* 32:14602–14616.
- Huang EP (1998) Synaptic transmission: spillover at central synapses. *Curr Biol* 8:R613–R615.
- Ito M, van Adel B, Kelly JB (1996) Sound localization after transection of the commissure of Probst in the albino rat. *J Neurophysiol* 76:3493–3502.
- Iwahori N (1986) A Golgi study on the dorsal nucleus of the lateral lemniscus in the mouse. *Neurosci Res* 3:196–212.
- Jeffress LA (1948) A place theory of sound localization. *J Comp Physiol Psychol* 41:35–39.
- Jones MV, Westbrook GL (1995) Desensitized states prolong GABAA channel responses to brief agonist pulses. *Neuron* 15:181–191.
- Joshi I, Shokralla S, Titis P, Wang LY (2004) The role of AMPA receptor gating in the development of high-fidelity neurotransmission at the calyx of Held synapse. *J Neurosci* 24:183–196.

- Kandler K, Friauf E (1995) Development of electrical membrane properties and discharge characteristics of superior olivary complex neurons in fetal and postnatal rats. *Eur J Neurosci* 7:1773–1790.
- Kandler K, Clause A, Noh J (2009) Tonotopic reorganization of developing auditory brainstem circuits. *Nat Neurosci* 12:711–717.
- Kane ES, Barone LM (1980) The dorsal nucleus of the lateral lemniscus in the cat: neuronal types and their distributions. *J Comp Neurol* 192:797–826.
- Kapfer C, Seidl AH, Schweizer H, Grothe B (2002) Experience-dependent refinement of inhibitory inputs to auditory coincidence-detector neurons. *Nat Neurosci* 5:247–253.
- Karayannis T, Elfant D, Huerta-Ocampo I, Teki S, Scott RS, Rusakov DA, Jones MV, Capogna M (2010) Slow GABA transient and receptor desensitization shape synaptic responses evoked by hippocampal neurogliaform cells. *J Neurosci* 30:9898–9909.
- Kelly JB, Buckthought AD, Kidd SA (1998) Monaural and binaural response properties of single neurons in the rat's dorsal nucleus of the lateral lemniscus. *Hear Res* 122:25–40.
- Kelly JB, Kidd SA (2000) NMDA and AMPA receptors in the dorsal nucleus of the lateral lemniscus shape binaural responses in rat inferior colliculus. *J Neurophysiol* 83:1403–1414.
- Kelly JB, Liscum A, van Adel B, Ito M (1998) Projections from the superior olive and lateral lemniscus to tonotopic regions of the rat's inferior colliculus. *Hear Res* 116:43–54.
- Kelly JB, van Adel BA, Ito M (2009) Anatomical projections of the nuclei of the lateral lemniscus in the albino rat (*Rattus norvegicus*). *J Comp Neurol* 512:573–593.
- Kim G, Kandler K (2003) Elimination and strengthening of glycinergic/GABAergic connections during tonotopic map formation. *Nat Neurosci* 6:282–290.
- Koch C (1999) *Biophysics of Computation: Information Processing in Single Neurons* New York: Oxford University Press.
- Koch U, Braun M, Kapfer C, Grothe B (2004) Distribution of HCN1 and HCN2 in rat auditory brainstem nuclei. *Eur J Neurosci* 20:79–91.
- Koch U, Grothe B (2003) Hyperpolarization-activated current (I_h) in the inferior colliculus: distribution and contribution to temporal processing. *J Neurophysiol* 90:3679–3687.

- Kopp-Scheinflug C, Tozer AJB, Robinson SW, Tempel BL, Hennig MH, Forsythe ID (2011) The sound of silence: ionic mechanisms encoding sound termination. *Neuron* 71:911–925.
- Kremkow J, Aertsen A, Kumar A (2010) Gating of signal propagation in spiking neural networks by balanced and correlated excitation and inhibition. *J Neurosci* 30:15760–15768.
- Kullmann PH, Kandler K (2001) Glycinergic/GABAergic synapses in the lateral superior olive are excitatory in neonatal C57Bl/6J mice. *Brain Res Dev Brain Res* 131:143–147.
- Kuwada S, Fitzpatrick DC, Batra R, Ostapoff EM (2006) Sensitivity to interaural time differences in the dorsal nucleus of the lateral lemniscus of the unanesthetized rabbit: comparison with other structures. *J Neurophysiol* 95:1309–1322.
- Leao KE, Leao RN, Sun H, Fyffe REW, Walmsley B (2006) Hyperpolarization-activated currents are differentially expressed in mice brainstem auditory nuclei. *J Physiol* 576:849–864.
- Lee N, Elias DO, Mason AC (2009) A precedence effect resolves phantom sound source illusions in the parasitoid fly *Ormia ochracea*. *Proc Natl Acad Sci U S A* 106:6357–6362.
- Lesica NA, Lingner A, Grothe B (2010) Population coding of interaural time differences in gerbils and barn owls. *J Neurosci* 30:11696–11702.
- Löhrke S, Srinivasan G, Oberhofer M, Doncheva E, Friauf E (2005) Shift from depolarizing to hyperpolarizing glycine action occurs at different perinatal ages in superior olivary complex nuclei. *Eur J Neurosci* 22:2708–2722.
- Li L, Kelly JB (1992) Inhibitory influence of the dorsal nucleus of the lateral lemniscus on binaural responses in the rat's inferior colliculus. *J Neurosci* 12:4530–4539.
- Li N, Pollak GD (2013) Circuits that innervate excitatory-inhibitory cells in the inferior colliculus obtained with in vivo whole cell recordings. *J Neurosci* 33:6367–6379.
- Litovsky RY, Colburn HS, Yost WA, Guzman SJ (1999) The precedence effect. *J Acoust Soc Am* 106:1633–1654.
- Litovsky RY, McAlpine D (2010) *The Oxford Handbook of Auditory Science: The Auditory Brain*, chapter Physiological correlates of the precedence effect and binaural masking level differences, pp. 333–360 Oxford University Press.
- Litovsky RY, Yin TC (1998a) Physiological studies of the precedence effect in the inferior colliculus of the cat. I. Correlates of psychophysics. *J Neurophysiol* 80:1285–1301.

- Litovsky RY, Yin TC (1998b) Physiological studies of the precedence effect in the inferior colliculus of the cat. II. Neural mechanisms. *J Neurophysiol* 80:1302–1316.
- Liu G (2004) Local structural balance and functional interaction of excitatory and inhibitory synapses in hippocampal dendrites. *Nat Neurosci* 7:373–379.
- Lopez de Armentia M, Sah P (2003) Development and subunit composition of synaptic NMDA receptors in the amygdala: NR2B synapses in the adult central amygdala. *J Neurosci* 23:6876–6883.
- Lovett-Barron M, Turi GF, Kaifosh P, Lee PH, Bolze F, Sun XH, Nicoud JF, Zemelman BV, Sternson SM, Losonczy A (2012) Regulation of neuronal input transformations by tunable dendritic inhibition. *Nat Neurosci* 15:423–30, S1–3.
- Lu T, Trussell LO (2000) Inhibitory transmission mediated by asynchronous transmitter release. *Neuron* 26:683–694.
- Magnusson AK, Kapfer C, Grothe B, Koch U (2005) Maturation of glycinergic inhibition in the gerbil medial superior olive after hearing onset. *J Physiol* 568:497–512.
- Markovitz NS, Pollak GD (1993) The dorsal nucleus of the lateral lemniscus in the mustache bat: monaural properties. *Hear Res* 71:51–63.
- Markovitz NS, Pollak GD (1994) Binaural processing in the dorsal nucleus of the lateral lemniscus. *Hear Res* 73:121–140.
- Marshall VT, Gerhardt HC (2010) A precedence effect underlies preferences for calls with leading pulses in the grey treefrog, *Hyla versicolor*. *Anim Behav* 80:139–145.
- Maximov A, Südhof TC (2005) Autonomous function of synaptotagmin 1 in triggering synchronous release independent of asynchronous release. *Neuron* 48:547–554.
- McAlpine D, Jiang D, Palmer AR (2001) A neural code for low-frequency sound localization in mammals. *Nat Neurosci* 4:396–401.
- McAlpine D, Grothe B (2003) Sound localization and delay lines—do mammals fit the model? *Trends Neurosci* 26:347–350.
- Meffin H, Grothe B (2009) Selective filtering to spurious localization cues in the mammalian auditory brainstem. *J Acoust Soc Am* 126:2437–2454.
- Milenkovic I, Witte M, Turecek R, Heinrich M, Reinert T, Rübsamen R (2007) Development of chloride-mediated inhibition in neurons of the anteroventral cochlear nucleus of gerbil (*Meriones unguiculatus*). *J Neurophysiol* 98:1634–1644.

- Miles R, Tóth K, Gulyás AI, Hájos N, Freund TF (1996) Differences between somatic and dendritic inhibition in the hippocampus. *Neuron* 16:815–823.
- Mitchell SJ, Silver RA (2003) Shunting inhibition modulates neuronal gain during synaptic excitation. *Neuron* 38:433–445.
- Moore MJ, Caspary DM (1983) Strychnine blocks binaural inhibition in lateral superior olivary neurons. *J Neurosci* 3:237–242.
- Mysore SP, Knudsen EI (2012) Reciprocal inhibition of inhibition: a circuit motif for flexible categorization in stimulus selection. *Neuron* 73:193–205.
- Nusser Z, Naylor D, Mody I (2001) Synapse-specific contribution of the variation of transmitter concentration to the decay of inhibitory postsynaptic currents. *Biophys J* 80:1251–1261.
- Oliver DL (2000) Ascending efferent projections of the superior olivary complex. *Microsc Res Tech* 51:355–363.
- Oliver DL, Shneiderman A (1989) An EM study of the dorsal nucleus of the lateral lemniscus: inhibitory, commissural, synaptic connections between ascending auditory pathways. *J Neurosci* 9:967–982.
- Otsu Y, Shahrezaei V, Li B, Raymond LA, Delaney KR, Murphy TH (2004) Competition between phasic and asynchronous release for recovered synaptic vesicles at developing hippocampal autaptic synapses. *J Neurosci* 24:420–433.
- Overstreet LS, Westbrook GL (2003) Synapse density regulates independence at unitary inhibitory synapses. *J Neurosci* 23:2618–2626.
- Park TJ, Pollak GD (1993) GABA shapes sensitivity to interaural intensity disparities in the mustache bat's inferior colliculus: implications for encoding sound location. *J Neurosci* 13:2050–2067.
- Park TJ, Klug A, Holinstat M, Grothe B (2004) Interaural level difference processing in the lateral superior olive and the inferior colliculus. *J Neurophysiol* 92:289–301.
- Pecka M, Brand A, Behrend O, Grothe B (2008) Interaural time difference processing in the mammalian medial superior olive: the role of glycinergic inhibition. *J Neurosci* 28:6914–6925.
- Pecka M, Siveke I, Grothe B, Lesica NA (2010) Enhancement of ITD coding within the initial stages of the auditory pathway. *J Neurophysiol* 103:38–46.

- Pecka M, Zahn TP, Saunier-Rebori B, Siveke I, Felmy F, Wiegrebe L, Klug A, Pollak GD, Grothe B (2007) Inhibiting the inhibition: a neuronal network for sound localization in reverberant environments. *J Neurosci* 27:1782–1790.
- Peden DR, Petitjean CM, Herd MB, Durakoglugil MS, Rosahl TW, Wafford K, Homanics GE, Belelli D, Fritschy JM, Lambert JJ (2008) Developmental maturation of synaptic and extrasynaptic GABAA receptors in mouse thalamic ventrobasal neurones. *J Physiol* 586:965–987.
- Pollak GD, Burger RM, Klug A (2003) Dissecting the circuitry of the auditory system. *Trends Neurosci* 26:33–39.
- Pollak GD, Burger RM, Park TJ, Klug A, Bauer EE (2002) Roles of inhibition for transforming binaural properties in the brainstem auditory system. *Hear Res* 168:60–78.
- Porres CP (2012) Neural circuit analysis of the dorsal nucleus of the lateral lemniscus and new viral approaches to neural circuit analysis in Mongolian gerbils Ph.D. diss., LMU München.
- Porres CP, Meyer EMM, Grothe B, Felmy F (2011) NMDA currents modulate the synaptic input-output functions of neurons in the dorsal nucleus of the lateral lemniscus in Mongolian gerbils. *J Neurosci* 31:4511–4523.
- Pouille F, Scanziani M (2001) Enforcement of temporal fidelity in pyramidal cells by somatic feed-forward inhibition. *Science* 293:1159–1163.
- Rautenberg PL, Grothe B, Felmy F (2009) Quantification of the three-dimensional morphology of coincidence detector neurons in the medial superior olive of gerbils during late postnatal development. *J Comp Neurol* 517:385–396.
- Ravin R, Spira ME, Parnas H, Parnas I (1997) Simultaneous measurement of intracellular Ca²⁺ and asynchronous transmitter release from the same crayfish bouton. *J Physiol* 501 (Pt 2):251–262.
- Rayleigh O (1907) On our perception of sound direction. *Philosophical Magazine and Journal of Science* XIII:214–232.
- Rietzel HJ, Friauf E (1998) Neuron types in the rat lateral superior olive and developmental changes in the complexity of their dendritic arbors. *J Comp Neurol* 390:20–40.
- Roberts MT, Seeman SC, Golding NL (2013) A mechanistic understanding of the role of feedforward inhibition in the Mammalian sound localization circuitry. *Neuron* 78:923–935.
- Rose JE, Brugge JF, Anderson DJ, Hind JE (1967) Phase-locked response to low-frequency tones in single auditory nerve fibers of the squirrel monkey. *J Neurophysiol* 30:769–793.

- Saint Marie RL, Ostapoff EM, Morest DK, Wenthold RJ (1989) Glycine-immunoreactive projection of the cat lateral superior olive: possible role in midbrain ear dominance. *J Comp Neurol* 279:382–396.
- Sanes DH (1990) An in vitro analysis of sound localization mechanisms in the gerbil lateral superior olive. *J Neurosci* 10:3494–3506.
- Satake S, Inoue T, Imoto K (2012) Paired-pulse facilitation of multivesicular release and intersynaptic spillover of glutamate at rat cerebellar granule cell-interneurone synapses. *J Physiol* 590:5653–5675.
- Saunier-Rebori B (2008) The neural mechanisms of persistent inhibition in the DNLL of the gerbil (*Meriones unguiculatus*). Ph.D. diss., LMU München.
- Scott LL, Mathews PJ, Golding NL (2005) Posthearing developmental refinement of temporal processing in principal neurons of the medial superior olive. *J Neurosci* 25:7887–7895.
- Seidl AH, Grothe B (2005) Development of sound localization mechanisms in the mongolian gerbil is shaped by early acoustic experience. *J Neurophysiol* 94:1028–1036.
- Shinn-Cunningham BG, Zurek PM, Durlach NI (1993) Adjustment and discrimination measurements of the precedence effect. *J Acoust Soc Am* 93:2923–2932.
- Shneiderman A, Oliver DL, Henkel CK (1988) Connections of the dorsal nucleus of the lateral lemniscus: an inhibitory parallel pathway in the ascending auditory system? *J Comp Neurol* 276:188–208.
- Silver RA (2010) Neuronal arithmetic. *Nat Rev Neurosci* 11:474–489.
- Singer JH, Talley EM, Bayliss DA, Berger AJ (1998) Development of glycinergic synaptic transmission to rat brain stem motoneurons. *J Neurophysiol* 80:2608–2620.
- Siveke I (2007) Novel approaches for the investigation of sound localization in mammals. Ph.D. diss., LMU München.
- Siveke I, Ewert SD, Grothe B, Wiegrebe L (2008) Psychophysical and physiological evidence for fast binaural processing. *J Neurosci* 28:2043–2052.
- Siveke I, Pecka M, Seidl AH, Baudoux S, Grothe B (2006) Binaural response properties of low-frequency neurons in the gerbil dorsal nucleus of the lateral lemniscus. *J Neurophysiol* 96:1425–1440.

- Spangler KM, Warr WB, Henkel CK (1985) The projections of principal cells of the medial nucleus of the trapezoid body in the cat. *J Comp Neurol* 238:249–262.
- Spitzer MW, Bala ADS, Takahashi TT (2003) Auditory spatial discrimination by barn owls in simulated echoic conditions. *J Acoust Soc Am* 113:1631–1645.
- Steinert JR, Postlethwaite M, Jordan MD, Chernova T, Robinson SW, Forsythe ID (2010) NMDAR-mediated EPSCs are maintained and accelerate in time course during maturation of mouse and rat auditory brainstem in vitro. *J Physiol* 588:447–463.
- Stuart G (1999) Voltage-activated sodium channels amplify inhibition in neocortical pyramidal neurons. *Nat Neurosci* 2:144–150.
- Szabadics J, Tamás G, Soltesz I (2007) Different transmitter transients underlie presynaptic cell type specificity of GABAA,slow and GABAA,fast. *Proc Natl Acad Sci U S A* 104:14831–14836.
- Tang ZQ, Lu Y (2012) Two GABAA responses with distinct kinetics in a sound localization circuit. *J Physiol* 590:3787–3805.
- Taschenberger H, von Gersdorff H (2000) Fine-tuning an auditory synapse for speed and fidelity: developmental changes in presynaptic waveform, EPSC kinetics, and synaptic plasticity. *J Neurosci* 20:9162–9173.
- Trussell LO (2012) *Synaptic Mechanisms in the Auditory System*, chapter Inhibitory Neurons in the Auditory Brainstem, pp. 165–185 Springer, New York.
- Tsuchitani C, Boudreau JC (1967) Encoding of stimulus frequency and intensity by cat superior olive S-segment cells. *J Acoust Soc Am* 42:794–805.
- van der Heijden M, Lorteije JAM, Plauška A, Roberts MT, Golding NL, Borst JGG (2013) Directional hearing by linear summation of binaural inputs at the medial superior olive. *Neuron* 78:936–948.
- Vida I, Bartos M, Jonas P (2006) Shunting inhibition improves robustness of gamma oscillations in hippocampal interneuron networks by homogenizing firing rates. *Neuron* 49:107–117.
- von Békésy G (1970) Travelling waves as frequency analysers in the cochlea. *Nature* 225:1207–1209.
- Wallach H, Newman EB, Rosenzweig MR (1949) The precedence effect in sound localization. *Am J Psychol* 62:315–336.

- Wehr M, Zador AM (2003) Balanced inhibition underlies tuning and sharpens spike timing in auditory cortex. *Nature* 426:442–446.
- Wehr M, Zador AM (2005) Synaptic mechanisms of forward suppression in rat auditory cortex. *Neuron* 47:437–445.
- Werthat F, Alexandrova O, Grothe B, Koch U (2008) Experience-dependent refinement of the inhibitory axons projecting to the medial superior olive. *Dev Neurobiol* 68:1454–1462.
- Williams SR (2004) Spatial compartmentalization and functional impact of conductance in pyramidal neurons. *Nat Neurosci* 7:961–967.
- Williams SR, Stuart GJ (2003) Voltage- and site-dependent control of the somatic impact of dendritic IPSPs. *J Neurosci* 23:7358–7367.
- Wilson CJ (2005) The mechanism of intrinsic amplification of hyperpolarizations and spontaneous bursting in striatal cholinergic interneurons. *Neuron* 45:575–585.
- Wilson CJ (2007) GABAergic inhibition in the neostriatum. *Prog Brain Res* 160:91–110.
- Wolf M, Schuchmann M, Wiegrebe L (2010) Localization dominance and the effect of frequency in the Mongolian Gerbil, *Meriones unguiculatus*. *J Comp Physiol A Neuroethol Sens Neural Behav Physiol* 196:463–470.
- Wu SH, Kelly JB (1995a) In vitro brain slice studies of the rat's dorsal nucleus of the lateral lemniscus. I. Membrane and synaptic response properties. *J Neurophysiol* 73:780–793.
- Wu SH, Kelly JB (1995b) In vitro brain slice studies of the rat's dorsal nucleus of the lateral lemniscus. II. Physiological properties of biocytin-labeled neurons. *J Neurophysiol* 73:794–809.
- Wu SH, Kelly JB (1996) In vitro brain slice studies of the rat's dorsal nucleus of the lateral lemniscus. III. synaptic pharmacology. *J Neurophysiol* 75:1271–1282.
- Xie R, Manis PB (2013) Target-Specific IPSC Kinetics Promote Temporal Processing in Auditory Parallel Pathways. *J Neurosci* 33:1598–1614.
- Yang L, Pollak GD (1994) The roles of GABAergic and glycinergic inhibition on binaural processing in the dorsal nucleus of the lateral lemniscus of the mustache bat. *J Neurophysiol* 71:1999–2013.
- Yang L, Pollak GD (1998) Features of ipsilaterally evoked inhibition in the dorsal nucleus of the lateral lemniscus. *Hear Res* 122:125–141.

Zahn TP (2003) Neural Architecture for Echo Suppression during Sound Source Localization based on Spiking Neural Cell Models Ph.D. diss., TU Ilmenau.

Zucker RS (1999) Calcium- and activity-dependent synaptic plasticity. *Curr Opin Neurobiol* 9:305–313.

Nomenclature

AMPA 2-amino-3-(3-hydroxy-5-methyl-isoxazol-4-yl)propanoic acid

AP action potential

AVCN anterior ventral cochlear nucleus

CN cochlear nucleus

DNLL dorsal nucleus of the lateral lemniscus

GABA γ -aminobutyric acid

IC inferior colliculus

ILD interaural level difference

IPSC inhibitory postsynaptic current

IPSP inhibitory postsynaptic potential

ITD interaural time difference

LNTB lateral nucleus of the trapezoid body

LSO lateral superior olive

MNTB medial nucleus of the trapezoid body

MSO medial superior olive

NMDA N-methyl-D-aspartate

PI persistent inhibition

Eidesstattliche Versicherung/ Affidavit

Hiermit versichere ich an Eides statt, dass ich die vorliegende Dissertation *Development and physiology of signal integration in the DNLL* selbstständig angefertigt habe, mich außer der angegebenen keiner weiteren Hilfsmittel bedient und alle Erkenntnisse, die aus dem Schrifttum ganz oder annähernd übernommen sind, als solche kenntlich gemacht und nach ihrer Herkunft unter Bezeichnung der Fundstelle einzeln nachgewiesen habe.

I hereby confirm that the dissertation *Development and physiology of signal integration in the DNLL* is the result of my own work and that I have only used sources or materials listed and specified in the dissertation.

München, den

Munich, date

Contributions

2 Physiological development of DNLL neurons

Julian Ammer (J.J.A.), Benedikt Grothe (B.G.), and Felix Felmy (F.F.) conception and design of research; J.J.A. and F.F. performed experiments; F.F. contributed all data and analysis to Figure 1. F.F. contributed data to Figures 2,3 and 4 and recorded all data for Figure 7. J.J.A. analyzed all electrophysiological data. J.J.A., B.G., and F.F. interpreted results of experiments; J.J.A. (Figures 2-8) and F.F. prepared figures (Figure 1); J.J.A. and F.F. drafted manuscript; J.J.A., B.G., and F.F. edited and revised manuscript; J.J.A., B.G., and F.F. approved final version of manuscript.

3 Long lasting inhibition in the DNLL

Julian Ammer (J.J.A.) and Felix Felmy (F.F.) conception and design of research; J.J.A. performed all experiments; J.J.A. analyzed all data; J.J.A. and F.F. interpreted results of experiments; J.J.A. prepared all figures; J.J.A. and F.F. drafted manuscript; J.J.A. and F.F. edited and revised manuscript.

Signature Felix Felmy

Acknowledgements

Thank you...

... Felix Felmy for your great support, supervision and enthusiasm during the last years. I enjoyed working with you and in your group. Although I will never be able to remember all the details and numbers, I hope to have learned from your meticulous look at raw data and your talent to break down a problem into a logical series of experiments.

... Benedikt Grothe for your support and always helpful input. I enjoyed having the systems background of your lab when fiddling with my synapses.

... Martin Stemmler, Bernd Sutor and Volker Scheuss for valuable input and discussions during my thesis committees.

... Delwen, Christian, Mike and Hanna for proofreading and plenty of helpful comments.

... Christoph Kirst and Ida Siveke for collaborations that were not part of this thesis, but a lot of fun.

...the GSN office team for their help, instantaneous reimbursements and the organization of a trillion of wonderful social events.

... to those who had to share an office with me (Eli, Christian, Chrissi) and got a trauma from listening to ever the same tunes.

...all the neurobio crew on the third floor for their help. Especially to those who keep everything running: Claudia, Hilde, Melanie, Olga, Horst, Dieter, Monika, Sabrina and Simone. Also to all those who became my friends, joined me for burgers or just beer after work and contributed to the good times outside the lab. Special thanks here to the home-cyclers, the retreat late-nighters, the next-door PhDs, the football crew aka VfB Martinsried, the happy hour team and to the crazies from Cologne and Australia who made the start in Munich a lot easier.

...den besten Eltern und der besten Schwester. Danke, dass ihr immer für mich da seid.

...Hanna, dafür, dass du selbst München zu meinem Zuhause gemacht hast.